

Title:

Integration of metamaterials in a mobile phone for reduction of the peak SAR in the head.

Theme:

Study of the effects of the implementation of SRRs on dipole antennas and PIFAs.

Thesis period:

MOB10, spring semester 2009

Thesis group: 09gr1113

Participants:

Guesdon Maxime
Métivier-Mervaud Edouard
Sermouh Adil

Supervisors:

Gert Frølund Pederson
Ivan Bonev Bonev

Copies: 5

Number of pages: 70

Date: 2nd June 2009

Abstract:

This thesis focuses on the use of metamaterials in mobile phone devices in order to improve antenna performances, e.g. to investigate if they can reduce the peak of SAR in the human head. The purpose is to present metamaterials in a general way as many researches do not provide general background and knowledge, and focus on very specific uses and topics.

As many researches focus on the use of metamaterials with antennas, the second objective is to analyze if they could possibly improve the performances of antennas. Thanks to FDTD simulations, several configurations have been investigated.

The first comparison has been done on a dipole antenna with and without metamaterials in terms of S11 parameter, gain, bandwidth, radiation efficiency, and SAR in a cube of tissue standing for a human head.

The second case dealing with more realistical configurations has been done with PIFAs without changing the overall volume of the antennas according to actual manufacturing standards. To appreciate the effects of SRRs, the fields have been investigated in the close vicinity of the antenna corresponding to the most exposed area of a human head.

The effective reduction of the fields thanks to metamaterials is investigated because improving user's safety compliance and handset performances is a major interest of mobile phone designers.

Preface

This report is written by project group 09gr1113 at the Department of Electronics at Aalborg University during the 10th semester at Mobile Communications (1st February 2009-2nd June 2009). The project concerns the “Integration of metamaterials in a mobile phone for reduction of the peak SAR in the head”.

The work is presented in three main parts, the first focuses on theoretical comprehension of metamaterials and their use, the second one depicts the simulations achieved and the last one is an appendix contains basic knowledge about antennas, FDTD and SAR.

The first part proposes a definition of metamaterials as well as usual classifications and applications. The second chapter explains the simulation performed for this study and the important parameters that have to be investigated, like SAR, E and H fields.

In the appendix, basic definitions about antennas are reminded and the particularities of small antennas are pointed out, linking them to the typical problem of mobile design.

As a conclusion, relevance of metamaterials coupled with mobile handset is discussed according to antennas performances and aimed reduction of SAR.

Aalborg University, 2nd June, 2009

We would like to thank all the people that helped to write this thesis, especially Pr. Gert Pederson and Ivan Bonev Bonev for their precious advice and supervising but also the Aalborg University for letting us use the supercomputer for FDTD simulations. Finally, thanks to Infineon for the interest they put in our project.

Guesdon Maxime
<guesdon@kom.aau.dk>

Métivier-Mervaud Edouard
<metivier@kom.aau.dk>

Sermouh Adil
<sermouh@kom.aau.dk>

Table of Contents

Preface	3
Table of Contents	5
Metamaterials	8
1. Definition	8
2. Classification.....	9
2.1. Sign of Parameters.....	9
2.1.1. DPS	9
2.1.2. DNG.....	10
2.1.3. ENG & MNG – plasmonic media.....	10
2.2. Bi-Anisotropic Materials	11
2.2.1. Example of bianisotropic metamaterials: chiral materials	11
3. Fabrication	12
3.1. 2D metamaterials	12
3.1.1. Split-Ring Resonators (SRRs)	12
3.1.2. Inclusions.....	15
3.1.3. Thin-wire structure	16
3.2. 3D metamaterials.....	18
3.2.1. Isotropic 3D SRR.....	18
3.2.2. Ceramic sphere	18
3.2.3. Lattices.....	19
3.3. Transmission lines	21
3.3.1. Example of SRR	21
3.3.2. Example of Thin Wires.....	21
3.4. Summary.....	22
4. What has been done so far	23
4.1. Antennas	23
4.1.1. DNG Shell	23
4.1.2. Thin wires	23
4.1.3. Increase of the directivity.....	23
4.1.4. Reduction of the SAR with SRR.....	24
4.2. Filters.....	24
4.2.1. Basic approach of different kind of filters	24
4.2.2. Relations with electronic filters	24
4.2.3. Advantages of a DNG metamaterial	25
4.3. Tuning and Theory	25
4.3.1. Reduce the electrical size of a SRR	25
4.4. Define the resonant frequency of a SRR from the substrate.....	26
4.5. Q factor analysis of different types of SRRs	27
4.6. Summary.....	28
Simulations	29
1. Modeling	29
1.1. Introduction	29
1.2. Antennas	30
1.2.1. Dipole antenna	30
1.2.2. Planar Inverted F-Antenna (PIFA).....	30
1.3. Metamaterials	31
1.3.1. Design	31
1.3.2. Implementation	33
2. Dipole investigations.....	33
2.1. Dipole and metamaterials in free space.	33

2.1.1.	Electric and magnetic fields investigations.....	33
2.1.2.	Conclusion	35
2.2.	Dipole with a Cube of tissue and metamaterials.....	35
2.2.1.	Configuration	35
2.2.2.	S11 parameter	37
2.2.3.	Total absorption	38
2.2.4.	Bandwidth.....	39
2.2.5.	Gain.....	39
2.2.6.	Electric and magnetic fields investigation	40
2.2.7.	SAR.....	42
2.2.8.	Conclusion	43
3.	PIFA investigations.....	44
3.1.	PIFA and SRRs in free space.....	44
3.1.1.	PIFA ‘Bottom’	44
3.1.2.	PIFA ‘Top’	52
3.1.3.	PIFA ‘Crossed’	56
3.1.4.	Comparison between PIFAs	58
3.1.5.	Additional layers of SRRs	60
3.1.6.	Conclusion	61
3.2.	PIFA with SRR and Cube.....	62
3.2.1.	Configuration.....	62
3.2.2.	Electric field investigations.....	62
3.2.3.	Conclusion	63
4.	Conclusions and improvements	64
4.1.	Conclusions	64
4.1.1.	Dipole investigations	64
4.1.2.	PIFA investigations.....	64
4.2.	Improvements	65
	List of Figures.....	66
	List of Tables	68
	Bibliography	69
	List of Abbreviations	70
	Appendix.....	I
	Antennas	II
1.	Antenna parameters.....	II
1.1.	Radiation pattern.....	II
1.2.	Input Impedance	III
1.3.	S11.....	III
1.3.1.	VSWR.....	III
1.3.2.	Reflexion coefficient.....	III
1.3.3.	Mismatch Loss	IV
1.3.4.	Return Loss	IV
1.4.	Radiation efficiency.....	IV
1.5.	Total Radiated Power (TRP) and Total Isotropic Sensitivity (TIS).....	V
1.6.	Bandwidth.....	V
2.	Small antennas	VI
2.1.	Definition of ‘small’	VI
2.2.	Problems encountered.....	VI
2.3.	Q-factor.....	VI
3.	Antenna design in portable devices.....	VII
3.1.	Classes ([26]).....	VII
3.1.1.	Whip antennas.....	VII
3.1.2.	Meanders and coils	VII
3.1.3.	Dual-band whips and coils.....	VIII
3.1.4.	Early internal antennas.....	VIII
3.1.5.	Dual-band internal antennas	VIII
3.1.6.	Triple-, quad-, penta-band antennas.....	IX

3.1.7.	Multiple antennas.....	IX
3.1.8.	Additional services	IX
FDTD method.....		X
1.	FDTD	X
1.1.	Method choice	X
1.2.	Why using FDTD method?.....	X
1.2.1.	Advantages.....	X
1.2.2.	Drawbacks	XI
1.3.	Principles	XI
1.4.	Yee algorithm	XII
1.5.	Absorbing Boundaries Conditions.....	XII
1.5.1.	Definition.....	XII
1.5.2.	Solution.....	XIII
1.6.	Models	XIII
1.6.1.	Drude Model	XIII
1.6.2.	Lorentz Model.....	XIV
SAR – Specific Absorption Rate		XV
1.	Introduction.....	XV
2.	Definition	XV
3.	Simulations.....	XVI

Metamaterials

In this chapter the main concepts that cover the topic of metamaterials are introduced. The first part gives a brief definition of what is actually a metamaterial and explains how they have been discovered. Then, in the next section, the study of the different parameters and behaviors leads to a classification of metamaterials. Finally the two last parts deal with the way to build these metamaterials and will expose the latest releases.

1. Definition

Even if the definitions of metamaterials occasionally differ from each other, they are most of the time referring to the metamaterials as media whose electromagnetic responses are different from those of their constituent components.

They are also often referred as materials with properties that cannot be found in nature.

They are mainly built on multiplying in a periodic manner various types of artificially fabricated media in a background substrate. Such a structure is called a lattice, and the elements are optically small resonant particles, usually much smaller than the operating wavelength. Most of the time, they are complex-shape metal inclusions operating in different frequency ranges. The particle characteristic size δ and the maximal period of lattices a are assumed to be much smaller than the wavelength in the lattice matrix in most of the metamaterials at the frequency of particle resonance. This assumption leads to homogenize metamaterials on explaining their exotic properties in terms of conventional material parameters (Quasi-static theory of lattices [1]). Even though they are small, the parameters δ and a are given for most of the practical cases by equation (1.1) [2]

$$0.01 \leq \frac{(a, \delta)}{\lambda} \leq 0.2 \quad (1.1)$$

The very first goal of the metamaterials was to create better conductors, closer to ideal insulators, on breaking the previously established basic rules of physics.

The discovery of the bianisotropic and chiral materials (2.2) brought a main question: do these materials still belong to the category of classical materials? In chiral media, the symmetry or antisymmetry of the internal structure is responsible for macroscopic effects. Whereas the bi-anisotropy defines a material that displays both anisotropy (the macroscopic response depends on the type of excitation) and electromagnetic behaviors [3].

Then, the discovery of Victor Veselago (1966) has created a revolution. Parameters that always have been assumed to be positive could finally also be negative. These materials possess backward wave propagation and negative refraction when both permittivity and permeability are negative or in certain frequency regions.

These successive discoveries have made this topic one of the most interesting in the past few years. Lots of researches focus on metamaterials nowadays in order to find applications concerning a wide range of domains.

2. Classification

It has been a long time now since scientists try to understand metamaterials, and it is not an easy task. The main problem remains the understanding of the internal structure of a metamaterial because it contains a very high degree of freedom that prevent from sorting everything. That is why the following classification also focuses on the macroscopic aspect as in the paper [4].

2.1. Sign of Parameters

A basic classification could be established regarding the sign of the permittivity and the permeability of the materials. This common classification is divided in four parts of positive and negative values that let us distinguish the regions of forward and backward propagation (see Figure 2.1)

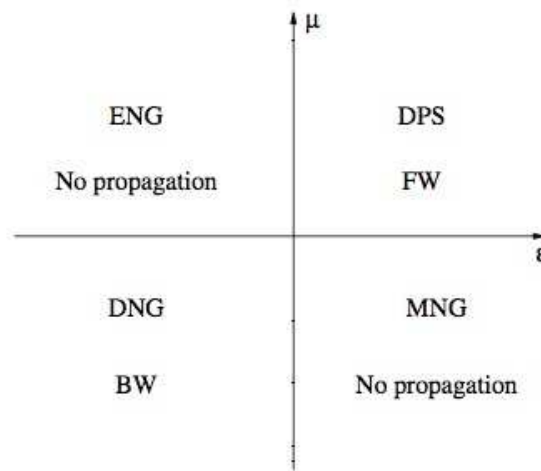


Figure 2.1 : Basic classification of materials in the ϵ, μ plane [31]

2.1.1. DPS

The common materials are ordinary Double Positive (DPS) which means that both permittivity and permeability are positive, therefore the waves are propagating forward. The DPS materials could also be classified in term of their dielectric parameters magnitude. Magnetic materials that have permeability values different from 1 are called 'ordinary' electromagnetic materials. Nevertheless some values can be very large or very small compared to the unity, so they can be regrouped into electromagnetic classes, as in the Figure 2.2.

Following this classification the Perfect Electric Conductors (PEC) and Perfect Magnetic Conductors (PMC) can be distinguished. Knowing that the PEC is defined by $\epsilon \rightarrow \infty, \mu \rightarrow 0$, and the PMC by $\epsilon \rightarrow 0, \mu \rightarrow \infty$, the PEC has extremely small impedance also called Zero-Impedance Medium (ZIM) and its conductivity σ is infinite. The PMC has an extremely large impedance, called Infinite-Impedance Medium (IIM).

Another material has also been studied the past few years, which is a Perfect ElectroMagnetic Conductor (PEMC). It is the only fully isotropic medium regardless to the movement of the observer. It has been proved that PEMC medium causes many interesting effects, which may find applications in antenna engineering.

These materials obey to others relations between the flux and fields [31]:

$$\begin{aligned} D &= M \cdot B \\ D &= -M \cdot E \end{aligned} \tag{2.1}$$

Where M is the real scalar admittance-type quantity. The special case of PEC comes with the choices $1/M = 0$, and the one of PMC with $M = 0$.

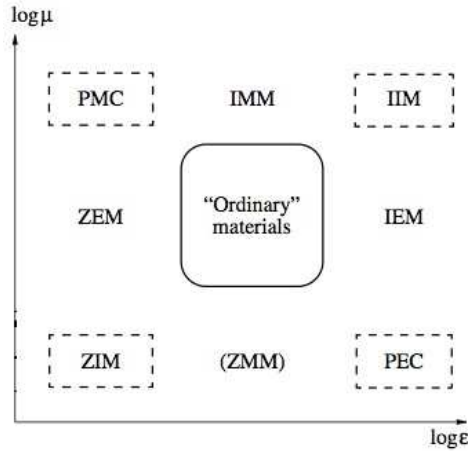


Figure 2.2 : Classification of extreme materials in the ϵ, μ plane [31]

*ZIM: zero-index material; IIM: infinite-index material;
 ZEM: zero-electric material; IEM: infinite-electric material;
 ZMM: zero-magnetic material; IMM: infinite-magnetic material.*

Materials with these extreme parameter amplitudes have been recently recognized for their potential applications, like increasing the directivity of planar antennas, cloaking objects, and squeezing electromagnetic and optical energy.

2.1.2. DNG

New materials have been recently found. They have properties that cannot usually be found in nature, and even more they have different behaviors than the ones of their component elements. They are called the Double Negative Materials (DNG) and belong to this new kind, the metamaterials. Both permittivity and permeability are negative so the waves are propagating backward, and the refractive index is negative. Such a media is capable of focusing electromagnetic radiations when placed in a way to have a lens.

2.1.3. ENG & MNG – plasmonic media

Then, the two remaining possibilities are the Epsilon Negative (ENG) and Mu Negative (MNG). With these parameters, the waves are not allowed to propagate into uniform medium. As the wave propagation in isotropic homogeneous media is in function of e^{-jkz} , where the wave number $ik = \omega\sqrt{\mu\epsilon}$, the square root gives an imaginary wave number.

2.2. Bi-Anisotropic Materials

A bi-anisotropic material displays both anisotropy and electromagnetic behaviors. Considering a magneto-electric coupling in the material, the wave propagation obeys to other relations between the different fields demonstrated in [31].

$$D = \varepsilon \cdot E + (\chi - j \cdot \kappa) \cdot H \quad (2.2)$$

$$B = (\chi + j \cdot \kappa) \cdot E + \mu \cdot H \quad (2.3)$$

With κ , the chirality parameter,
 χ , the non-reciprocity parameter.

The plane waves in these mediums are propagating with the wave number:

$$k_{\pm} = k_0 \cdot \left(\sqrt{\mu \cdot \varepsilon - \chi^2} \pm \kappa \right) \quad (2.4)$$

With k_0 , the free space wave number $[m^{-1}]$

The two waves can now be either backward or forward because the wave number depends on the magnitude of the four parameters. The relation between the fields is therefore [31]:

$$\begin{pmatrix} D \\ B \end{pmatrix} = \begin{pmatrix} \varepsilon & \chi - j \cdot \kappa \\ \chi + j \cdot \kappa & \mu \end{pmatrix} \cdot \begin{pmatrix} E \\ H \end{pmatrix} \quad (2.5)$$

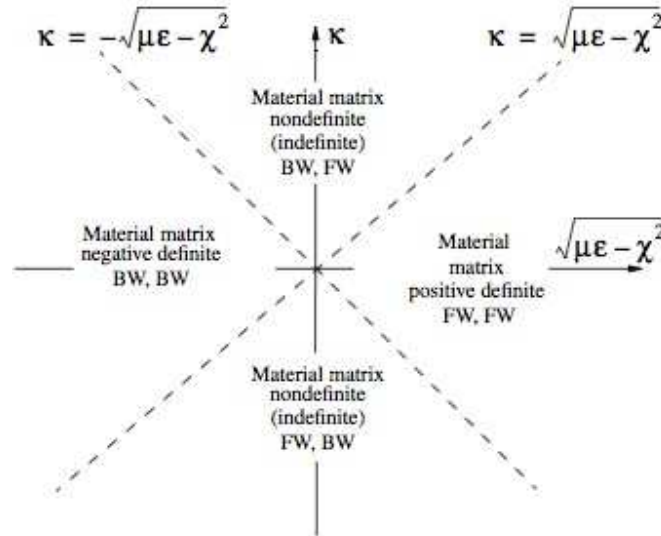


Figure 2.3 : Classification of bi-isotropic materials [30]

2.2.1. Example of bianisotropic metamaterials: chiral materials

In chiral media, the geometrical nature of the structure of the internal elements leads to macroscopic effects thanks to its antisymmetry, like the rotation of the polarization of the propagation field plane (rotary power). This rotary power comes from the magnetoelectric coupling caused by the chiral elements.

3. Fabrication

Here are presented some of the most widespread metamaterials that could be useful to understand this study. Nevertheless more information about the different fabrication techniques could be found in the paper [5].

3.1. 2D metamaterials

As the required feature sizes of fabrication are very small, most of the 2D metamaterials are fabricated using electron-beam lithography (EBL). EBL is still the most spread technique even if it is quite complicated to build wide areas because of cost and time efficiency. For rapid prototyping of metamaterials, focused-ion beam (FIB) techniques can be used. The principle of FIB is that a focused beam of gallium ions is used to sputter atoms from the surface or to implant gallium atoms into the top few nanometers of the surface, making it amorphous [5]. When the large-scale fabrication is aimed, then the interference lithography is mainly used. This fabrication technique is based on the superposition of two or more coherent optical beams forming a standing wave pattern. Nevertheless a promising large-scale fabrication technique is arising from the Nano-imprint lithography (NIL). Metal nanostructures are thus obtained by printing directly on metal substrates without any further processing step.

3.1.1. Split-Ring Resonators (SRRs)

The SRRs are used to generate magnetic resonance and to provide negative permeability.

3.1.1.1. Basic SRR

a. Design

The SRR presented in the Figure 3.1 has an expected resonance at 10 GHz ($\lambda=30\text{mm}$), and can be created on printing a metalized copper layer on a Printed Circuit Board (PCB).

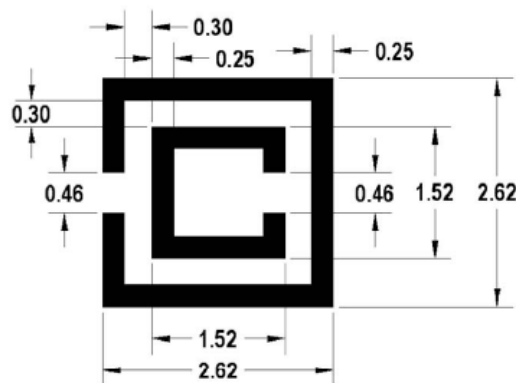


Figure 3.1 : Dimensions in millimeter of a SRR pattern in mm [6]

When designing a SRR, the first parameter to take into account is the frequency range where it is effective. Let us have a look to the curve that the parameter μ_{eff} describes in the Figure 3.2:

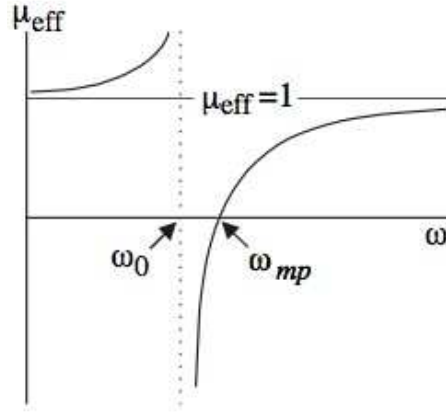


Figure 3.2. Discontinuity of the permittivity [32]

The range of frequency between $[\omega_0 : \omega_{mp}]$, respectively the resonant and plasma frequencies, will be the frequency range where the medium exhibits negative permittivity (in the case where they are taken for $\mu_{eff} = 0$). These parameters can be found thanks to the equations below [32]. ω_0 is the frequency where μ_{eff} diverges.

$$\omega_0 = \sqrt{\frac{3lc_0^2}{\pi r^3 \log\left(\frac{2c}{d}\right)}} \quad (3.1)$$

$$\omega_{pm} = \sqrt{\frac{\omega_0^2}{1 - \frac{\pi r^2}{a^2}}} \quad (3.2)$$

Where:

- c is the ring width [m]
- d is the gap between the inner and the outer rings [m]
- l is gap between the different layers [m]
- r is the radius of the first inner ring [m]
- c_0 the celerity in free space [m.s⁻¹]

The choice of the dimensions is therefore very important because it leads to different resonance frequencies. All the parameters of the SRR influence the negativity properties, such as increasing the bandwidth or the values of μ_{eff} for example. The model used to simulate these properties is given by these two equations [32]:

$$\mu_{eff} = 1 - \frac{\frac{\pi r^2}{a^2}}{1 + \frac{2l\sigma}{\omega r \mu_0} i - \frac{3lc_0^2}{\pi \omega^2 \ln \frac{2c}{d} r^3}} \quad (3.3)$$

$$\epsilon_{eff} = 1 - \frac{\omega_{pm}^2}{\omega^2} \quad (3.4)$$

Where:

- σ is the conductivity of the metallic part (=0 for perfect conductors) [S.m⁻¹]
- a is the lattice constant, the gap between two SRR centers in the same layer [m]

On tuning the different parameters, one can obtain a SRR resonating at a specified frequency.

b. Incidence of the gap orientation

In [6], the incidence of the orientation of the gap of the SRR is studied depending on the E-field direction, by studying the S parameters S11 and S21. The Figure 3.3 shows the different orientations studied.

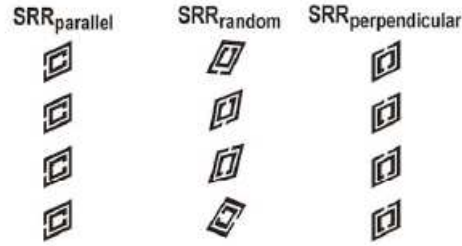


Figure 3.3 : $SRR_{parallel}$, SRR_{random} , $SRR_{perpendicular}$

$SRR_{parallel}$ —gaps in the split rings parallel to the incident E field to realize a dielectric resonance;
 SRR_{random} —randomly oriented gaps to realize simultaneous dielectric and magnetic resonances;
 $SRR_{perpendicular}$ —gap oriented perpendicular to the E-field to realize a strong magnetic resonance.

The NRW (Nicolson-Ross-Weir) method is used to deduce mathematically the values of the parameters by using the S parameters. The far field is simulated with two horns equipped with divergent lenses, and placed on both sides of the structure. They deliver a plane wave to the structure and the S parameters are measured.

The conclusions of this study show that the nature of the plasmonic resonance depends a lot on the orientation of the SRR gaps (see Figure 3.3):

- For E-field parallel disposition to the SRR gap, an electrical resonance is found
- For E-field perpendicular disposition to the SRR gap, a magnetic resonance is found
- For random disposition, both electric and magnetic resonances are found
- For particular frequencies, the resonances are not very deep and the real part of μ and ϵ still be positive leading to negative index behavior

c. Influence of the substrate

In [7], it is demonstrated that the response of SRRs could also be tuned by changing its substrate layer properties (most often the FR4 substrate). The thickness of this layer affects a lot the responses. It could change the electrical size by reducing the resonance frequency.

The main breakthrough of the thickness modulation of the substrate is that it keeps the permittivity of the metamaterial as it was and decreases the resonant frequency of the metamaterials. Therefore the properties of the substrate or even its thickness are good tools to tune the metamaterial, and for example define the resonant frequency of SRRs.

d. Polarization of a SRR

Basically, to understand how a SRR polarization occurs, an H field excitation in the axis of the SRR is considered as depicted in Figure 3.4:

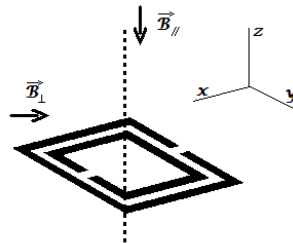


Figure 3.4 : Orientation of B-fields on a SRR structures

As it will be explained further in the following part (§4.2), this simple SRR structure will behave as a stop-band for the GSM frequencies. To be able to see the best processing of this structure, a H field is directed towards the structures along its axis (-z). Obviously, the SRR presents a simple negative material [8] and would be able to observe that specific behavior.

First, the magnetic component of the EM waves creates a huge electric capacitance between the two rings of the SRR. Therefore, a great E field is created along this gap and because of that, the field coupling determines ϵ as a negative value. In Figure 3.5, this effect is depicted:

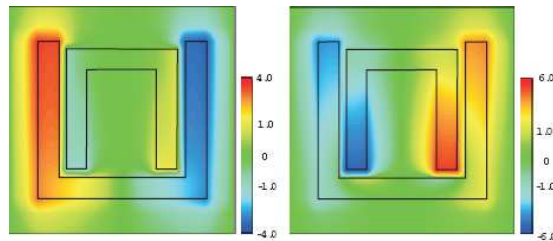


Figure 3.5 : Excitation of the U-shaped SRR by electric field [9]

This U-shaped SRR acts just like a C-shaped SRR. In blue and red, the positive and negative electric poles show the new capacitance created between the ring gaps. Then, only ϵ is negative and μ still positive turning the exposed SRR into a stop-band filter for its resonant frequency defined by its own physical size parameters.

In the case of a perpendicular polarization (perpendicular to the SRR axis), a similar effect appears: only μ becomes negative. Except for the magnetic field created, (as depicted on Figure 3.6) the response behaves the same but for magnetic waves.

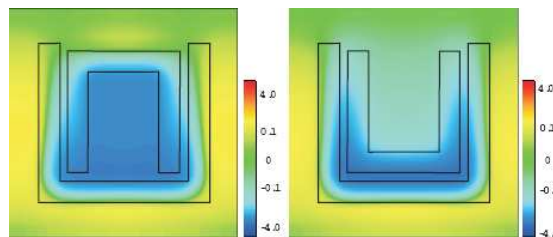


Figure 3.6 : Excitation of the U-shaped SRR by magnetic field [9]

Finally, it can be said that the difference of stop-band localizations in the spectrum is due to the difference between electric and magnetic response of the SRR.

3.1.2. Inclusions

Inclusions are used for melting different designs having different properties, in order to obtain a medium which would combine them. CLS (half Jerusalem cross meaning Capacitive Loaded Strips) are designed for dielectric-like responses and SRR for magnetic-like responses. Therefore to get a DNG media, those two designs could melt as shown on Figure 3.7 :

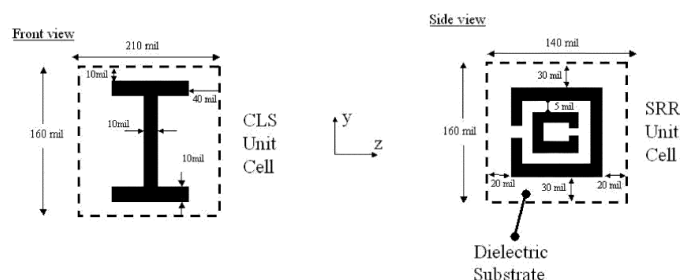


Figure 3.7 : Design of CLS on the left, and SRR on the right (1 mil = $2.54 \cdot 10^{-2}$ mm).[10]

As it can be seen in the Figure 3.8, the structure contains both of the previous studied inclusions, in a planar media. In red, a CLS is repeated in a way that two CLS contain in the same plane (yz) a SRR structure. As both of the inclusions are in the structure, the whole design has electric and magnetic responses.

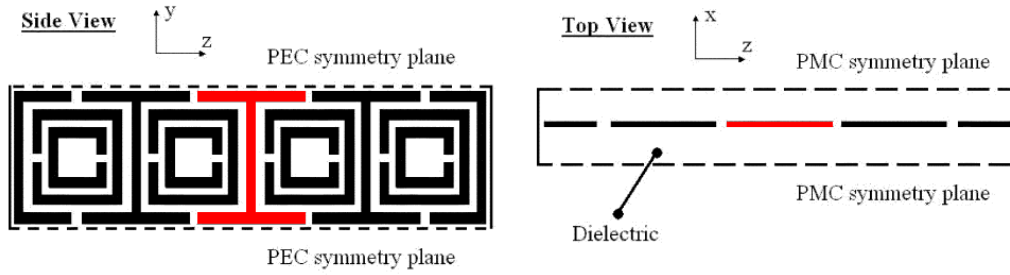


Figure 3.8 : Planar MM designed with CLS and SRR

This kind of hybrid materials able to reproduce the different electric and magnetic responses has already been used in the past to create HFSS (High Frequency Selective Surfaces) and dielectric applications.

A PMC (Perfect Magnetic Conductor) and a PEC (Perfect Electric Conductor) send respectively a magnetic and an electric impulse all around the structure that have to be tested. If we superimpose the two spectrum responses, it appears clearly that for a specific range of frequencies, CLS and SRR show a total reflectivity. Thus, they influence the effective permittivity and permeability of the whole structure ($S_{11} \approx 1$ and $S_{21} \approx 0$)

When both SRR and CLS structures are responding by quasi-only reflections, the media is becoming DNG as it has been proved in [10].

3.1.3. Thin-wire structure

3.1.3.1. Definition

Rotman stated 60 years ago that this structure could be used to simulate the plasma medium because its effective permittivity is expressed the same way (3.5) [12].

$$\epsilon_{eff} = 1 - \frac{\omega_p^2}{\omega^2} \quad (3.5)$$

Where ϵ is the permittivity [F.m⁻¹]
 ω is the radial frequency [rad.s⁻¹]

With:

$$\omega_p = \frac{1}{a^2 \cdot L' \cdot \epsilon_0} \quad (3.6)$$

Where a is the size of the wires ($\Delta x = \Delta y = a$) [m]
 L' is normalized self inductor/unit length [H.m⁻¹]

Then Pendry stated that a negative permittivity effect occurs in the thin-wire if $\omega \ll \omega_p$ leading to ENG metamaterials. In order to shrink the size of the unit cells of the structure a thin-wire based ENG metamaterials loaded with uniformly distributed inductances lowers the plasma frequency.

The thin-wire structure of metamaterials is defined as a pattern of parallel wires small enough to have relevant electromagnetic responses as seen in Figure 3.9 :

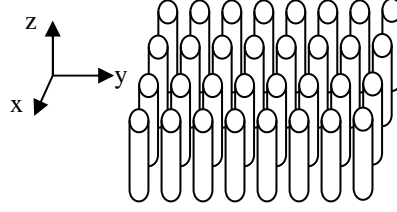


Figure 3.9 : Arrangement of thin-wire structure for metamaterials

This structure is designed to have spacing between wires very small compared to the wavelength. As a consequence, the electromagnetic responses are modified (material turned into ENG metamaterial for example) due to the inner reactance and capacitance of this new structure. According to the paper [11] the relative permittivity of this structure is defined as (3.7) and (3.8) if there is no component along the z-vector:

$$\epsilon_{\text{reff}} = \epsilon'_{\text{reff}} - j \cdot \epsilon''_{\text{reff}} = 1 - \left[\frac{(f_p^2)}{f^2 - j \cdot \gamma \cdot f} \right] \quad (3.7)$$

Where f_p is the plasma frequency [Hz]
 ϵ is the permittivity [F.m⁻¹]
 γ is the loss

With:

$$f_p = c \cdot \left[d \cdot \sqrt{2 \cdot \pi \left(\ln \left(\frac{d}{2 \cdot \pi \cdot r_0} \right) + 0.5275 \right)} \right]^{-1} \quad (3.8)$$

Where f_p is the plasma frequency [Hz]
 c is the speed of light [m.s⁻¹]
 d is the lattice constant [m]
 r_0 is the wire radius [m]

3.1.3.2. Different types of thin-wire structures

There are two main kinds of thin-wires: continuous and discontinuous ones. According to the paper [12], continuous thin wires structures behave like high-pass filter, which means that the effective permittivity takes negative values below the plasma frequency (3.6). On the other hand, discontinuous thin wire structures act as the same filters but with a lower edge turning them into stop-band filters around the resonant frequency.

The combination with other structures previously described is not excluded. As it can be imagined, an alternation of layers of SRR and thin-wires could be made to obtain different relevant responses of the metamaterials thus created. Indeed, the SRRs layer structure leads to negative permeability and thin wires based structures to negative permittivity. Therefore, a superposition of both will give a DNG metamaterial (see example at Figure 3.13).

3.1.3.1. Polarization of a thin wire

A single thin wire represents also a SNG material and acts as a stop-band too. The main difference is that the thin wires structure would change the electromagnetic parameters that are not changed by a layer of SRR alone (See Figure 3.13). As the thin wires structure is not polarized the same way the SRR is, it acts on different parameters.

3.2. 3D metamaterials

According to the paper [13], several difficulties on fabricating 3D metamaterials have to be faced. For example, SRRs are difficult to be made electrically small at optical frequencies. Some DNG materials based on resonant dielectric elements could be the solution to overcome these issues. In the paper [14], an isotropic DNG material with magneto-dielectric particles having high permittivity and high permeability is proposed. It is shown that the material can have magnetic and electric resonances over a common range of frequencies.

For more information about the last fabrication of complex 3D structures, refer to the paper [5].

3.2.1. Isotropic 3D SRR

One of the most challenging tasks in the design of metamaterials was to reach the isotropy. Several attempts have been made in that way and some recent 3D design have been proved to present isotropy properties, like the ones presented in the Figure 3.10:

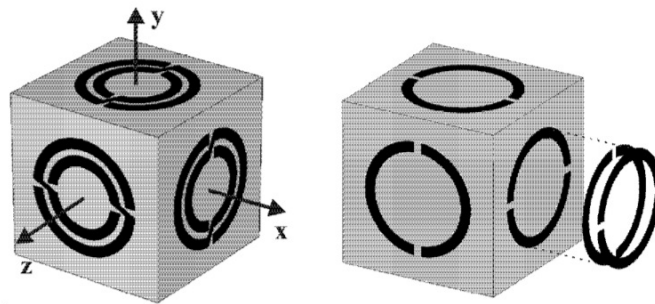


Figure 3.10 : Two types of isotropic magnetic 3D cubical resonators

3.2.2. Ceramic sphere

In the paper [3], a DNG material built up with ceramic spheres and a conducting wire frame has been proposed. The spheres are placed periodically in a conducting wire frame and drive a magnetic resonance, which simulates an artificial plasma medium with a negative permittivity.

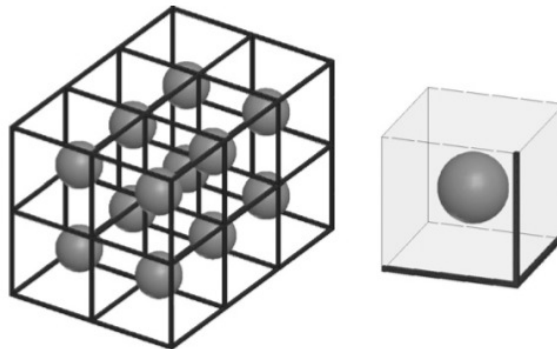


Figure 3.11 : Scheme of 3D DNG metamaterial with dielectric particles and conducting wire frame

In this configuration, the sphere radius is $r=2.7\text{mm}$ ($r=\lambda/20$ at 6GHz) and its dielectric constant is $\epsilon_r=88.3$ (the dielectric constant of the polymer foam is $\epsilon=1.05$). The radius of the wire is 0.5 mm ($\lambda/10$ at 6GHz) and the lattice constant is 6.7 mm ($\lambda/8$ at 6GHz).

It is also proved that due to the negative permeability provided by the ceramic spheres, the transmission coefficient is quite low in the frequency range studied (about -80dB). The metal wires tested without the ceramic spheres lead to a transmission lower than -100dB on the same examined frequency range. Nevertheless the transmission of the waveguide loaded with the composite turns up to -10dB. This metamaterial is also proved to give a backward propagation in the frequency range of 5.64–6.34 GHz. The electric field distribution also shows unmatched impedance and thus verifies the double negativity properties of this material.

3.2.3. Lattices

In general the metamaterials lattices can be described as particles that possess electric and magnetic polarization. They can have two different geometric properties as depicted in the Figure 3.12. In the first one (a) the particles both have electric and magnetic moments. In the second one (b) the electric and magnetic scattering devices are different particles. Both of the cases have an electric field averaged over the unit cell along the x-axis direction, and an averaged magnetic field along the y-axis.

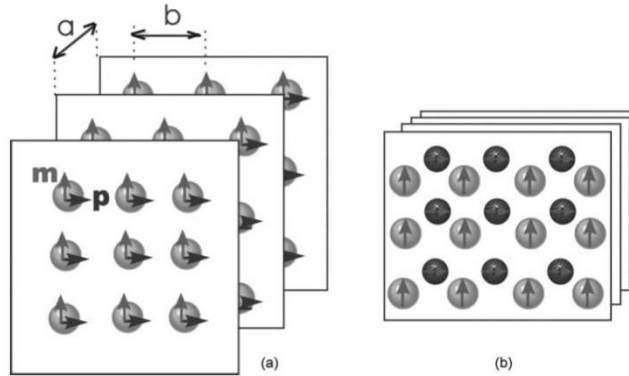


Figure 3.12 : Metamaterials with both electric and magnetic polarization presented as a set of crystal planes [15].

To simplify the calculations, when studying the plane-wave reflection from such a lattice the particles can be replaced by point p - and m -dipoles forming parallel grids away from each other by a distance a . This structure is also called crystal plane and is modeled as infinitely thin sheets with polarization and magnetization surface currents defined as J_e and J_m .

3.2.3.1. I-m-lattices

The I-m-lattice is nothing more than a lattice comprising thin wires and magnetic dipole scattering devices known as Split-Ring Resonators (SRRs). The front view of this metamaterial is shown in the Figure 3.13. In this example, one element is responsible for the resonant magnetic scattering, and thus the negative value of the effective permeability within a narrow frequency range above the resonant frequency, whereas the other one is responsible for the negative permittivity.

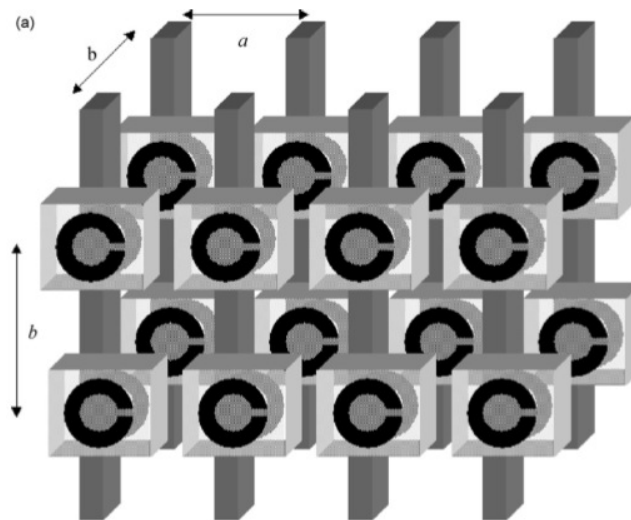


Figure 3.13 : Front view of an I-m-lattice metamaterial [15]

The index of refraction (n) is given by the relation:

$$n = \sqrt{\frac{\epsilon \cdot \mu}{\epsilon_0 \cdot \mu_0}} \quad (3.9)$$

Where	ϵ is the permittivity	[F.m ⁻¹]
	μ is the permeability	[A.m ⁻¹]
	ϵ_0 is the free-space permittivity	[F.m ⁻¹]
	μ_0 is the free-space permeability.	[A.m ⁻¹]

When the frequency is near the resonant frequency of the SRR the magnetic field drives the permeability below zero on the high frequency side of the resonance and the resonant response of the wires in the electric fields.

According to the paper [15], the electromagnetic response of a thin infinite wire to the local electric field is the axial current I . If the wave propagates at an angle with respect to the wire axis, spatial dispersion is observed in the lattice at all frequencies. However, if the propagation holds in the orthogonal plane the low-frequency spatial dispersion is absent and the lattice can introduce the local negative permittivity. On the other hand, the SRRs give the resonant permeability. Therefore the I–m-lattice behaves as a uni-axial variant of the double negative medium. In I–m-lattices the spatial dispersion can arise in the backward wave region even if the period at these frequencies is optically small.

3.2.3.2. Polarization

In a typical case, the SRR provides a μ negative and the thin wire layer turns ϵ into a negative value in the whole structure. The combination of both shows exactly the cumulative effects of SRR and thin wires. Therefore, a DNG material is obtained ($\mu < 0$, $\epsilon < 0$) and the implementation of a negative refraction index pass-band could be done. (See Figure 3.14).

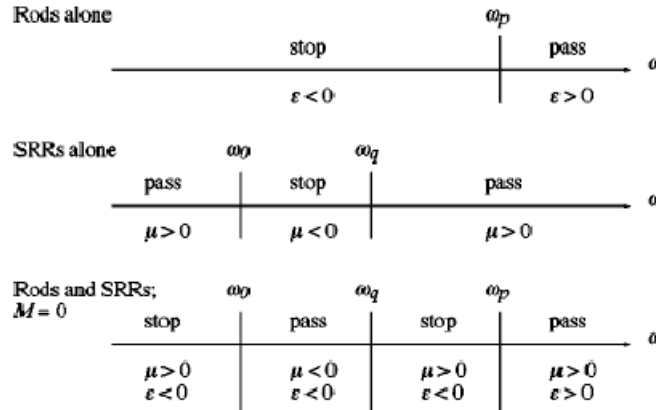


Figure 3.14 : Sum up of the different combinations of structures and their effects

3.2.3.3. P-m-lattices

This lattice could be built as a pair of p-dipole and m-dipole formed by two perfectly conducting Ω -particles placed in a way that cancels the bi-anisotropy as shown in the Figure 3.15. These Ω -particles can be printed on two sides of a thin dielectric plate. In the paper [15], the inner radius of the loops in Ω -particles is equal to $R_{in} = 2.2$ mm, and the outer one to $R_{in} = 2.4$ mm. The distance between particles is equal to $q = 0.5$ mm and the host medium is free space. This design has electric and magnetic dipole resonances at 4 GHz.

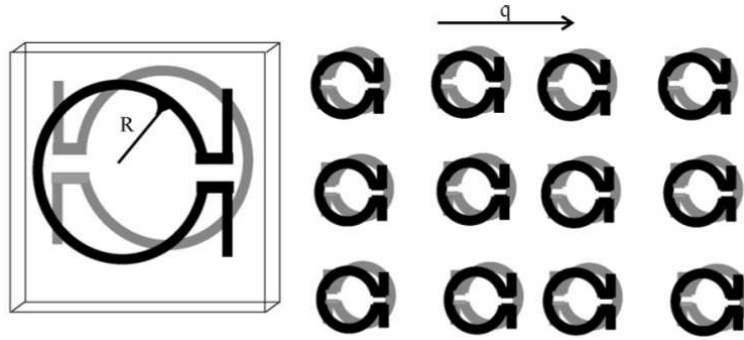


Figure 3.15 : The lattice geometry of a p-m crystal

P–m-lattices as well as I–m-lattices can exhibit the partial stop-band in the backward wave regions, so that these structures cannot be described in terms of local material parameters.

3.3. Transmission lines

The transmission lines are used to model metamaterials by creating analogues circuits. When a metamaterial consists in two parallel straight conductors, as in lattices for example, it can be modeled by a sequence of impedances and admittances. Instead of solving the problems on the built metamaterials, they can be solved easily by computing techniques thanks to the transmission line modeling where the electromagnetic fields are represented by electrical circuits.

3.3.1. Example of SRR

In the paper [16] an equivalent circuit standing for a SRR is given and the calculation of the parameters of L and C in the presence of a dielectric substrate is discussed in [17]. Therefore, the simplest equivalent circuit model (neglecting losses) for the SRR unit cell is given in the Figure 3.16. C_s is the capacitance between the gaps.

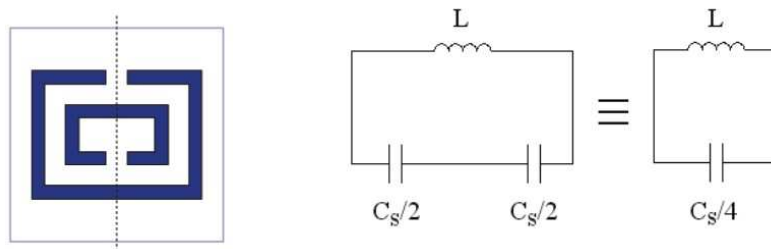


Figure 3.16. A SRR and its Equivalent Circuit

The SRR structure under the excitation of the incident wave treated as an equivalent L-C circuit has a resonance frequency of:

$$f = \frac{1}{2 \cdot \pi \cdot \sqrt{L \cdot C}} \quad (3.10)$$

Where C is equal to $C_s/4$.

3.3.2. Example of Thin Wires

Based on previous studies ([18]) and simulations to confirm the analogy, the transmission line theory relies on the equivalent circuit of inclusions among a layer. As a matter of fact, the thin wires of a single

structure could be assimilated to inductances on an electrical circuit. The main idea of this theory is to be able to modify at will the structure to simulate and appreciate theoretical results before manufacturing them.

This method is especially accurate for the far field cases and allows determining the effective permittivity of a medium. As it could be predicted, this theory is matching with the previous ones (Pendry's model) and according to it ([18]), an asymmetric arrangement of thin wires could also lead to relevant (negative) electromagnetic responses.

Thus, the equivalent circuit for the thin wire structure could be represented as a grid of inductances on Figure 3.17 :

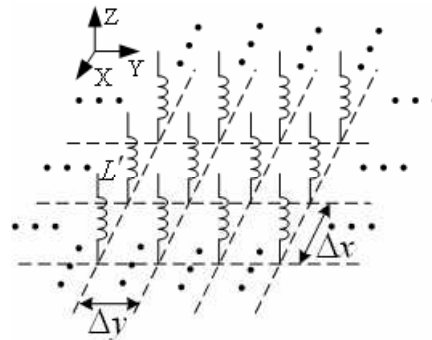


Figure 3.17 : Equivalent circuit of thin wire array with inductor array. ([18])

3.4. Summary

- As most of the researches have been done on SRRs, they are the most explained designs. In fact, it has been seen that layers of SRRs can provide negative permeability at a specific resonant frequency depending of the SRR dimensions. In this peculiar negative region, the material turns into stop-band filter. This is why SRRs have been chosen among all kind metamaterials in order to test their impact on the reduction of the peak E field as their dimensions and their fabrication are compatible with modern antenna design.

- Nowadays, GSM frequencies used are roughly between 1GHz and 5GHz, that is why choosing SRRs is a smart choice as their size is reducing while increasing the resonant frequency of the metamaterial.

- It has been shown that the dimensions of the metamaterial are the main parameters as they influence its resonant frequency. Reducing the size of the SRRs when keeping the same resonant frequency is an important issue as miniaturization is a hot topic in mobile devices. To see the dimensions of the SRR chosen for this study refer to 1.3.1.

- There is actually no relevant study concerning the impact of the number of SRRs layers and the coupling effects between the different elements on the metamaterial macroscopic effectiveness, like field reduction or gain.

4. What has been done so far

4.1. Antennas

4.1.1. DNG Shell

The structure of a DNG shell has been investigated in the paper [19], a small electric dipole antenna is surrounded by a DNG shell in such a way that the DNG shell acts as a distributed matching network between the dipole antenna and free space. The radiated power is thus increased. When matched, this structure can be summed up as a resonant CL circuit formed by the dipole antenna and the DNG shell, respectively capacitor and inductor. As defined in the Figure 4.1, the DNG spherical shell is defined by its inner radius r_1 and its outer radius r_2 .

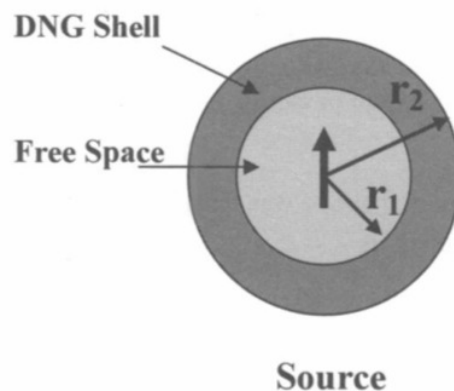


Figure 4.1 : Dipole antenna surrounded by a DNG shell

Recent works have oriented researchers to investigate the possibility of reciprocity between the radiation and scattering resonances for a variety of nested metamaterial shells. It could also be guessed that matching an electrically small antenna with an ENG material alone could be done in order to enhance the radiated power gain when the dipole and the shell are resonating. Indeed, an electrically small ENG shell also acts like a capacitive element but as the permittivity is negative, it finally acts an inductor and thus its combination with the dipole forms an LC resonator. And this perspective is quite interesting as ENG materials can be made easier than DNGs.

4.1.2. Thin wires

Small enough thin wires layer (arranged the way previously described in 3.1.3) could lead to interesting structures, but the question to ask is about the implementation of such structures at GSM band into a mobile phone. According to previous studies ([20]), the sizes of thin wires operating at this band region are too large for practical applications in mobile and small antenna designs. Therefore, to be able to implement such structures into mobile phones, a new theoretical approach of those thin wires has to be investigated.

4.1.3. Increase of the directivity

In [21] the study of the radiation pattern of an antenna is done with a S-shaped metamaterial. The gain of the antenna is thus increased by approximately 6 dBi, but the beam width is reduced by 37.5%. This discovery could be used in point to point transmission as for example between two buildings, where the directivity is a relevant parameter. Moreover other studies have proved that the directivity of an antenna could be increased with for example the use of directive antennas.

4.1.4. Reduction of the SAR with SRR

In previous studies ([20]), some important contents have been described for a better understanding on how metamaterials such as SRRs work. They were investigated with a simplified model of the head, symbolized by a cube of tissue, and a dipole antenna. The distance between the head and the antenna in this paper is equal to 25mm and does not match a realistic handling of a user in common life. The configuration used in this paper is depicted in the Figure 4.2.

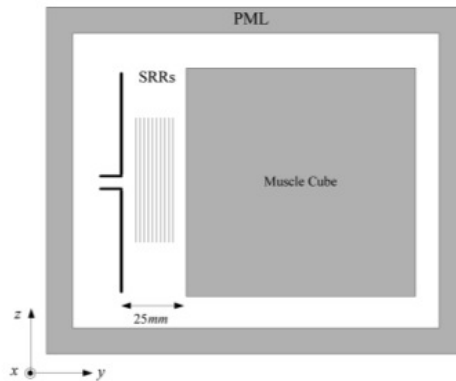


Figure 4.2 : Configuration for the SAR calculation

The different layers of SRRs provide a reduction of the SAR_{1g} maximum by almost 38% at a frequency of 1800MHz. Distances and modeling of the metamaterials used in this study do not allow concluding on the benefit of those kinds of structures compared to simple dielectric bricks or metal plates. A more precise model for metamaterial and realistic distances has to be simulated.

4.2. Filters

4.2.1. Basic approach of different kind of filters

Electronic filters are commonly used in electric circuits to perform signal processing functions especially to remove (or attenuate) specific unwanted frequencies or enhance wanted ones. Filters could be active or passive, analogical or digital, and appear under 4 different categories: High-pass, Low-pass, Stop-band, and Pass-band. The different effects of these ones are summed up in Figure 4.3:

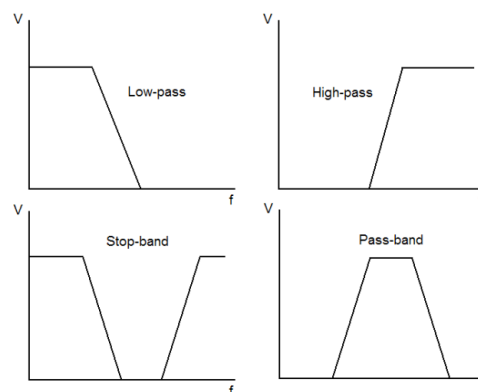


Figure 4.3 : The different types of filters

4.2.2. Relations with electronic filters

As metamaterials could behave like the different kind of filters depending on their electromagnetic parameters, an analogy can be done between metamaterials and electronic filters. The aim of this study is to stop the electromagnetic waves incoming at 1800MHz. The focus is thus set especially on stop-band and pass-band

filters. It is already known that a SNG material behaves as a stop-band and a DNG as a negative refraction index pass-band filter [8].

As a result, when implementing a stop-band metamaterials for specific frequencies, the EM waves are attenuated through the structure and protect the user from dangerous EM waves.

4.2.3. Advantages of a DNG metamaterial

To go further, a negative refraction index pass-band filter could be considered for DNG metamaterials. Indeed, implementing this kind of metamaterials could lead to the redirection of the EM waves incoming. First, if this filter is perfectly done, all the EM waves are back scattered and not absorbed by the user head. Secondly, the EM waves are redirected way back and could be used for base stations to communicate. This last procedure results in an enhancement of the QoS of the communication.

With the SNG metamaterials, the result is only the loss of the EM waves oriented towards the metamaterial structure: it appears to be a solution but surely not the best one. That is why the DNG is privileged.

It is also important to highlight the fact that this negative refraction index appears there and the electromagnetic waves are back scattered which is not the case in simple transmission (normal pass-band filter when double positive parameters). Therefore, DPS metamaterial cannot behave as the wanted pass-band as it does not stop any EM waves through the structure.

4.3. Tuning and Theory

4.3.1. Reduce the electrical size of a SRR

The paper [22] focuses on the reduction of the electrical size of a single split finger ring (Table 4.1) on modifying the width of its structure. The electromagnetic response and the resonant frequency are changed. The λ_0 is then increased which leads to a lower electrical size as given by the formula below:

$$Electrical_size = \frac{Ring_diameter}{Wavelength} \quad (4.1)$$

In this paper [22], it is admitted that the C-shaped SRR is one of the most common SRR because it is really easy to build. Indeed, for such a structure only one ring is needed but on the other hand the electrical size is about 1/10. That is why only a few parameters have an impact on the electrical size.

When creating a BC-SRR, more parameters can be modified in order to increase λ as it can be noticed in the equation of the electrical size, like the gap between the two rings (see Table 4.2).

$$Electrical_size_{BC-SRR} = \frac{2.(r+c)}{\lambda_0} \quad (4.2)$$

The main goal is reached since the electrical size is reduced. The BC-SRR has almost the same size than the C-shaped SRR but has a lower electrical size at around $\lambda/300$ for the BC-SRR against $\lambda/10$ for the C-shaped.

According to this paper [22], actually the smallest electrical size is found in the Enkrich structure where the fabrication limits are reached. The subject of this part is mainly about the BC-SRR but suggests that the same procedure could be followed for others SRR types as EC-SRR (Edge-Coupled SRR) or VS-SRR (Vertical-Spiral SRR).

Nevertheless, recent studies based on the same principle have proposed another similar design. In the paper [16], the Double sided SRR (DSRR) design is discussed (Figure 4.4).

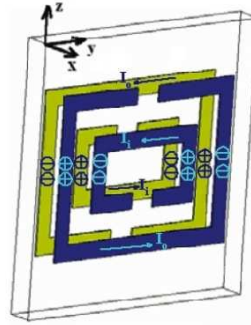


Figure 4.4. Design of a DSRR

The DSRR is basically a combination of two inverted SRRs on both sides of the substrate. This particular design leads to an even higher coupling between the two SRRs. A maximum reduction of almost 29% of the resonant frequency is reached by using DSRR instead of SRR. In other words, the DSRR structure can provide much better miniaturization in RF design applications.

This discovery could lead to several applications in domains such as the design of Radio Frequency technologies and wireless technologies in general, like the enhancement of small antennas on mobile devices, but could also be used for metamaterial structures or in filters.

4.4. Define the resonant frequency of a SRR from the substrate

The thickness of the substrate where the metamaterials are placed has a role in their resonant frequency. In the paper [7], two antennas facing each other have been used in order to deduce the properties of the material, and the S parameters are calculated (see Figure 4.5). This technique is known as the NRW method (Nicolson-Ross-Weir) and is useful to create a plane wave exposition of the metamaterial (Far-field). Therefore, the complex permittivity and permeability could be extracted and studied.

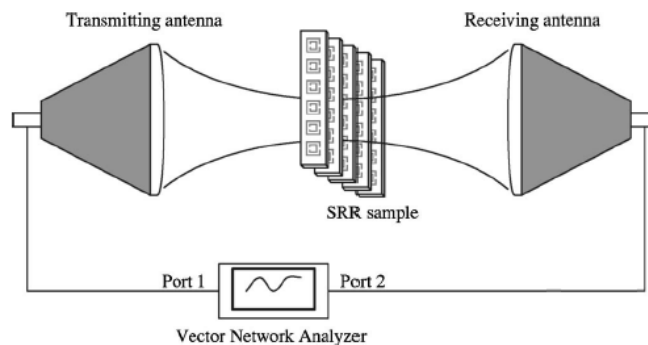


Figure 4.5 : Measurement of S parameter for a layer of SRRs

Different techniques could be used to reduce the thickness of the substrate:

- Heating (increase temperature to make the structure thinner)
- External magnetic fields that create the effect that the substrate is less thick
- Mechanical stress (using force to compress the structure)

Different tunable materials could also be used as the substrate layer:

- Ferroelectric thin films
- Liquid crystals layer
- Very low loss layer used as filters and phase shifters

Thanks to the experiments, it has been found that the resonance frequency is changed by the thickness of the substrate layer. The reason of this decrease of resonance frequency could be explained by the fact that when the substrate thickness increases, the capacitance (defined by the coupling between the inner and outer ring) increases also, bringing a reduced resonance frequency. It saturates because the field caused by the capacitor is confined in a smaller region while the electrical size of the substrate increases.

As a conclusion, it is known that there are multiple ways to reduce the resonance frequency with SRR metamaterial, for example by defining proper size parameters of the different gaps, splits, etc... But tuning these microscopic scaled gaps is a bit more difficult than changing the substrate thickness or properties. As the geometrical size of the metal structure is usually fixed and hard to change, and as the gaps are too small to be tuned precisely, these substrate techniques allow reaching much more precision about lowering or defining the resonance frequency.

4.5. Q factor analysis of different types of SRRs

The paper [23] investigates the influence of the different configurations of the rings on the Q factor. For more information about the Q factor, see 2.3. The results found are summed up in the Table 4.1 and Table 4.2.

Type (thick)	Single Split Finger Ring (big)	Single Split Double Finger Rings	Shielded Finger Rings	Finger SRR	Single Split Finger Ring (small)
Geo.					
f_{meas}	1.86	2.03	2.96	1.53	2.78
f_{sim}	1.955	2.071	2.926	1.562	2.829
Q_{meas}	16.9	19.6	89.2	39.4	15.4
Q_{sim}	17.3	21.3	272.1	44.5	14.9

Table 4.1 : Five configurations of finger rings [23]

(Outer ring: $\varnothing=22$ mm, inner ring: $\varnothing=15$ mm, split gap width: 2 mm, ring width: 1 mm, ring thickness: 5 mm)

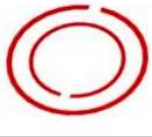
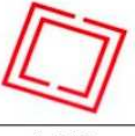
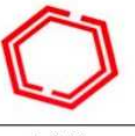
Type	SRR (thin)	BC-SRR (thin)	Spiral-SRR (thin)	VS-SRR (thin)
Geo.				
f_{sim}	1.921	1.263	1.041	0.6348
Q_{sim}	34.4	133.6	183.7	348.9
Type	Quadrangle SRR (thin)	Hexagon SRR (thin)	Quadrangle SRR (thick)	Hexagon SRR (thick)
Geo.				
f_{sim}	1.512	1.841	1.232	1.260
Q_{sim}	52.4	80.7	71.7	151.6

Table 4.2 : Planar and vertical configurations (same sizes than in the previous table) [23]

It can be noticed that similar element sizes lead to similar material loss, and the different radiations can be verified by the calculated and measured Q factors. First of all, only one structure in the Table 4.1 against 4 in the Table 4.2 is displaying Q values above 100. They have similar material loss but much smaller radiation loss, which can be identified as the main reason for higher Q values.

It is shown in the paper [23] that in the case of a classical SRR configuration, the E field amplitude is higher at the ends of the split ring, while the distributed capacitance is in comparison smaller (the distributed capacitance is located in the radial direction and between the inner and outer rings).

For the case of the spiral SRR and VS-SRR, the E field within the split gap is weakened due to the zero potential difference at the conjunction. The power thus circulates within the element, and less power is radiated. In the BC-SRR case, no wave propagation is established and no power is radiated. The E field is concentrated vertically due to the broadside coupling. In the Shielded Finger Ring (SFR) the shielding prevents power radiation, which could be useful in the case where additional reduction of radiation is needed. In general, the SRRs which are not in circle shapes are interesting for assembling into planar arrays because they are easier to arrange between each others.

Finally, the conclusion of this study is that thicker elements have higher Q factors than thinner ones. This is partially because of their smaller material loss and radiation loss, the relative magnitude of material and radiation losses therefore determine the value of Q. The investigation of the metamaterial elements did not verify the uniformity of surface current, but rather emphasized its influence on the radiation efficiency, Q factor and resonant frequency. A combination of the BC-SRR and the spiral structure seems to be the best possible trade-off, but it has to be pointed out that the transmission efficiency is greatly influenced by the effective coupling between neighboring elements.

4.6. Summary

- Various studies about the improvement of antenna parameters have been done, but only a few focuses on small antennas. Based on those studies, this thesis aims more realistic situations as it considers a real antenna volume and practical distances. Those distances take into account the operating position of a mobile phone where the antenna is less than 5mm away from the user head. In opposition to most of the studies, the SRRs are implemented inside a PIFA in order to investigate their influence on the antenna, and not only on the radiated fields far from the antenna. The objective is to build an antenna coupled with metamaterials not only to reduce de SAR, but also to keep a good trade-off with the other parameters.

- It has been seen that the substrate could be tuned to improve some parameters but none is used in this study, in order to be able to isolate the effects of the metamaterial structure itself.

Simulations

T*his part exposes all the results from the FDTD simulations. First, the objective of this project is described, then the way the different structures have been designed, and investigated. The next sections will first deal with the results linked to a dipole antenna, and then with the PIFA. Both cases are studied with an array of SRR and a cube of tissue modeling a simplified human head.*

1. Modeling

1.1. Introduction

The simulation part has been divided into two main parts. The first one is the study of a dipole in order to get some basic knowledge about the influence of the distance between the antenna and the head, and the resonance of the SRR designed. The second part will treat the PIFA case, which is much more likely in actual devices simulations with realistic distances in a way that it could be possible to create a real phone with those dimensions. Unlike most recent antennas, a PIFA has been chosen because it is still a reference model for internal antennas, which could resonate at a unique frequency of 1800MHz which is the center frequency of the GSM 1800 standards.

The goal of this study is to reduce the peak of SAR, and more generally the fields that are absorbed by the tissues in the head. In order to reach this goal, arrays of SRR resonating at the same frequency that the antenna (1800 MHz) have been designed. Around the resonance frequency, the permeability becomes negative, and in this bandwidth where those values are negative the SRR provides high magnetic impedance and is supposed to act as a stop band.

Since the study is based on the enhancement of a small antenna, it is difficult to predict its behavior as it is interacting with the near field, which is complex. Nevertheless E and H fields will mainly be discussed, as the SAR is time consuming due to its high requirement in computing power. Other features allowing to appreciate the effectiveness of the antennas design like the bandwidth, the radiation efficiency, the radiation patterns and the Smith charts are depicted in this study.

1.2. Antennas

1.2.1. Dipole antenna

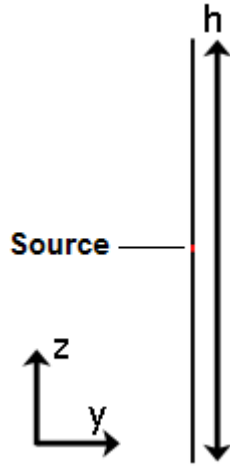


Figure 1.1 : Detailed dipole model used in the simulations

The first simulations are used as a basic example to describe the behavior of a dipole when SRRs are added. The theoretical length for a dipole to resonate at 1.8GHz is half the wavelength calculated here:

$$\lambda = \frac{c}{f} = \frac{300 \cdot 10^6}{1,8 \cdot 10^9} = 16,7 \text{ cm} \quad (1.1)$$

The dipole designed has a total size of $h=8\text{cm}$. The results of the simulations with a dipole, a SRRs layer and a cube will be shown later in the report. In order to be matched, the real part of the antenna impedance has to be the closest possible to 50Ω . In other words, when the antenna is resonating at the required frequency, $\text{Re}[Z]=50\Omega$. The length of a monopole is usually estimated to $l=\lambda/4$ to fill this condition.

1.2.2. Planar Inverted F-Antenna (PIFA)

Here are the dimensions of the PIFA used in the simulations and the positions of the source and the short circuit in order to match the antenna to 50Ω .

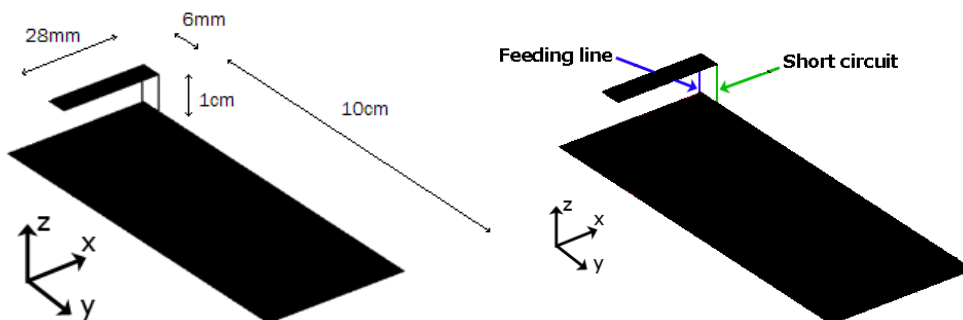


Figure 1.2 : Detailed PIFA models used in the simulations

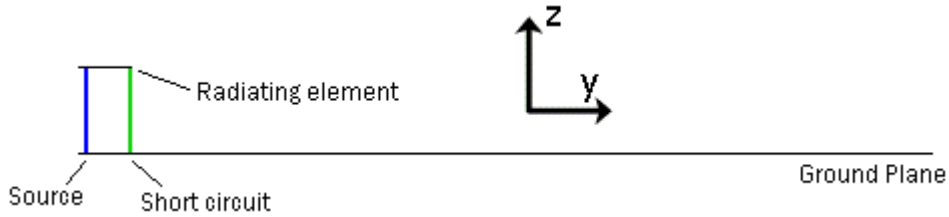


Figure 1.3 : PIFA used for simulations

This antenna resonates at 1.8GHz. The Figure 1.4 shows the S11 parameter corresponding to this antenna:

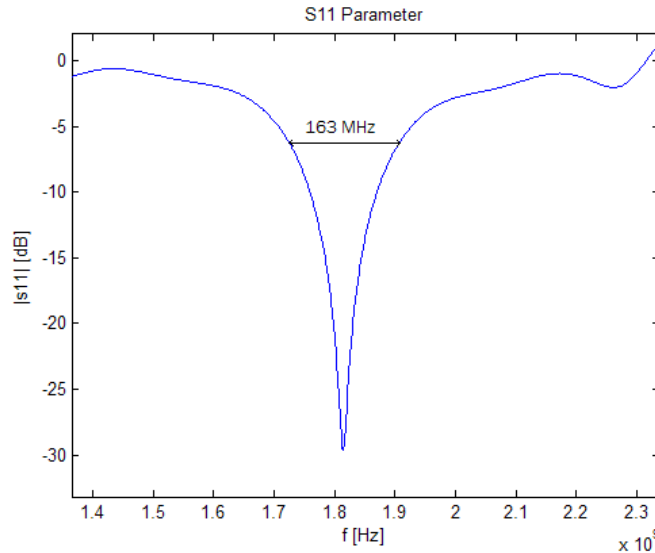


Figure 1.4 : S11 parameter showing the resonance of the PIFA

It can also be noticed that the bandwidth is equal to 163MHz at -6dB. The domain is free space and no loss is the antenna is considered so its radiation efficiency is 1.

1.3. Metamaterials

1.3.1. Design

For this report, only basic Split-Ring Resonators (SRRs) have been simulated, as they are the simplest structure used to make metamaterials. It has been previously explained that many different structures derived from SRR exist, but this one is simple to design in a FDTD simulator since a model directly describes its dimensions.

Here are the dimensions for a square SRR resonating at 1.8GHz:

$$C = 1. \cdot 10^{-3}m$$

$$d = 0.2. \cdot 10^{-3}m$$

$$l = 0.2. \cdot 10^{-3}m$$

$$r = 4. \cdot 10^{-3}m$$

$$\text{Total size} = 2. (r + (2C) + d) = 1,24. \cdot 10^{-2}m$$

$$a = \text{Total size} + 6. \cdot 10^{-3}m$$

Ring width

Gap between inner and outer ring

Gap between the different layers

Radius of the first inner ring

Total size of one SRR

Lattice constant, distance between two ring centers

(The distance between two consecutive SRR is equal to $6.10^{-3} m$)

Those dimensions are depicted in Figure 1.5 :

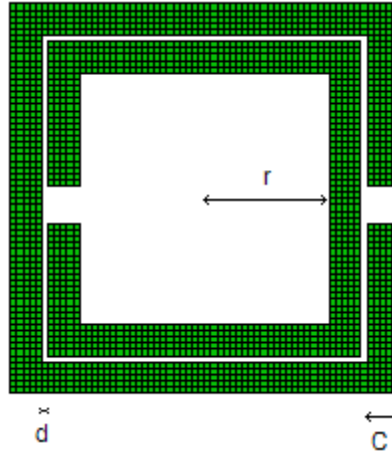


Figure 1.5 : Shape and dimensions of the square SRR used

To verify the dimensions of the SRR, it is possible to calculate the μ_{eff} (1.2) as shown before (3.3):

$$\mu_{eff} = 1 - \frac{\frac{\pi r^2}{a^2}}{1 + \frac{2l\sigma}{\omega r \mu_0} + \frac{3lc_0^2}{\pi\omega^2 \ln\left(\frac{2C}{d}\right)r^3}} \quad (1.2)$$

Where σ is the resistance per length (0 in this case as a perfect conductor is assumed to design the SRR), C_0 is the speed of light. Therefore the formula can be simplified as:

$$\mu_{eff} = 1 - \frac{\frac{\pi r^2}{a^2}}{1 + \frac{3lc_0^2}{\pi\omega^2 \ln\left(\frac{2C}{d}\right)r^3}} \quad (1.3)$$

designed above.

The following plot shows μ_{eff} for the ring

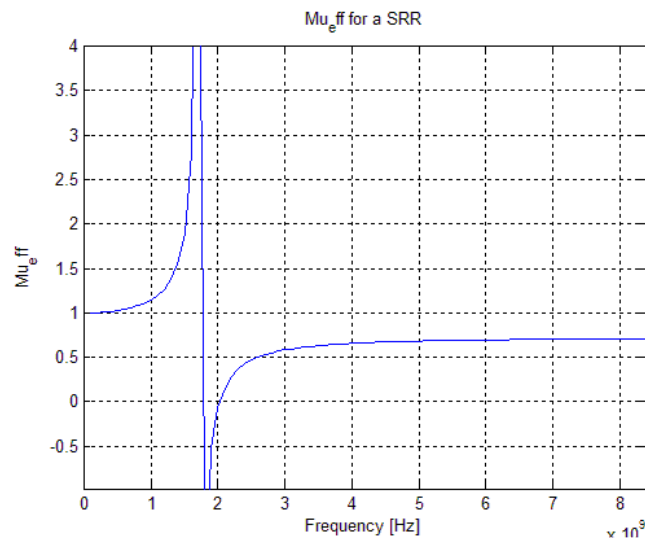


Figure 1.6 : μ_{eff} plot showing the resonance

A SRR designed with the previous dimensions resonating at 1.8GHz. It is also possible to get the plasma frequency from the graph, by checking the value corresponding to $\mu_{eff} = 0$. It is very close to 2GHz in this example. This means that negative permittivity will be achieved between 1.8GHz and the plasma frequency.

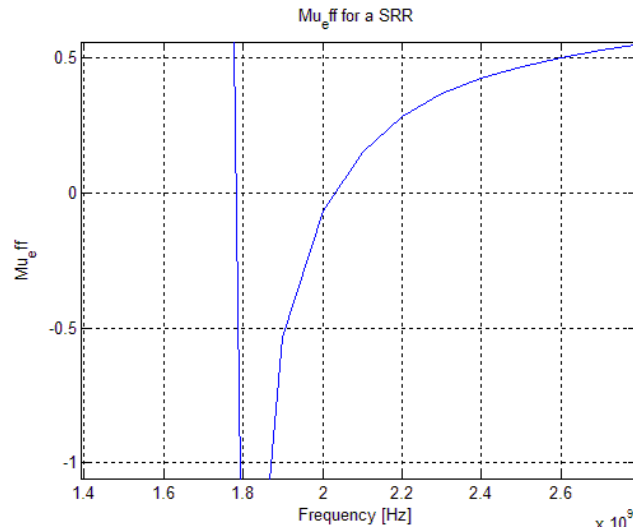


Figure 1.7 : closer look at the resonance in μ_{eff}

1.3.2. Implementation

For the simulations which have been done for this study, metamaterial sheets have been added to a dipole antenna and a PIFA:

- In the case of the dipole, a single layer of 3 columns and 6 rows of SRRs has been added 4mm away from the antenna as it covers the tissues behind it.
- In the case of the PIFA, a layer of 3 columns and 2 rows of SRRs has been included in various positions between the ground plane and the radiating element and under the ground plane. The purpose is here to investigate a realistic implementation of metamaterials inside an antenna.
- In addition to these configurations, more layers have been included in the PIFA.

As the SRRs are implemented in the near field region, their orientation cannot be defined according to the directions of the fields that are unpredictable.

2. Dipole investigations

2.1. Dipole and metamaterials in free space.

2.1.1. Electric and magnetic fields investigations

The first case investigated is the direct influence of a layer of SRRs on a dipole antenna. The next figure shows this configuration. The distance between the SRRs layer and the antenna is set to $x = 4\text{mm}$ because this distance will allow studying their impact in the near field region.

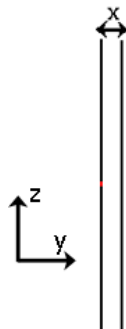


Figure 2.1 : Detailed dipole with SRR configuration used in simulation

Different planes have been studied at different distances in order to investigate the impact of the distance on the reduction of the fields. This configuration shown by the figure below will be used to compare the dipole alone and the dipole with a layer of SRRs.

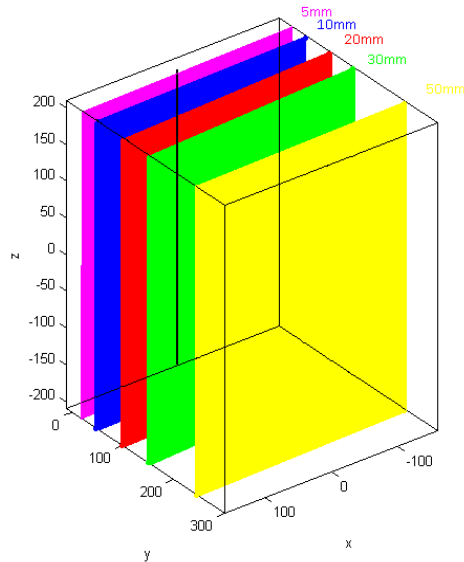


Figure 2.2 : Different planes where the fields are studied (dipole case) (cell size = 0.2mm)

The two next plots show the comparison between the electric and magnetic fields for the SRR and dipole alone configurations.

a. Electric field

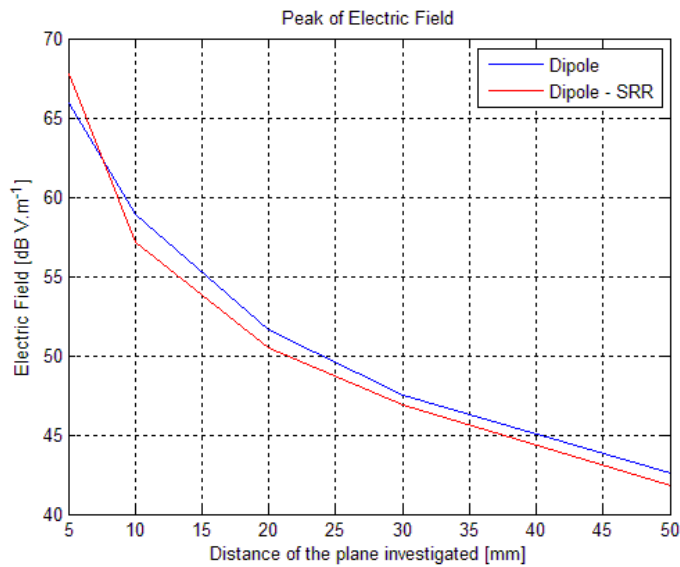


Figure 2.3 : E field peak plot on different planes

This graph shows that from 20mm away from the antenna, the SRRs reduce the peak of electric field by approximately 1dB V.m⁻¹, and 2dB V.m⁻¹ between 7 and 20mm. For distances lower than 7mm, the peak E field is increased. In term of ratios, the decrease observed at 10mm distance represents 3.3% whereas the decrease observed at 50mm represents 2.3% of the total field. The impact is getting lower while increasing the distance after the 7mm plane.

b. Magnetic field

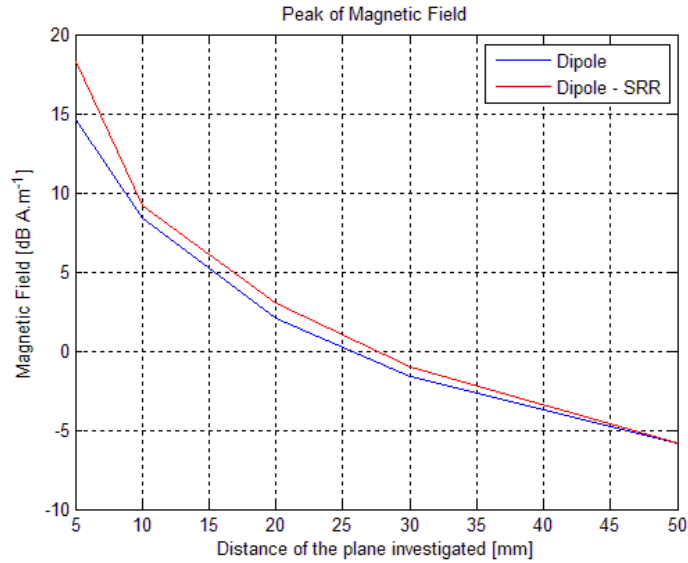


Figure 2.4 : H field peak plot on different planes

The peak of magnetic field is increased in the dipole with metamaterials configuration by less than 1dB $A.m^{-1}$ for distances between 10 and 30mm, and is almost equivalent to the case without metamaterials for distances between 30 and 50mm. In the first plane of 5mm, the difference is 3.5dB $A.m^{-1}$.

2.1.2. Conclusion

The effect of the metamaterial layer varies according to the distance where the fields are extracted. For distances lower than 7mm, the peaks of electric and magnetic fields are higher in the case with metamaterials are reduced for higher distances only in the case of the electric field.

2.2. Dipole with a Cube of tissue and metamaterials

In this part, a cube of tissue is included in the models to study the effect of metamaterials on the antenna parameters when an absorbing element such as a human head is interfering. The first paragraph describes the configuration studied, then the SAR, the S11 parameter, the total absorption, the bandwidth, the gain and the fields are investigated.

2.2.1. Configuration

Before trying to analyze the impact of the metamaterial, the behavior of a dipole with a cube of tissue has to be studied. The influence of a cube of tissue on a dipole antenna depending on the distance between them will be explained.

- The distance x between the dipole and the layer of metamaterials has been set to 4mm as it is the maximum acceptable value to be realistic and does not change the resonant frequency of the antenna too much.
- The distance d is varying from 5mm to 29mm.
- The cube stands for a cube of tissue. Its relative permittivity is equal to 49.4 which has been demonstrated to be the value of human brain used in [20]; the relative permeability is set to 1, and its conductivity to 1.53. The cube is 60x60x60mm.

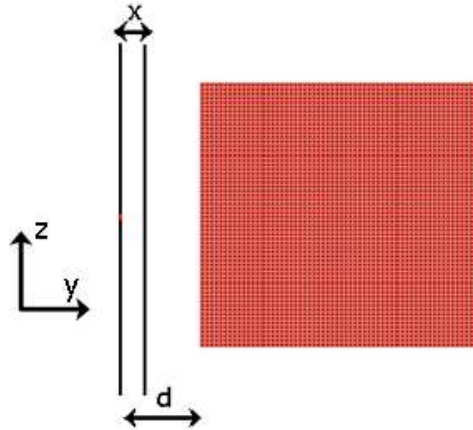


Figure 2.5 : Dipole with SRR and cube configuration

Then the influence of a layer of SRRs between the cube and the antenna is investigated for the same distances.

Different parameters will be investigated, such as the peak of SAR and average for SAR 1g and 10g for the dipole and cube configuration, then the radiation efficiency, the bandwidth, the gain, the mismatch loss for both configurations. Finally, the electric and magnetic fields are extracted from the first part of the cube in order to be compared.

The following figure shows the part of the cube where the fields are studied (in blue). This studied part has a size of 60*30*60mm and has been chosen because the highest values of the electric and magnetic fields peaks are in it, and that most waves are absorbed there. The section of the cube that has been selected to be studied is the most relevant one as the impact on the near field in the purpose of our study and the peaks will be in the first half.

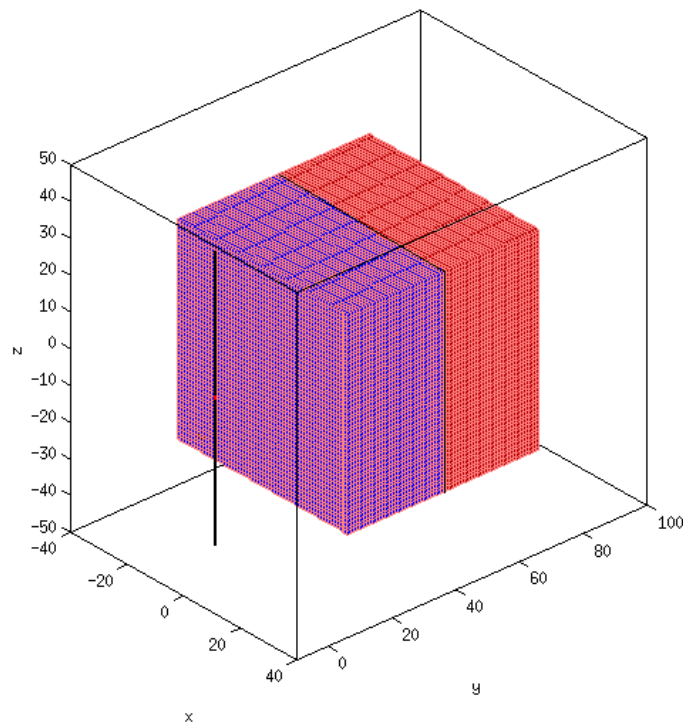


Figure 2.6 : Investigation of E and H fields in the purple array

2.2.2. S11 parameter

The following plot represents the S11 parameters for different distances between the cube and the dipole. The Figure 2.7 only shows the results for the dipole and the cube and the dipole alone as a reference (depicted as a dashed curve).

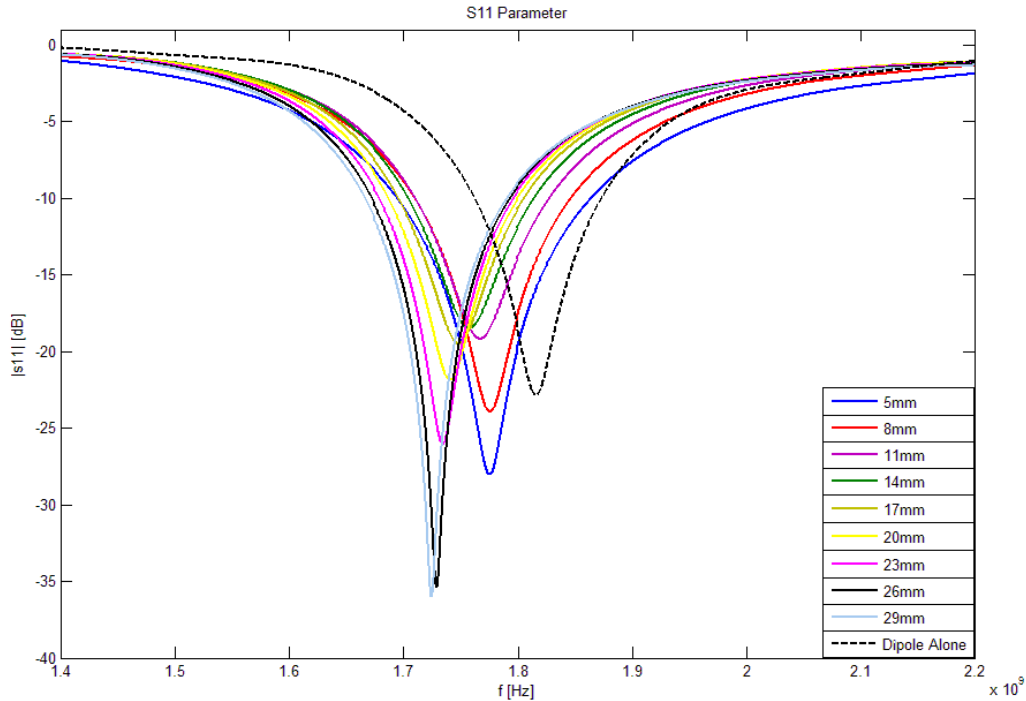


Figure 2.7 : S11 parameters for dipole and cube configuration at different distances

It can be observed that the presence of an absorbing element close to the antenna has an impact on the resonant frequency. In fact, the resonant frequency is shifted to lower values, with a minimum shift of 20MHz between the lowest distance investigated (5mm) and the dipole alone. The maximum shift is about 90MHz between the highest distance investigated (29mm) and the dipole alone. For this worst case that is the distance of 29mm, the return loss is equal to 5dB at 1.88GHz, which is equal to a mismatch loss of 1.65dB. According to the distances studied, the further away the absorbing element is from the antenna, the higher the shift is.

Nevertheless, for all the distances between 11mm and 5mm, the return loss is always lower than -6dB, which is the threshold to calculate the bandwidth. All the other distances from 14mm to 29mm have a return loss between, -5dB and -6dB. In other words, the return loss has unacceptable values in terms of bandwidth coverage for GSM 1800 standards when the resonant frequency is shifted too much. As a comparison, the return loss of the dipole alone is around -10dB, which is 0.46dB of mismatch loss.

In the following Figure 2.8, the dipole with SRR and cube configuration is depicted in terms of S11 parameter for different distances between the antenna and the cube.

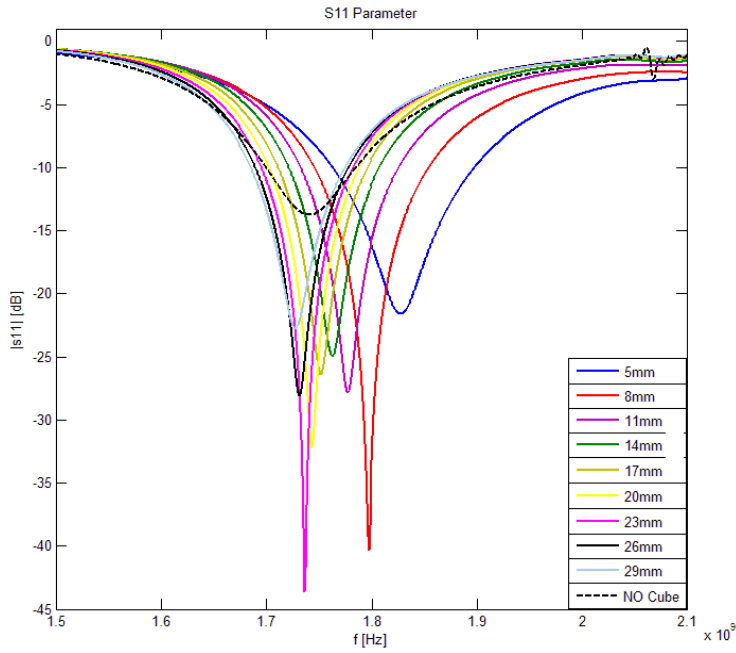


Figure 2.8 : S11 parameters for dipole with SRR (at 4mm) and cube configuration at different distances

The dipole with SRRs layer has a shift in frequencies around 65MHz compared to the dipole alone, and its return loss is around -5dB which corresponds to a mismatch loss of 1.65dB. The covered bandwidth does not fit the GSM 1800 standards anymore. In the case of the cube included at 5mm with SRRs, the resonant frequency is shifted by +50MHz in comparison with the case without SRRs. When the cube is included at high distances (29mm) from the antenna, there is no shift in frequencies between with and without SRRs.

The shift between the distance 29mm and the case without cube is -20MHz. In the case of dipole with a SRRs layer, the closer the absorbing element is from the antenna, the higher the shift is.

2.2.3. Total absorption

Here is the plot comparing the absorption loss according to the distance between the dipole and the cube in the cases of a dipole alone or with metamaterials.

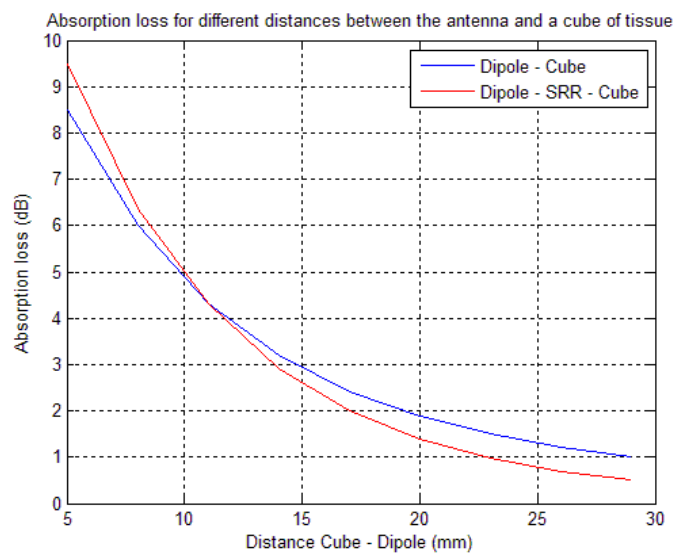


Figure 2.9 : Absorption loss depending on the distance (dipole-cube)

At 5mm distance, the dipole with SRR and cube configuration has an absorption loss 1dB higher than the case without SRR. This difference tends to reduce while increasing the distance until the distance 12mm

where the curves cross. The difference is then increasing the other way around, and the case with SRR is providing a gain up to 0.5dB less at 29mm distance. The same kind of results as in free space is noticeable, meaning that the case with SRR starts to provide a reduction of the fields located at a certain distance from the antenna.

2.2.4. Bandwidth

This plot shows the variation of bandwidth for the dipole when the cube is shifted, with and without SRRs. To compare the bandwidth of the dipole alone and dipole with a layer of SRRs in free-space are shown. The bandwidth has been calculated with the threshold of -6dB.

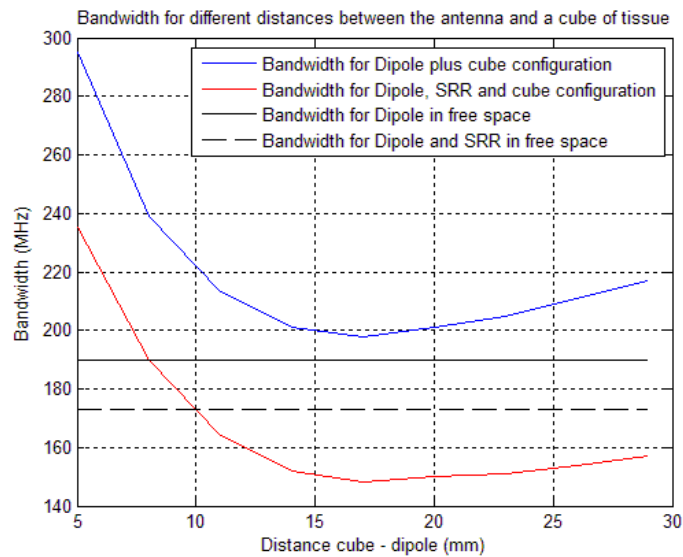


Figure 2.10 : Variation of effective bandwidth depending on the distance {dipole-cube}

What can be observed in this graph is that adding a cube of tissue near the dipole is increasing the bandwidth of the antenna, which is higher than in the free-space case. Adding a layer of SRRs close to the antenna decreases this bandwidth to reach a value lower than the free-space case. The only exception is the case where the cube is really close to the antenna (less than 8mm), where the bandwidth is higher than the one of the dipole in free space. At 5mm, it is increased from 190MHz to 238MHz. The bandwidth of the case with SRR and cube configuration still reaches the bandwidth requirement of the GSM 1800 (can be found in the Table 1.1 of the Appendix) for distances below than 10mm.

2.2.5. Gain

Radiation patterns are not such relevant parameters for small antennas because the orientation between the handset and the base station is unpredictable. That is why a gain in directivity is for example not aimed in such studies. Anyways, the Figure 2.11 shows the different patterns of a dipole alone, and a dipole with a cube a different distances. It can be observed that no much improvement is appreciable.

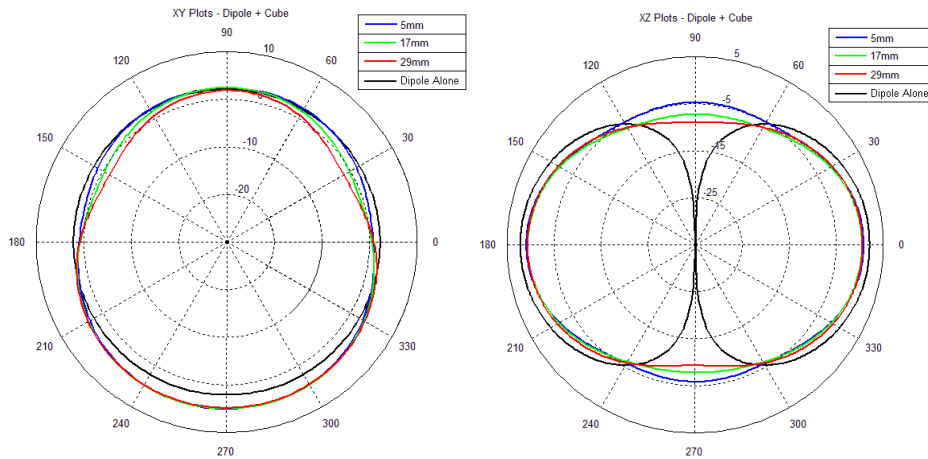


Figure 2.11 : Radiation patterns of dipole and cube for three distances (dB)

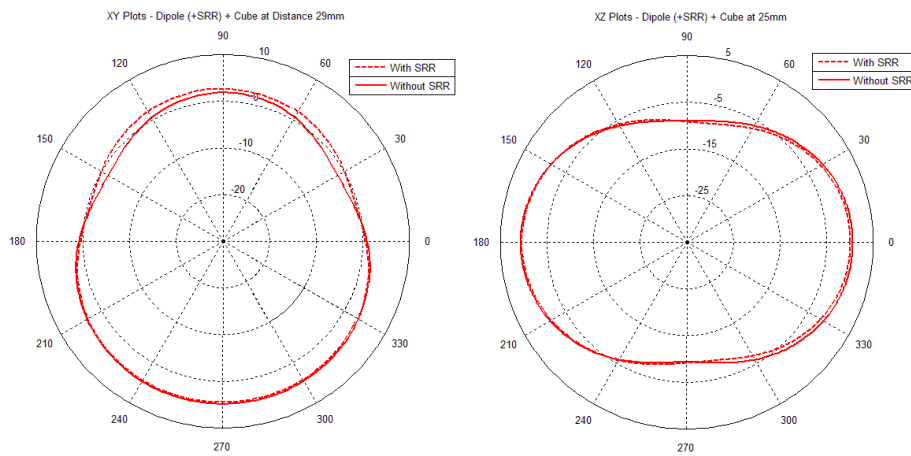


Figure 2.12 : Radiation patterns for high distance with and without SRR (dB)

In the Figure 2.12 the difference of the patterns with and without SRR at 29mm distance can be observed. First of all, the other curves plotted for other distance have not been presented here because they do not add any specific information. Secondly, the highest difference appears in the plane 29mm and is still too small to be taken into consideration.

2.2.6. Electric and magnetic fields investigation

The Figure 2.13 represents the decrease of the peak E field in function of the distance from the antenna for both cases, with and without metamaterials. The decrease is observed inside the cube of tissue depicted in the Figure 2.6. The total decrease for both cases is around 15 dB V.m^{-1} between the planes 5 and 29mm.

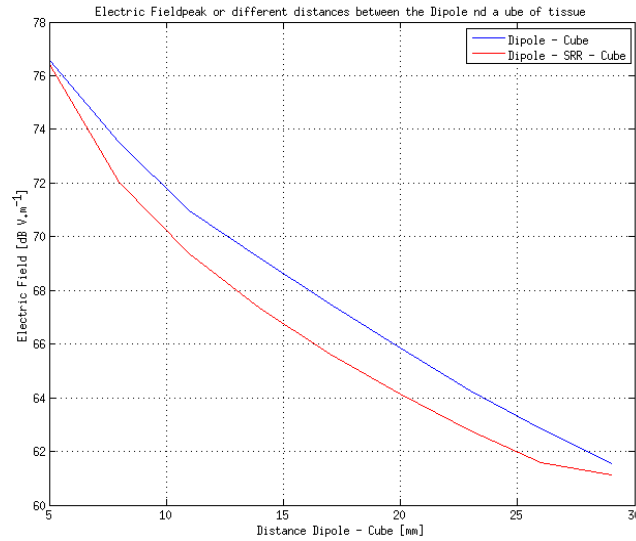


Figure 2.13 : E field peak plot on the different planes

In the Figure 2.13, both cases are quite the same with the two extreme distances taken, i.e. 5 and 29 mm. In the plane of 8mm the difference is 2 dB V.m⁻¹, and this difference remains constant until the plane 20mm. It is finally reduced to 1.7dB for 26mm and 0.5dB for 29mm. This constant decrease represents 2.7% reduction for the 8mm plane, and 3% for the 20mm plane. The impact on the peak E field is thus increasing from the distance 5 to 20mm, and then decreasing from 20 to 29mm. The Figure 2.14 is basically the same plot but for the H field peak.

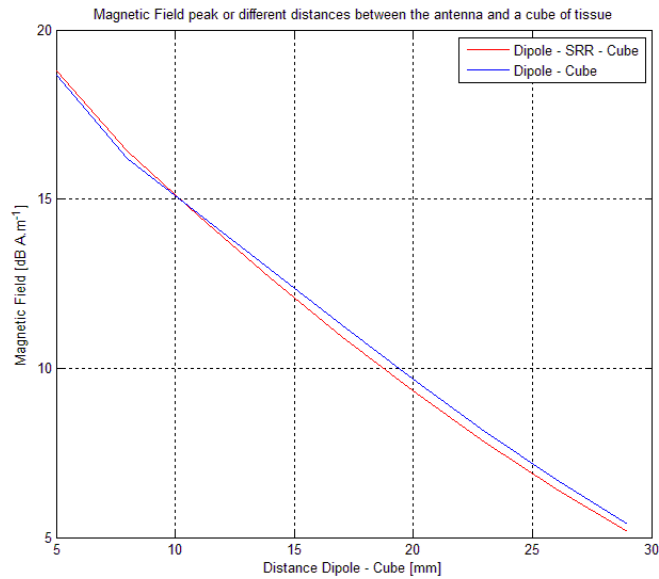


Figure 2.14 : H field peak plot on the different planes

The decrease is this time around 13 dB A.m⁻¹ from 5 to 29mm, but not real advantage or disadvantage could be appreciated. The highest difference around 0.4 dB A.m⁻¹ and could only be observed further away than 10 mm distance.

2.2.7. SAR

The following graph shows the peak of SAR calculated for a dipole with the cube configuration. It shows the influence of the distance on the SAR.

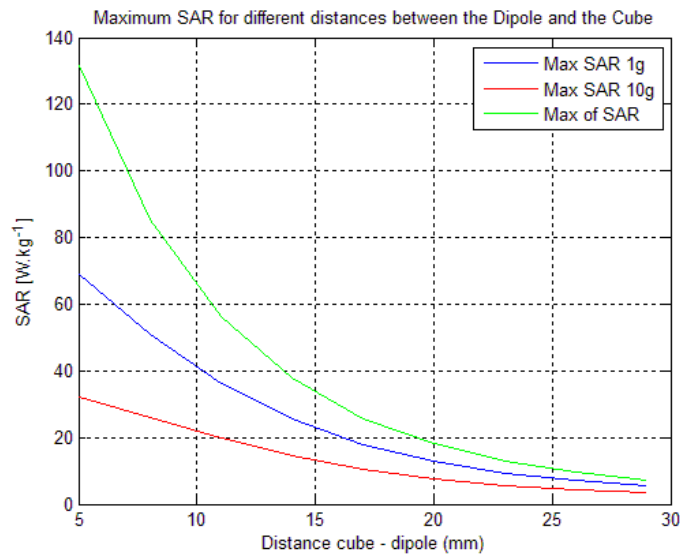


Figure 2.15 : SAR peak plot for dipole and cube configuration

This plot clearly shows the influence of the distance of a tissue on the SAR. The SAR is basically high for distances lower than 15mm and decreases fast until it reaches a lower and more stable value at 20-25mm. This decrease could easily be because the fields are reduced for higher distances in free space. A smaller SAR is thus expected for high distances compared to low ones because the more the fields are penetrating the tissues, the more they are absorbed.

Two calculations have been done to compare the peak SAR in the case with and without metamaterials for a cube 5mm far from the antenna. Here is the table with the results:

Configuration	Peak SAR	Maximum 1g
With SRRs layer	117 W.kg ⁻¹	61 W.kg ⁻¹
Without SRRs layer	131 W.kg ⁻¹	74 W.kg ⁻¹

Table 2.1 : SAR values with and without SRRs layer

These results show that for a distance of 5mm between the dipole and the cube, the SAR is reduced in the case with metamaterials. It has been shown in Figure 2.13 that the electric field can be lower in the SRRs configuration.

2.2.8. Conclusion

- Without the cube of tissue, adding SRRs to a dipole in free space shifts the frequency resonance by 50MHz lower, and reduces the return loss from -10dB to -5dB.

- Without the SRRs, adding an absorbing element close to the dipole antenna shifts the resonance frequency to lower values.

- In the case of a dipole with SRRs, adding an absorbing element close to the dipole antenna shifts the resonance frequency to higher values.

- The absorption observed in the cube is increased in the metamaterial configuration for distances between the cube and the antenna lower than 10mm compared to the case without metamaterials, and is then reduced for higher distances.

- In free space, the bandwidth is reduced from almost 20MHz in the case with SRR compared to single dipole. When the distance between the dipole and the cube is from 8mm to 20mm, the difference between the bandwidth of the dipole and cube, and dipole with SRRs and cube is constantly equal to 50MHz, and is 60MHz anywhere else. The highest reduction is equal to 28% at the highest distance (29mm), and to 20% for small distances (5mm). Anyways, for distances below 10mm between the cube and the dipole, the SRR with cube still has a higher bandwidth than the dipole in free space.

- The SRRs layer gives a reduction of the peak electric up to 3%. The magnetic field is not affected as much as the electric field and remains more or less the same with or without SRR.

3. PIFA investigations

3.1. PIFA and SRRs in free space

The objective of this part is to investigate the influence of a layer of SRR on the basic PIFA described in the last chapter. Knowing that actual manufacturers are willing to reduce more and more the size of mobile devices, the challenge was to implement a layer of SRRs on a phone without changing the overall volume.

Therefore, several positions of the layer of SRRs have been tested in order to check their influence on the antenna. The resonant frequency and the bandwidth will be study and the peak of the electric and magnetic fields extracted for a portion of the space corresponding to the position of the head. Three sets of models have been investigated in the next paragraphs.

3.1.1. PIFA ‘Bottom’

This part shows the results obtained for a PIFA where both radiating element and layer of SRRs are on the opposite side of the region investigated. The following picture shows this configuration. In blue, red and green are drawn the three planes where the electric and magnetic fields are extracted. They respectively correspond to the planes 5mm, 10mm and 15mm below the antenna, and are sized 60*50mm. In other words this configuration is standing for a mobile device where the radiating element would be on the bottom of the antenna.

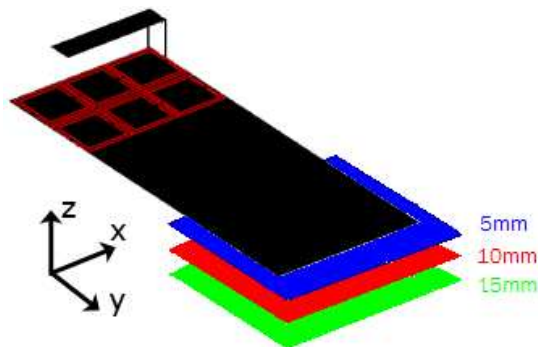


Figure 3.1 : Areas of E and H fields extraction for the PIFA ‘bottom’

Then, ten cases of SRR placement have been investigated by varying the distance C shown in the next picture from -1mm to 8mm.

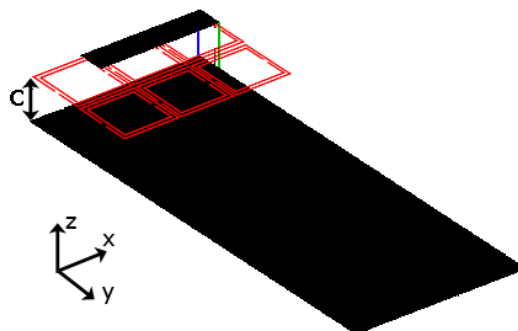


Figure 3.2 : Variation of the position of the SRR into the PIFA

In the next plots, the abscissa represents the different cases:

- Case 1 corresponds to $C=-1\text{mm}$, when the layer of SRRs is placed below the ground plane. In this specific case, the radiating element has been lower by 1mm in order to keep the same overall volume for the antenna.
- Case 2 corresponds to $C=0\text{mm}$, basically when there are no SRR (PIFA alone case).
- Case 3 corresponds to $C=1\text{mm}$,
- Case 4 to 10 correspond to the value of C from 2mm to 8mm.

It has to be precised in the case 1, the plane investigated is 1mm further from the ground plane and the fields are thus lower.

3.1.1.1. Resonant frequency

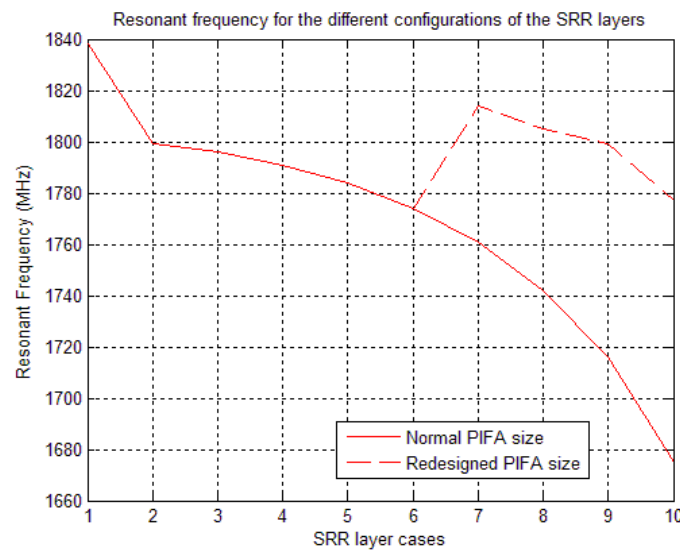


Figure 3.3 : Resonant frequencies for different PIFA models

The different positions of SRRs have an influence on the resonant frequency. The closer the SRRs are from the resonating element the bigger is the shift. In the cases 7 to 10, the antenna does not resonate around 1.8GHz anymore and the mismatch loss is dramatically increasing.

For these configurations, the antenna has been redesigned by changing the size of the radiating element in order to obtain the good resonant frequency again. The following plot shows the corrected PIFAs with the same configurations of metamaterials.

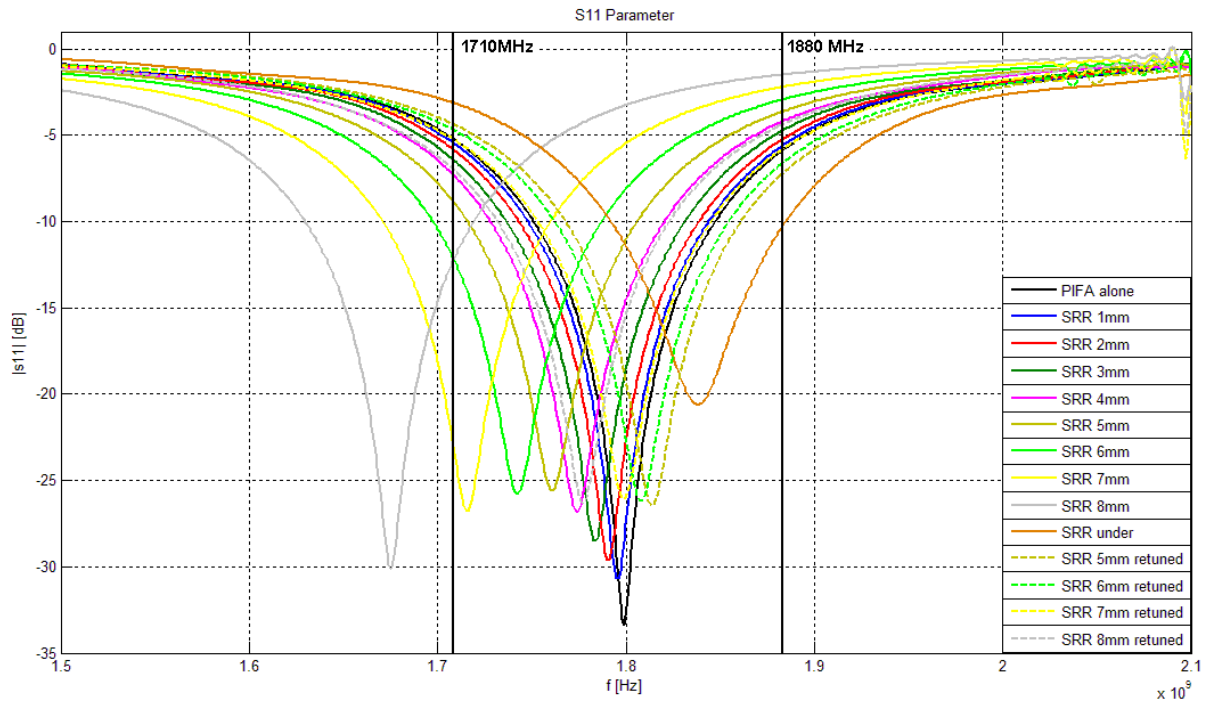


Figure 3.4 : S11 parameters for the different types of PIFA configurations investigated

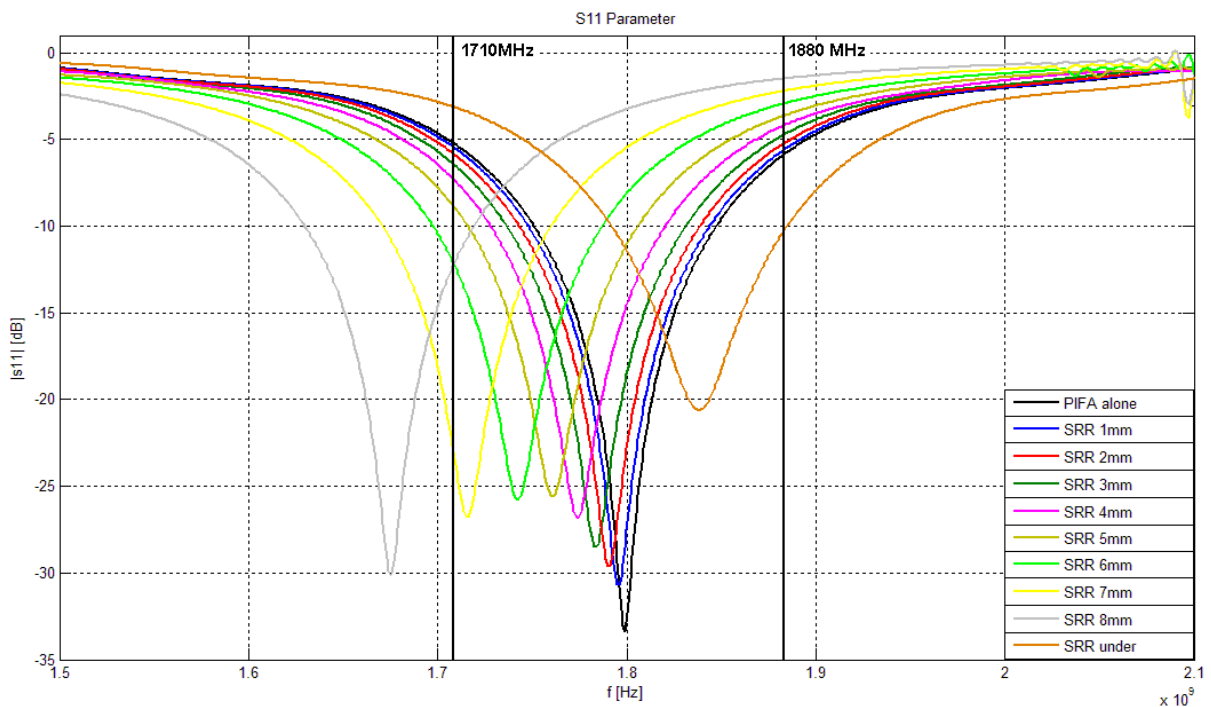


Figure 3.5 : Initial S11 parameter plots before retuning

This plot shows the shift of the resonant frequency of the antenna that occurs when adding a layer of SRR between the ground plane and the radiating element. It can be observed that the closer the layer is to the radiating element, the more the resonant frequency is shifted (by a maximum of 125MHz for the 8mm case). In this case, the return loss is equal to -3dB for 1800MHz, which corresponds to a mismatch loss of 3.02dB. The bandwidth corresponding to the GSM 1800 specifications (1710-1880MHz) is not covered anymore.

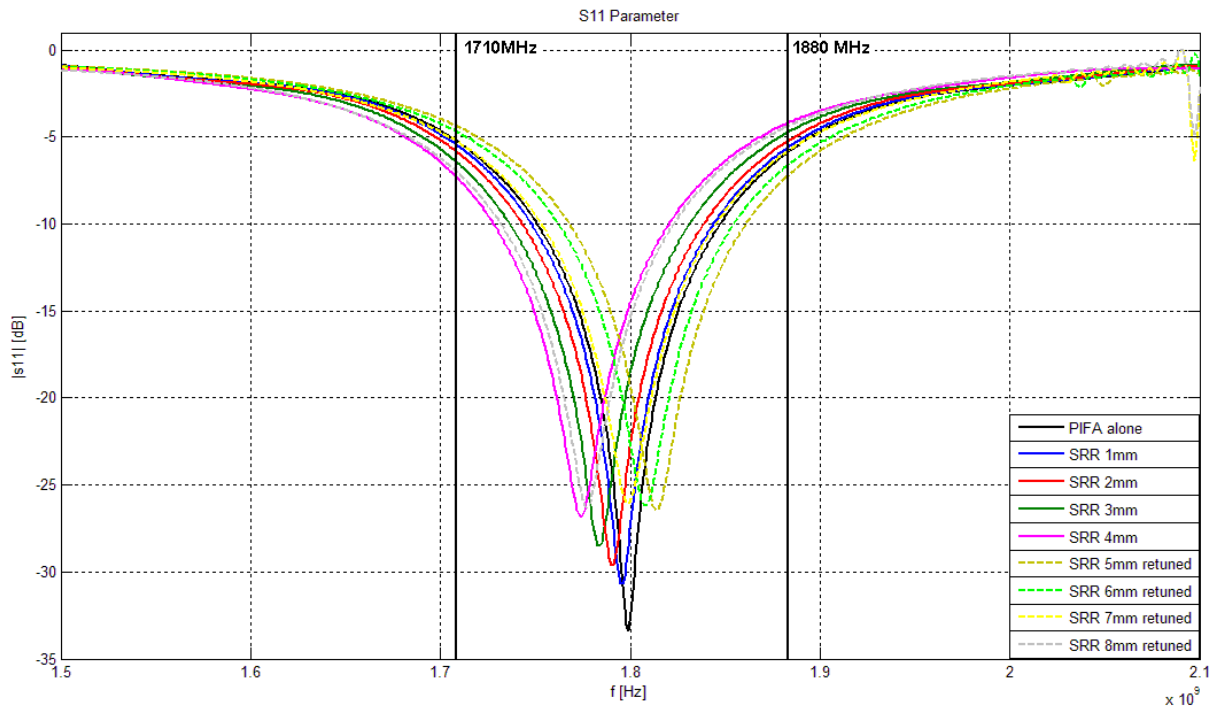


Figure 3.6 : S11 parameter plot after the retuning

These S11 parameters are obtained after retuning the antennas for the four worst cases (distance between the ground plane and the SRRs layer from 5mm to 8mm). Now, all the antennas are covering the GSM 1800 bandwidth and the maximum mismatch loss is equal to 2.55dB at 1880MHz, which is an acceptable value for a mobile phone to operate.

The Smith chart can also be plotted to study the influence of the SRRs layer on the antenna (see Figure 3.7):

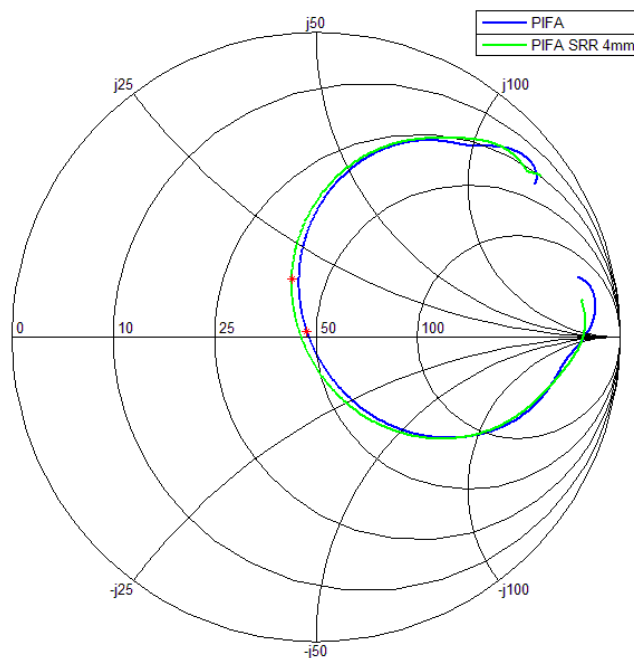


Figure 3.7 : Smith chart of the PIFA alone and with a SRRs layer at 4mm

The Figure 3.7 is a Smith chart showing both curves of the PIFA without SRR and the PIFA with the SRRs layer at 4mm. As it can be seen on the Figure 3.6 the case of 4mm is the worst matching and the most shifted case of the set because it is the case of highest distance between the ground plane and the radiating

element that has not been retuned. The red marker stands for the frequency 1.8GHz and allows comparing the two matching. The real part of the impedance at this frequency is 47.7Ω for the PIFA alone, and 40.2Ω for the other case. Knowing that it is the worst matching case, this value is still considered as acceptable.

3.1.1.2. Bandwidth

The variation of the bandwidth is too small to be plot. The table below shows this low variation with the different configurations:

Cases	Distance between the SRRs and the ground plane	Bandwidth
1	-1mm	162MHz
2	No SRRs layer	163MHz
3	1mm	163MHz
4	2mm	163MHz
5	3mm	161MHz
6	4mm	159MHz
7	5mm	158MHz
8	6mm	158MHz
9	7mm	157MHz
10	8mm	157MHz

Table 3.1 : Variation of the bandwidth for the different types of PIFA investigated

What can be pointed out is that the effective bandwidth of the PIFA is not really affected by the position of the layer of SRRs, since the maximum reduction is equal to 5MHz in the 8mm case.

3.1.1.3. Electric field investigation

The peak E field has been investigated for all the different SRRs layer configurations at 3 different distances in free space (see Figure 3.1), and plotted for both initial and retuned antennas. The set of figures below show the values of the 'bottom' PIFA.

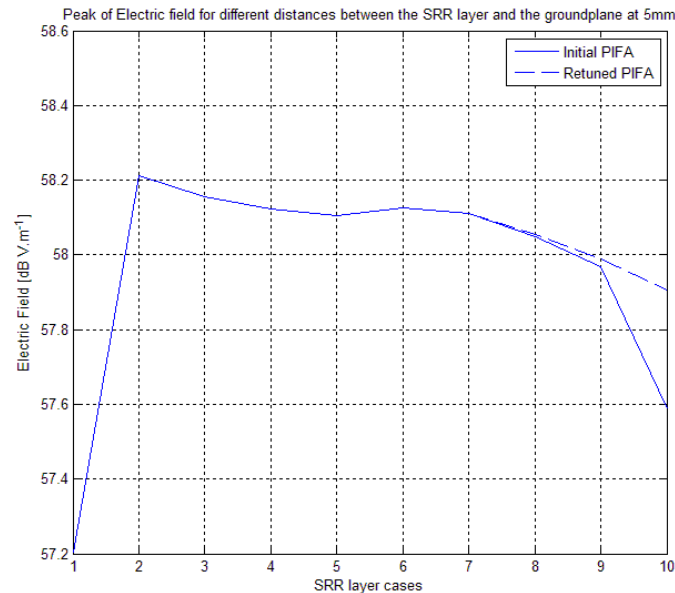


Figure 3.8 : E field peak plot depending on SRRs layer distance to the ground plane calculated at 5mm

An important decrease on the peak E field can be observed with the SRRs cases with the initial antennas but cannot leads to a straightforward conclusion as the resonant frequencies are shifted. Considering the fact that antennas resonating at 1.8GHz are compared, only retuned antennas can be trusted.

There is a decrease of 0.3 dB V.m^{-1} between the case without SRRs and the case 10 with SRRs at 8mm, whereas when the layer of SRRs is placed under the ground plane, the peak E field value is thus reduced by 1dB. This

configuration is the one showing the highest reduction of the peak E field without changing the bandwidth and the resonant frequency.

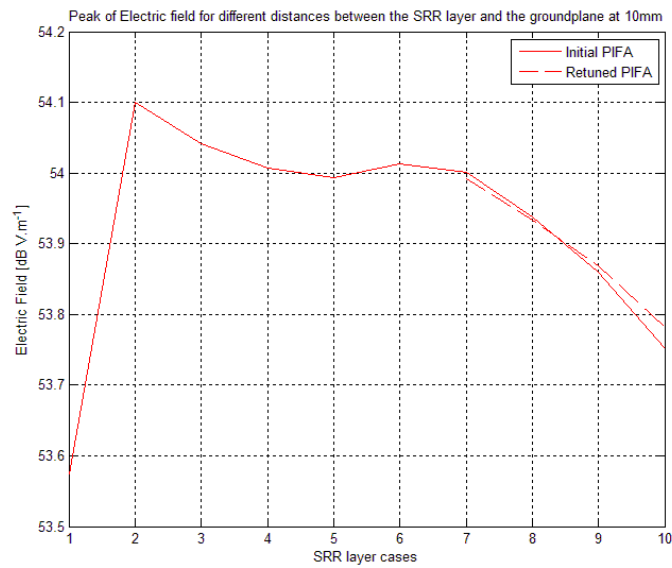


Figure 3.9 : E field peak plot depending on SRRs layer distance to the ground plane calculated at 10mm

The 10mm plane curve shows the same kind of shape, even though the retuned and initial PIFAs give almost the same reduction. The maximum decrease of the peak E field still occurs with the case 1 with a value around 0.5 dB V.m^{-1} . Nevertheless, the decrease between the case without SRRs and the case 10 is still 0.3 dB V.m^{-1} .

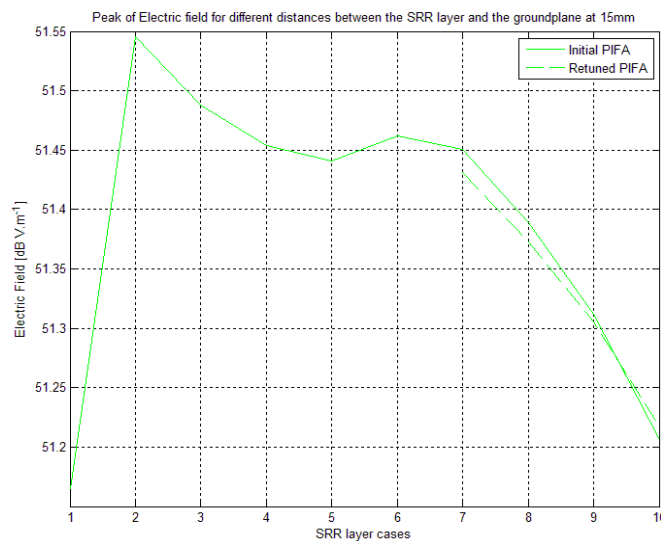


Figure 3.10 : E field peak plot depending on SRRs layer distance to the ground plane calculated at 15mm

The 15mm plane curve has also the same kind of shape, and the retuned antennas have only a slight difference in comparison to the initial ones. The peak E field is reduced almost the same with a SRRs layer under the ground plane or at 8mm, with a value around 0.4 dB V.m^{-1} .

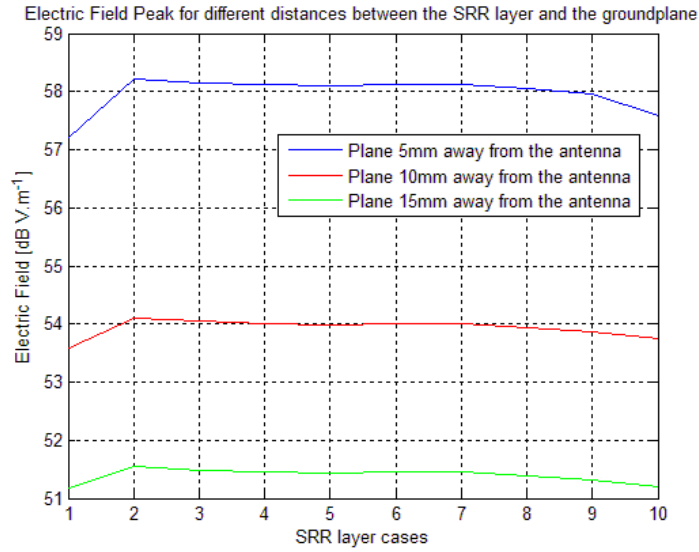


Figure 3.11 : E field peak plot depending on SRRs layer distance to the ground plane calculated in 3 planes

On the Figure 3.11, only the retuned PIFAs have been considered as the initial ones cannot all be used for a GSM standard. However, the peak of electric and magnetic fields in both cases (initial and retuned) are very similar as the variation is never more than 0.1dB.

As expected the peak E fields is reduced while increasing the distance, and the benefit obtained from the metamaterial is noticeable in terms of peak E fields even if not so big. But on the other hand it can be concluded that the further away the plane is studied from the antenna, the less the position of the SRRs layer matters just as in the 15mm case the peak E field is almost not reduced anymore.

3.1.1.4. Magnetic field investigation

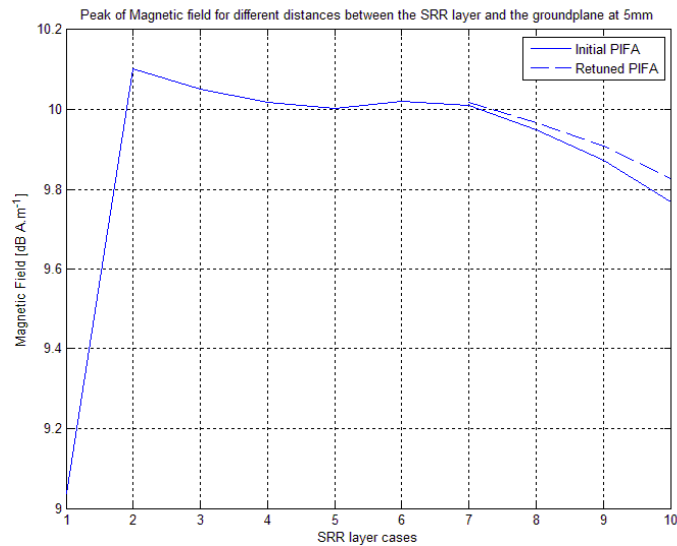


Figure 3.12 : H field peak plot depending on SRRs layer distance to the ground plane calculated at 5mm

The biggest impact on the peak magnetic field is still found with the case 1, and with a value of 1dB $A.m^{-1}$, whereas the reduction given by the case 10 is around 0.3dB $A.m^{-1}$. These decreases are the exact same ones than the ones of the peak E fields.

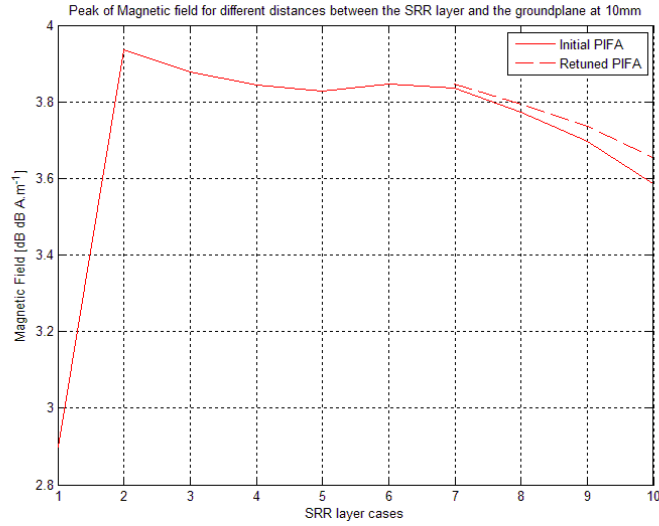


Figure 3.13 : H field peak plot depending on SRRs layer distance to the ground plane calculated at 10mm

The field is still reduced to 1dB less with the case 1, and to 0.25dB less with the case 10. The highest difference between the initial and retuned PIFAs is around 0.1dB and thus could be neglected.

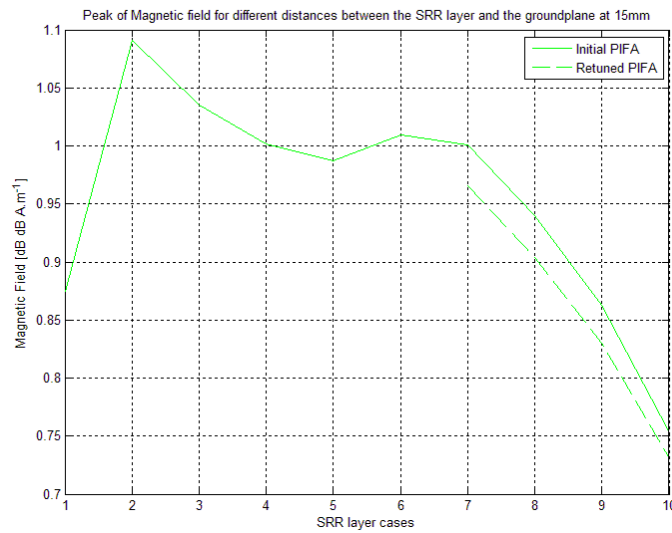


Figure 3.14 : H field peak plot depending on SRRs layer distance to the ground plane calculated at 15mm

In the 15mm plane, the peak magnetic field is reduced a lot and has a value in free space of almost 1.1 dB A.m^{-1} . The highest reduction of the field is not anymore the case 1, but this time the case 10 with almost 0.35 dB A.m^{-1} .

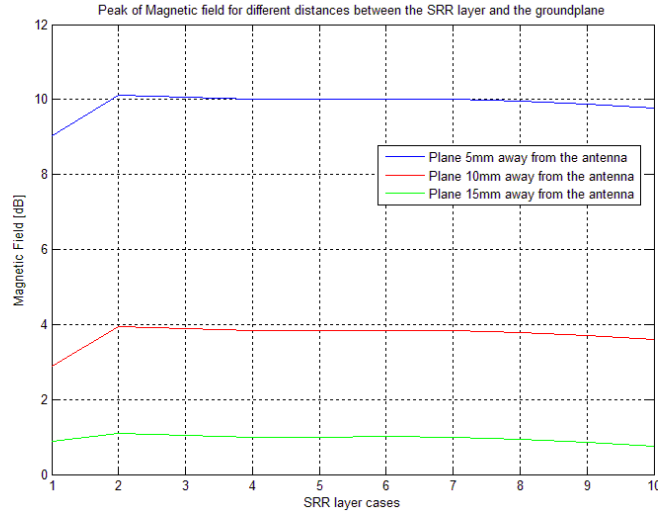


Figure 3.15 : E field peak plot depending on SRRs layer distance to the ground plane calculated in 3 planes

The effects of the SRRs layers are the same on the peak electric or magnetic field considering the shapes of the curves, and the further away the peak magnetic field is extracted from the antenna, the less the impact of the SRRs is.

3.1.2. PIFA ‘Top’

In this PIFA configuration both radiating element and layer of SRRs are on the same side, just above the planes that are investigated. This PIFA is called ‘Top’ because it stands for a mobile device where the radiating element would be on the top part of the handset. This configuration corresponds to the case where the user brain is on the same axis as the radiating element of the antenna. Of course this model does not take into account a fully realistic configuration, but the difference between both PIFA ‘top’ and ‘bottom’ allows to compare the absorption of a tissue right under the radiating element and farther.

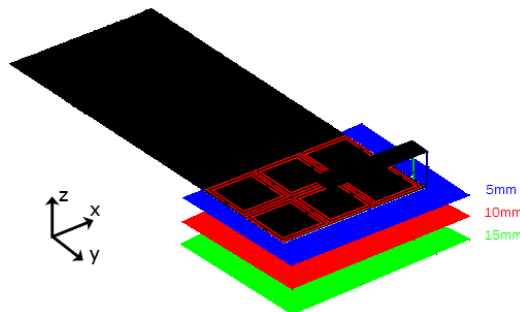


Figure 3.16 : Areas of E and H fields extraction for the PIFA ‘top’

The different SRR configurations are the same as for the PIFA ‘bottom’ and thus will not be explained again.

3.1.2.1. Resonant frequency and bandwidth

As this PIFA is only an inverted version compared to the PIFA ‘bottom’, the resonant frequencies and bandwidths for the different SRR cases are equivalent in free space. The same PIFAs have been retuned to resonate at the right frequency (cases 7 to 10).

3.1.2.2. Electric field investigation

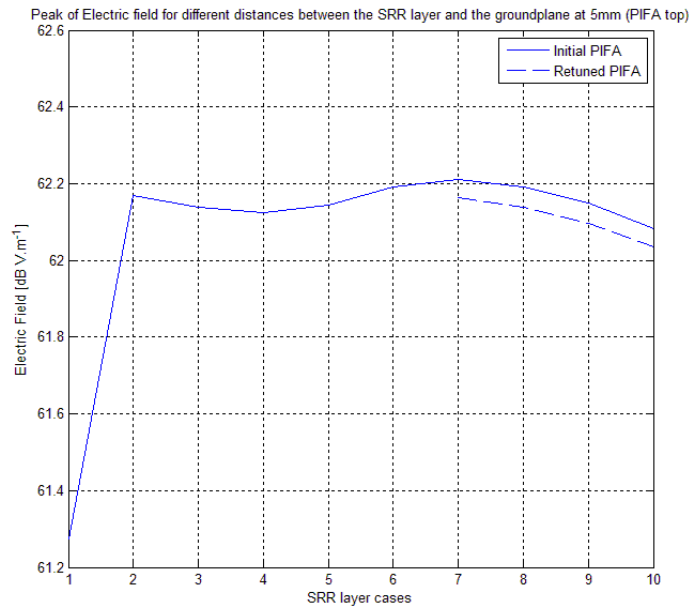


Figure 3.17 : E field peak plot depending on SRRs layer distance to the ground plane calculated at 5mm

In the 5mm plane, the peak E field in free space has a value of almost 62.2dB V.m^{-1} , whereas in the ‘bottom’ case this value is around 58.2dB A.m^{-1} . This first comparison is quite understandable as the plane is to a closer distance from the radiating element than in the ‘bottom’ case (see the Figure 3.1 and Figure 3.16). This highest reduction observed appears in the case 1 with a value of 0.9dB, whereas the difference between the case 2 and 10 is around 0.1dB.

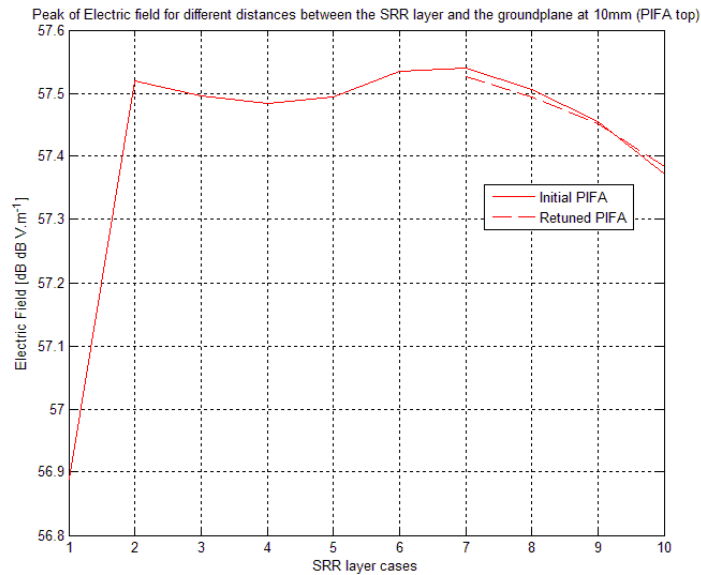


Figure 3.18 : E field peak plot depending on SRRs layer distance to the ground plane calculated at 10mm

In the 10mm plane, the difference between the highest reduction (case 1) and the case 2 is around 0.6dB, and is around 0.15dB between the case 2 and 10.

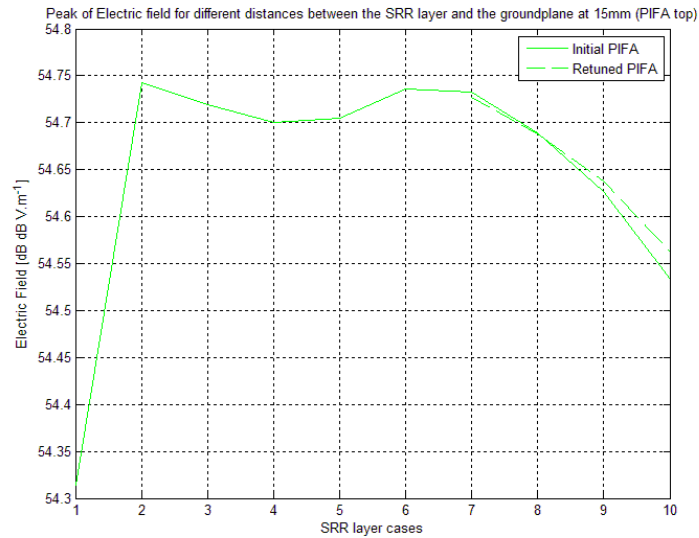


Figure 3.19 : E field peak plot depending on SRRs layer distance to the ground plane calculated at 15mm

The highest decrease of the peak E field is 0.45dB between the case 1 and 2 in the 15mm plane. The difference between the case 2 and 10 is rather increased to 0.2dB.

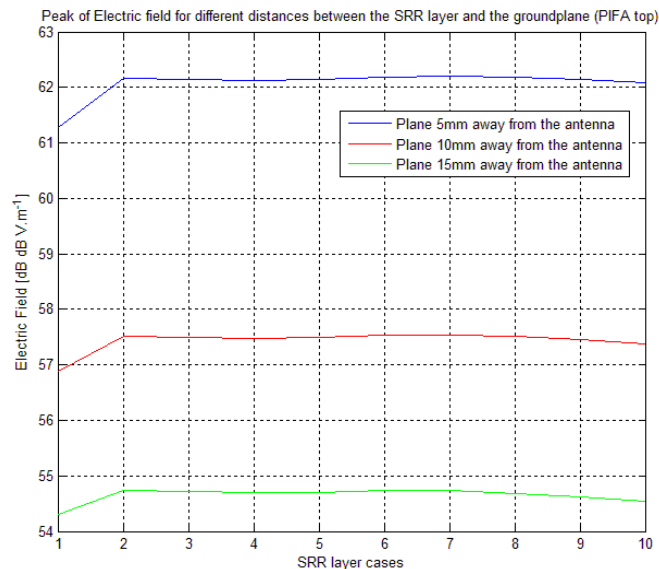


Figure 3.20 : E field peak plot depending on SRRs layer distance to the ground plane calculated in 3 planes

The Figure 3.2 exhibits the behaviors of the peak E field in all the cases for the 3 planes. It can be seen that increasing the distance has the same effect in free space on both 'bottom' and 'top' cases, but slightly different for the cases from 3 to 10. In these cases, the peak E field reduction gets bigger and bigger while increasing the distance, whereas the 'bottom' was exhibiting curves more and more flat.

3.1.2.3. Magnetic field investigation

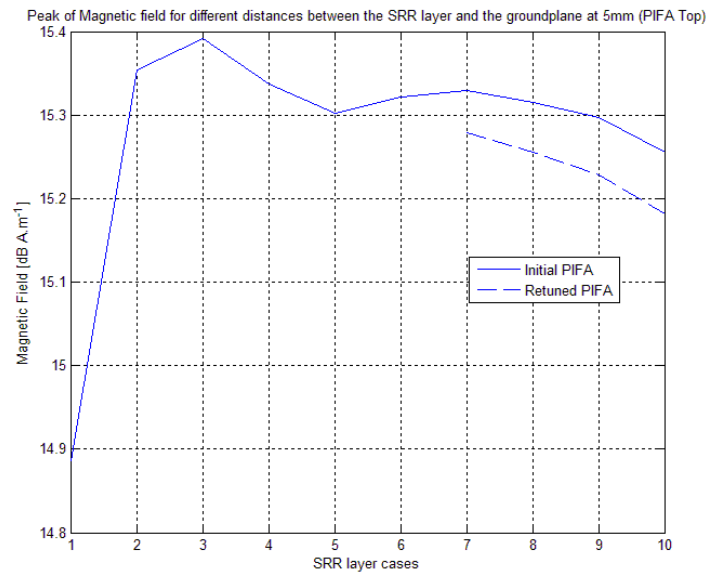


Figure 3.21 : H field peak plot depending on SRRs layer distance to the ground plane calculated at 5mm

The highest difference in term of peak magnetic field is given by the case 1 with a reduction of 0.45dB, while it is only about 0.16dB with the case 10.

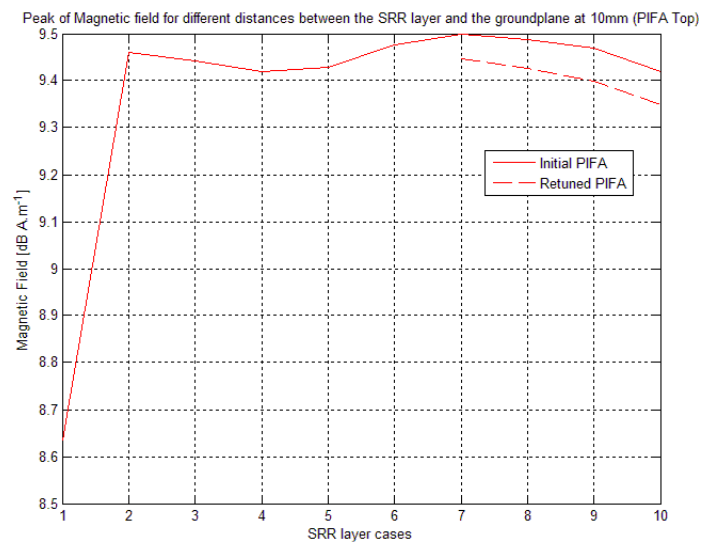


Figure 3.22 : H field peak plot depending on SRRs layer distance to the ground plane calculated at 10mm

The highest difference value is about 0.85dB between the cases 2 and 1, whereas it is only about 0.1dB between the case 2 and 10.

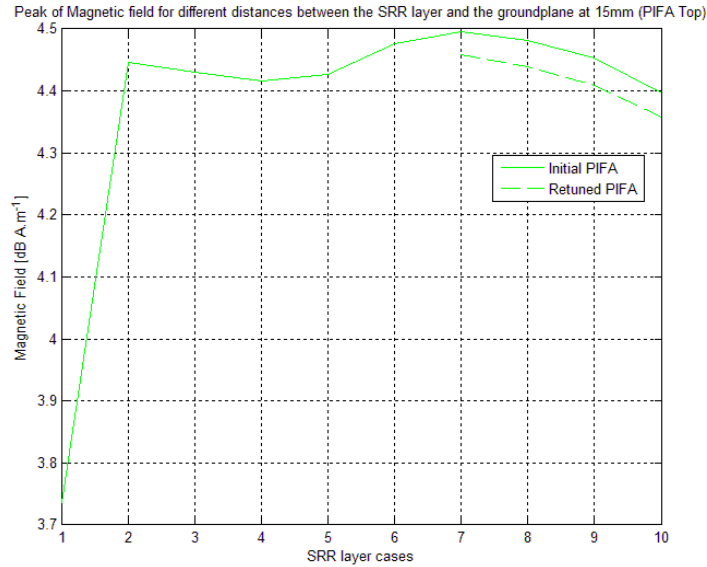


Figure 3.23 : H field peak plot depending on SRRs layer distance to the ground plane calculated at 15mm

The same kind of behavior is still observed, and the highest difference value is still found between the cases 2 and 1 with approximately 0.7dB and 0.1dB between the cases 2 and 10.

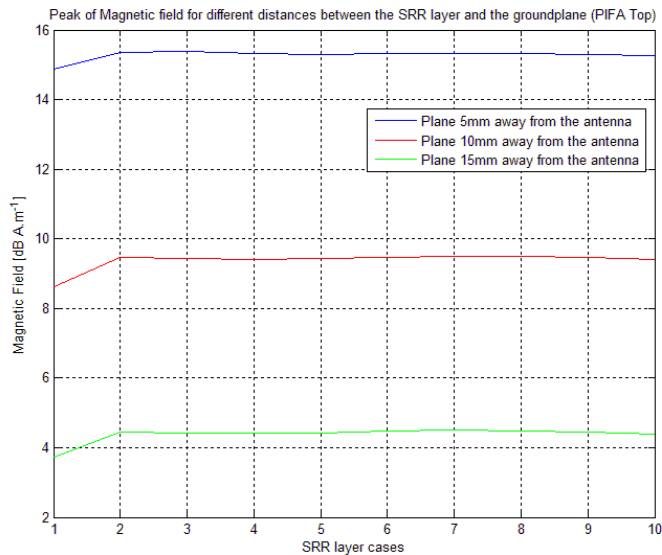


Figure 3.24 : H field peak plot depending on SRRs layer distance to the ground plane calculated in 3 planes

In the ‘bottom’ case, the peak magnetic field is reduced by 9dB $A.m^{-1}$ from the plane 5mm to 15mm, whereas in the ‘top’ case this value is around 11dB $A.m^{-1}$. The second noticeable difference is that case 10 is not reducing more the field on increasing the distance.

3.1.3. PIFA ‘Crossed’

This paragraph investigates the case where SRRs are not on the same side as the radiating element. The studied area is now only below this layer of SRRs. The distance C and the cases are still the same as in the previous PIFA configurations. As the results obtained show an equivalent reduction compared to the ‘bottom’ PIFA but worse results for cases 8 to 10, they are not described in details.

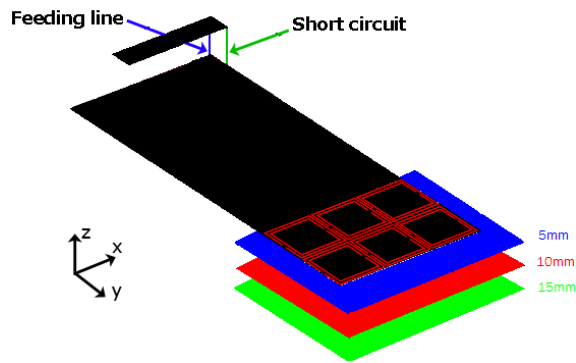


Figure 3.25 : Areas of E and H fields extraction for the PIFA ‘crossed’

3.1.3.1. Resonant frequency and bandwidth

In this model, the metamaterials only have a low influence on the resonant frequency of the antenna. The bandwidth is thus 162MHz, and the resonant frequency is equal to 1799MHz in all cases.

3.1.3.2. Electric field investigation

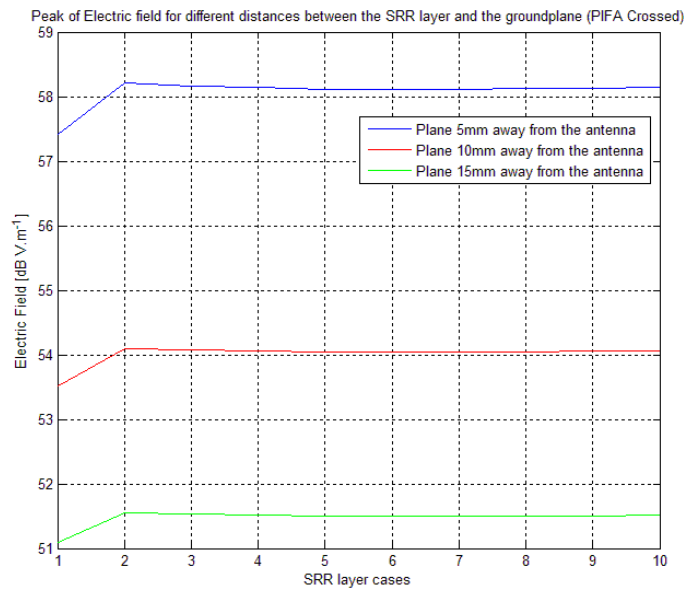


Figure 3.26 : E field peak plot depending on SRRs layer distance to the ground plane calculated in 3 planes

According to this figure, it appears that the changes brought by moving the SRRs layer within the PIFA modifies slightly the fields (case 2 to 10) while it is more remarkable with the SRRs layer under the ground plane.

As expected, the calculations at different distances from the antenna give lower electric fields as the distance increases.

3.1.3.3. Magnetic field investigation

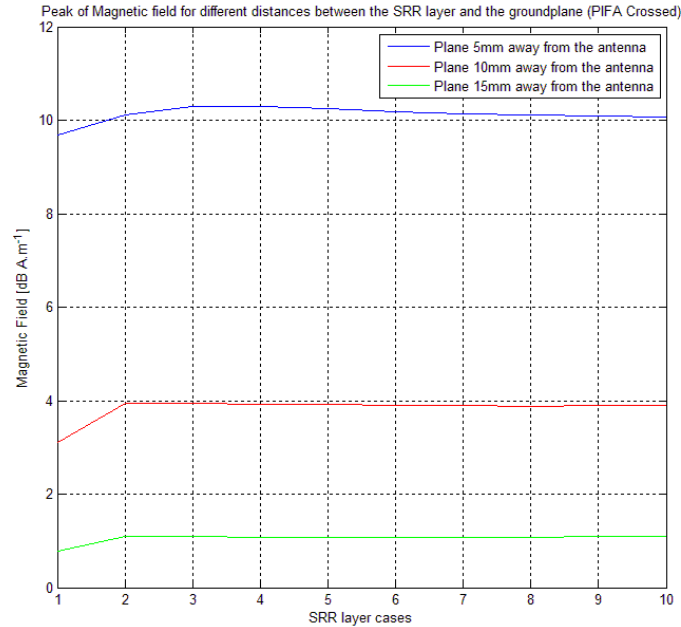


Figure 3.27 : H field peak plot depending on SRRs layer distance to the ground plane calculated in 3 planes

At small distances from the ground plane, the magnetic field seems to be enhanced for some of the configurations of the SRR cases. For higher distances, this field decreases slightly but this drop could not be considered as a relevant effect due to the SRRs layer.

As expected, the calculations at different distances from the antenna give lower magnetic fields as the distance increases.

3.1.4. Comparison between PIFAs

The Figure 3.28 regroups the peaks of the electric fields for the three different configurations of antennas with on the 3 different planes. The PIFA 'top' is the one showing the highest peak, as the radiating element is right above the investigated area. The two other PIFAs show close results, but in the cases 9 and 10 the field is reduced in the case of the PIFA 'bottom' by 0.5dB compared to the PIFA 'crossed'.

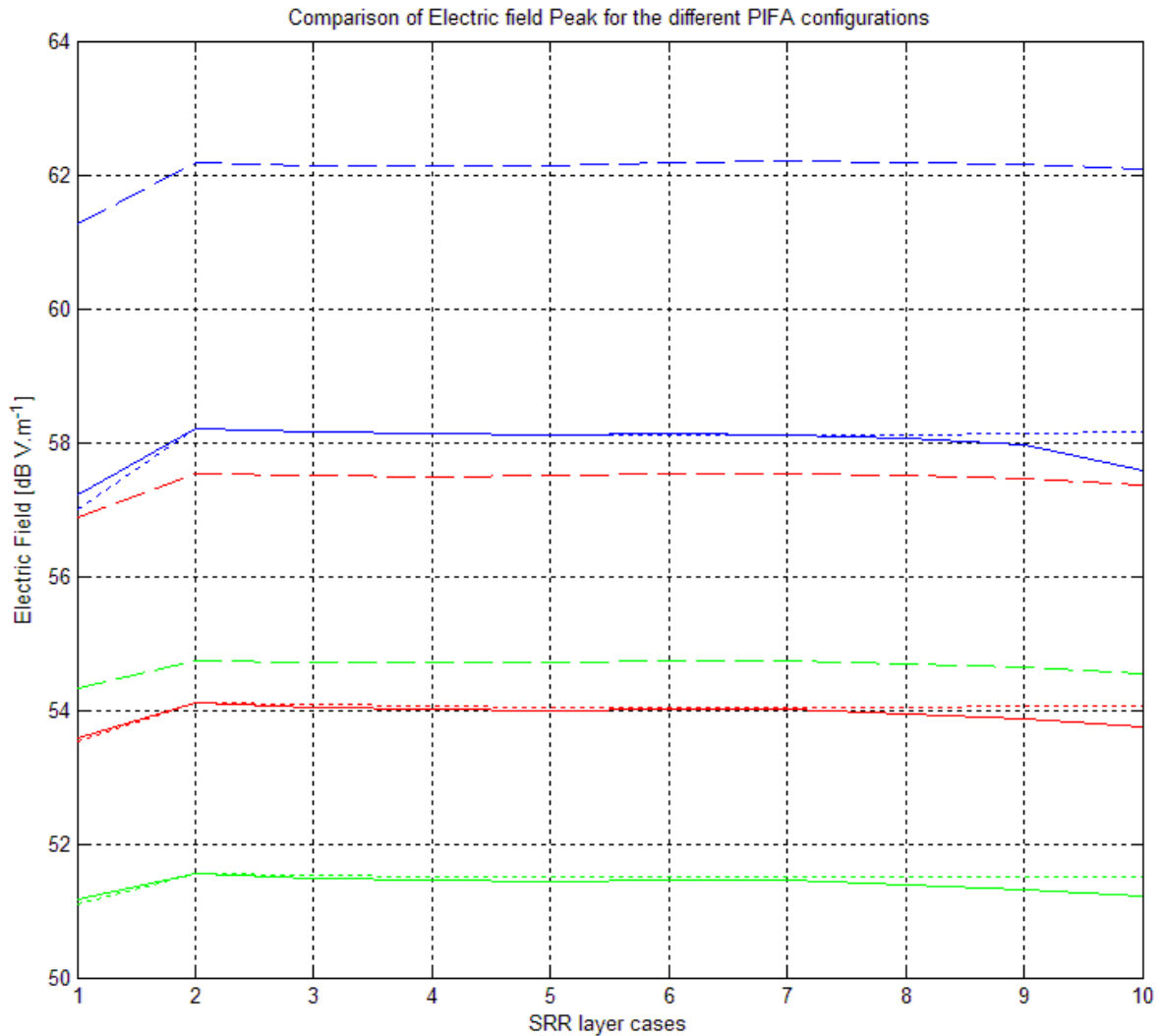
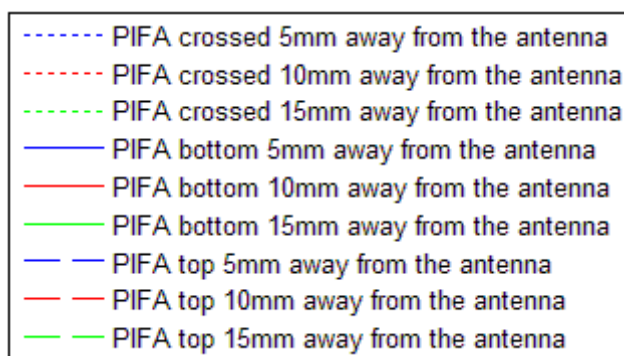


Figure 3.28 E fields of the 3 configurations and 3 distances



The case 1 cannot really be compared to the others as the field is calculated farther from the ground plane in this case. However, as the radiating element has been moved in this case to keep the same overall volume for the device, it can be considered at the best case to reduce the peak of the electric field. The reduction is around 1dB for the closest plane (5mm from the antenna) and 0.7dB for the plane 15mm from the antenna.

The third PIFA case shows that the influence of the SRRs layer on the reduction of the peak E field is reduced for the cases 6 to 8, contrarily to the PIFAs 'top' and 'bottom' where those cases were the most efficient.

3.1.5. Additional layers of SRRs

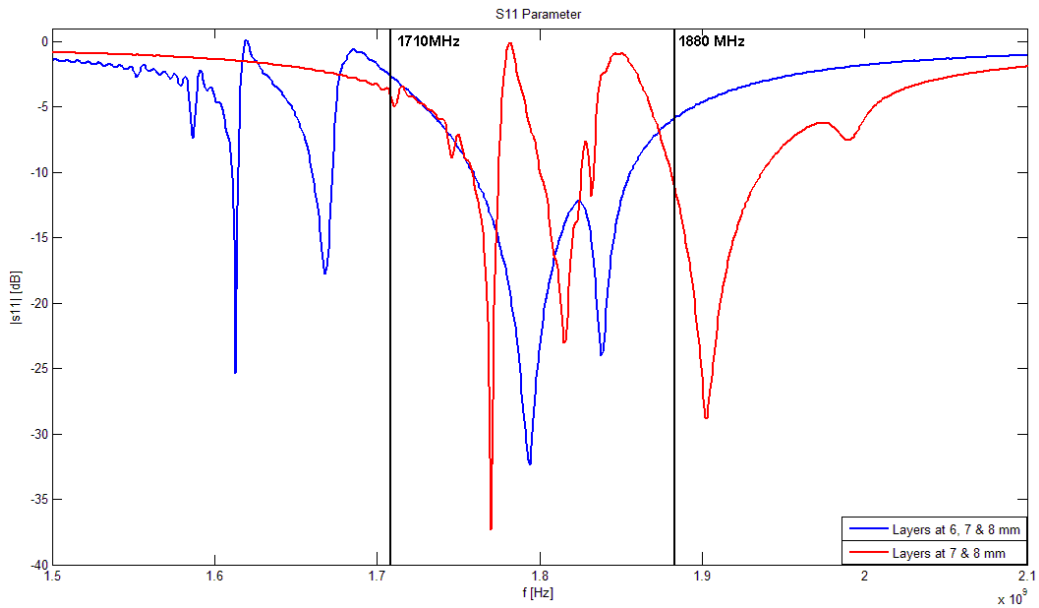


Figure 3.29 : S11 parameter for 2 and 3 layers of SRRs

The Figure 3.29 has been extracted from two different configurations. In the first one, both 9 and 10 cases have been added at the same time, it is to say two layers of SRR at 7 and 8mm away from the ground plane. The second case that is in blue is the same than the first one with another layer added at 6 mm.

It can be observed that unlike the case of 1 layer where the S11 exhibits only one resonant peak, these two are way more complicated to use for different reasons. First of all there is not only one clear resonant frequency of the antenna but several ones.

For the case of two layers, the peak is shifted to 1.77GHz and very narrowband. This result could be interpreted as a multiband antenna but the different peaks are also too close from each other to be exploited.

For the case of three layers, the main resonant peak is still at 1.8GHz and one more peak can be observed. The same conclusions can be extracted than from the other case since the peaks are too narrow and too close to be considered as a usable multiband antenna.

The next plot shows the peak E field calculation in the different planes 5mm, 10mm and 15mm away from the antenna for the 2 and 3 layers configuration.

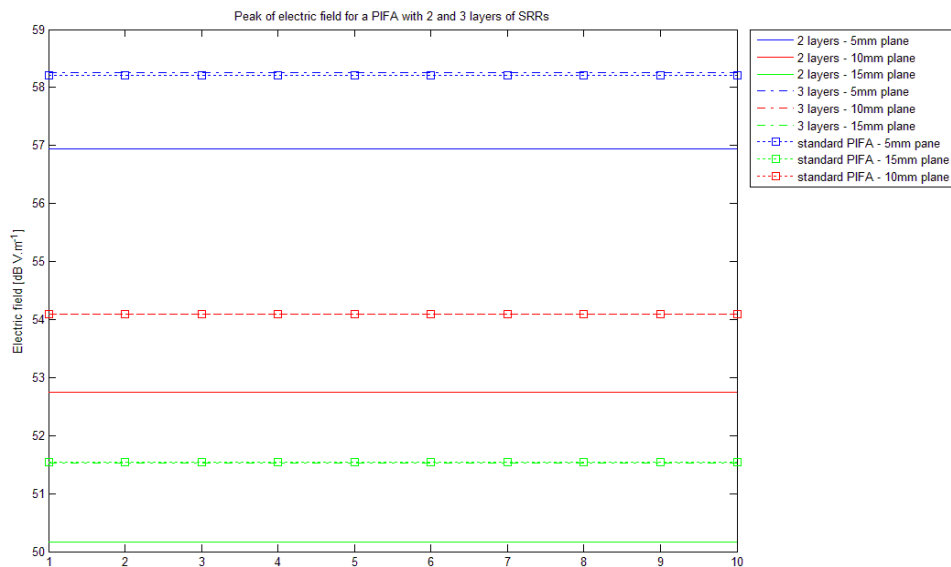


Figure 3.30 : Peak of electric field for a PIFA with 2 and 3 layers

The 2 layers case is obviously reducing the peak E field by approximately 1.3dB in all planes, whereas the 3 layers configuration does not show any improvement compared to the normal PIFA. Beyond these results, it can be observed that the narrowest bandwidth is observed for the 2 layers case, and it seems that the behavior of the antenna cannot be predicted when adding more layers. In fact, the highest reduction occurs with the worst S11 case.

3.1.6. Conclusion

- The position of the layer in the PIFA has an effect on the resonant frequency of the antenna. The closer the layer is from the radiating element, the lower the resonant frequency is.

- In the 3 PIFA configurations and all positions of the SRRs layers, the bandwidth is still very close to the original PIFA bandwidth which is a positive point.

- The closer the SRRs layer is from the radiating element, the bigger is the influence on the peak electric field. The influence is more important for the 'bottom' antenna configuration than for the 'top' antenna configuration. Like in the dipole case, the peak electric field reduction provided by the SRRs layer is bigger for high distances between this layer and the cube of tissue. That is why the SRRs show a higher reduction of the peak electric field in a 'bottom' antenna. However, the cube studied is too small to stand for a realistical case, as a human head would cover the whole surface of the handset, and the difference between the PIFA configurations would be reduced.

- The case 1 offers interesting results as it shows the best peak E field reduction for all configurations of PIFA, without reducing the operating bandwidth.

- All these results show nevertheless relatively small reduction compared to the field values. It can be considered that reducing the field by 1dB is not really effective over nearly 70dB (which is a reduction of approximately 2%). As this reduction is obtained without reducing the bandwidth, it is still an interesting improvement as it could probably be increased when altering other parameters, and keeping a good trade-off between these modifications. Concerning multiple layers simulations, it is difficult to foresee what would come out of such structures in terms of frequency. With more than one layer placed between the ground plane and the resonating element, the SRRs are excited by the fields and the different couplings occurring between the layers and the antenna influence the resonance, and this configuration needs further investigations for example by modifying the distances between the layers. The case with 2 layers of SRRs shows a reduction of 1.3dB where the case with 3 layers does not show any improvement. It has been shown that these two cases highly modify the antenna S11 parameter and it seems that this modification is not predictable. However, the 2 layers case shows the best peak E field reduction, and the distance between these SRRs layers could for example be investigated deeper.

3.2. PIFA with SRR and Cube

3.2.1. Configuration

This section investigates the peak of electric field in a cube of tissue placed at 1mm and 5mm of a PIFA antenna. Only the PIFAs ‘top’ and ‘bottom’ are taken into account as they show better reductions of the fields. The cube used is 30*30*30mm and has the same properties as in the dipole case. Two different distances between the cube and the antenna are investigated as the cube is placed 1mm or 5mm under the antenna. In these configurations, the peak of electric field will be investigated on three planes, which are located respectively 5mm, 10mm and 15mm under the antenna.

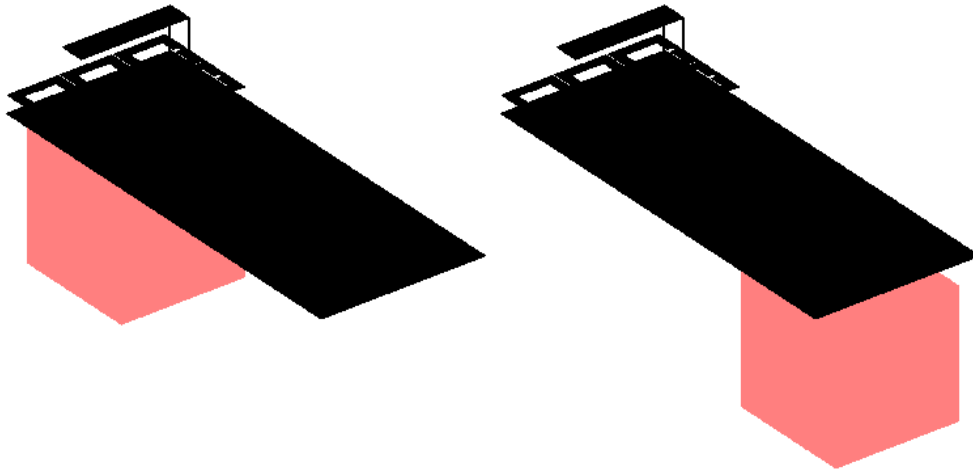


Figure 3.31 : positions of the cube of tissue for ‘top’ and ‘bottom’ simulations with SRRs layer

3.2.2. Electric field investigations

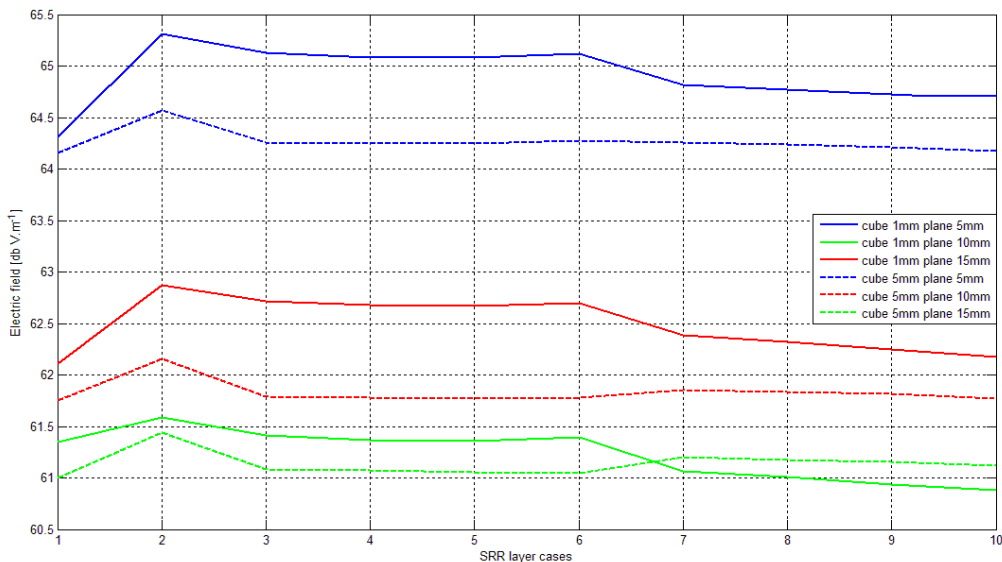


Figure 3.32 : Peaks E field at different planes into the cube place at 1mm and 5mm for a PIFA ‘bottom’

The Figure 3.32 depicts clearly the decrease of the peak E field in the cube depending on its distance to the antenna. Indeed, the reduction is more important for closer planes. For planes farther from the antenna, this difference tends to cancel out by nearly 2dB for plane at 5mm and around 0.5dB for the 15mm plane. The highest decrease of the peak E field is obtained in the case 1 (SRR under the ground plane). In this configuration,

the field is reduced by 1dB. In a general way, it can be observed that the case 1 and 10 show similar reduction of the peak E field.

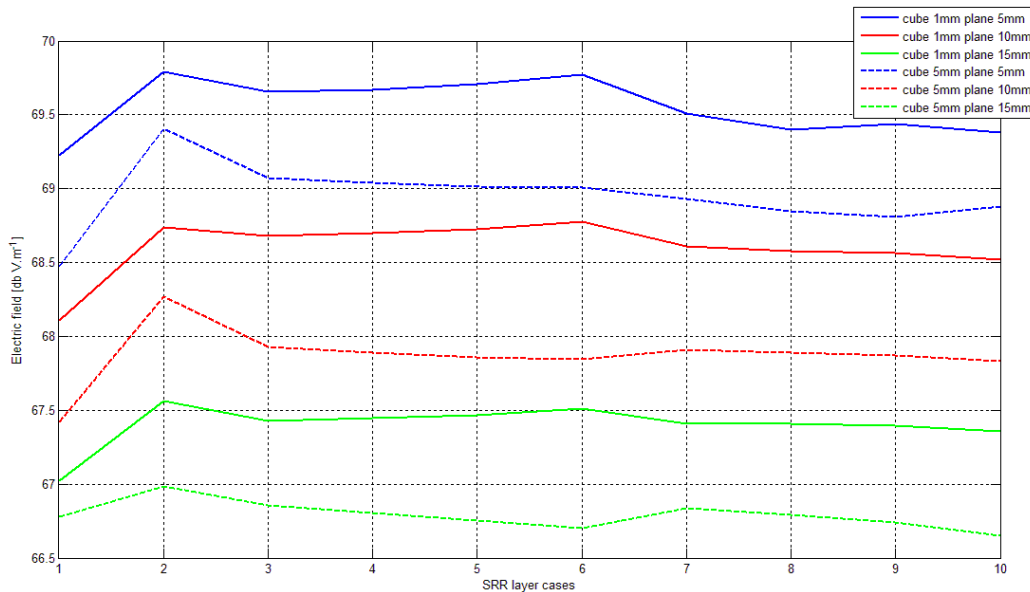


Figure 3.33 : Peaks E field at different planes into the cube place at 1mm and 5mm for a PIFA 'top'

In the case of the Figure 3.33, the same behaviors between 'top' and 'bottom' PIFAs could be expressed but this difference is clearer on the 'bottom' case though.

After seeing those figures depicting the fields behaviors inside the cube of tissue, the relevant fact that the case that is the most influenced by the SRR is obviously when the cube is placed at 5mm from the ground plane. The case of the SRR under the ground plane reduces the peak E field inside the cube of tissue and turns it into the best case of all, as the maximum reduction is close to 1dB when the cube is 5mm under the antenna.

It can also be observed that the cases 3 to 6 do not show a clear reduction of the peak E field in any plane. However, the cases 7 to 10 offer a reduction from 0.2dB to 0.7dB in the configuration where the cube is 5mm under the antenna.

In the case of the PIFA 'bottom', the best configuration (case 1) shows higher reduction than for the case 10, in opposition to the PIFA 'top' case.

When both PIFA types are compared, it can be seen that the PIFA 'bottom' shows a lower peak E field in all cases. In addition to that, the effect of SRRs on the peak E field of this configuration is more visible. This observation confirms the fact that SRRs are more effective in the peak E field reduction for higher distances observed, as the best reduction offered is in the PIFA 'bottom' cube 5mm configuration.

3.2.3. Conclusion

- For a cube placed at 1mm from the antenna, the highest reduction of the peak E field provided by the SRR is lower than 0.5dB in the case of PIFA 'top' and PIFA 'bottom'. At this stage, the peak electric field cannot be significantly reduced in the near field with the structures implemented.

- For a cube placed at 5mm from the antenna, the reduction is the highest (1dB for both antenna configurations depending on the SRRs position). The cases 1 and 7 to 10 show the highest reduction of the peak E field in all planes. The case 1 is the most interesting because it exhibits the best reduction of the peak E field. This is why additional configuration with more layers and a reduced distance between the radiating element and the ground plane should be investigated.

4. Conclusions and improvements

4.1. Conclusions

Metamaterials could have many uses in upcoming technologies especially for lenses and filters. A lot of promising theories praising the advantages of these new kinds of engineered materials have been written, but only a few shows convincing practical applications. They still should be investigated for antennas in mobile communications as their properties could provide new features for user safety. This study therefore aims at the absorption reduction of the tissues in terms of SAR, peak E and H fields while keeping a good trade-off with the main antenna parameters. All the results for the dipole and PIFAs point out that a SRRs layer has more influence on the peak E field reduction when it is investigated far from the antenna. As the studies presented in the first part of this thesis (part 1) do not investigate metamaterials in the near field of the antenna, these results cannot be compared and show the difference of behavior of SRRs in the two cases.

4.1.1. Dipole investigations

First of all, the simple dipole case had been studied to understand the influence of a metamaterial layer (SRRs layer) on the resonance of the antenna. Then, a cube standing for human tissue had been included to consider the impact of the user's head near the antenna.

Adding a layer of SRRs close to the antenna (4mm) reduces the bandwidth covered by the antenna by 20MHz. When a cube of tissue is inserted at different distances from the antenna (from 5mm to 29mm), the SRRs layer reduces the bandwidth covered by a relatively constant value around 55MHz.

It has been shown that the layer of SRRs provides a reduction of the peak E field and the total absorption when the cube of tissue is placed after a certain threshold (respectively around 8mm and 10mm), the highest reduction achievable being around 3% for the peak electric field. Underneath these values, the effect is inverted and the SRRs show an increase of these parameters. To investigate the reason of such variation all the components of the fields should be investigated in the close vicinity of the SRRs layer, or additional and larger layers could be added.

After those studies, a PIFA antenna had been included instead of the dipole for a more realistic case. Therefore, the same investigations have been led and the simulation results are explained in the following paragraphs.

4.1.2. PIFA investigations

A SRRs layer has been included at different distances from the radiating element of a PIFA designed to cover the GSM 1800 requirements, by step of 1mm. Ten cases have thus been designed and are explained in chapter 3.1.1.

Adding a layer of SRRs in the PIFA does not reduce the bandwidth covered by the antenna by more than 5MHz (see Table 3.1) and the real part of the impedance by more than 7Ω (see Figure 3.7). In a general way, the closest the layer is from the radiating element, the highest reduction on the antenna resonant frequency is. As the objective of this study is to build an antenna coupled with metamaterials usable for the GSM 1800 standards, some cases had to be retuned in order to fit the required bandwidth.

The best configuration investigated is the case 1 where the layer of SRRs is placed under the ground plane of the antenna. When more layers are added in the antenna, the covered bandwidth is highly influenced. For 2 and 3 layers, additional simulations are needed to study the variations of the S11 parameter that appear. However, the case where 2 layers are included shows the best reduction of the peak E field in free space ($1.3\text{dB V}\cdot\text{m}^{-1}$ at most), at the expense of the bandwidth covered by the antenna. In the case that this bandwidth issue could be avoided, the cases of multiple layers might bring remarkable peak E field reduction.

In the opposite of the multiple layers cases, the cases 1 and 8 offer the highest reduction for both PIFA configurations ('top' and 'bottom') without degrading the bandwidth of the antenna.

Nevertheless, the case 1 seems to be more promising as the distance between the radiating element and the ground plane is reduced without decreasing the bandwidth. It is to say that some more configurations with more layers and reduced distances between the radiating element and the ground plane could maybe preserve the bandwidth and decrease the peak E field. In the case where those results are generalized, they could be considered as a good achievement in favor of the reduction of the peak SAR in the human head.

4.2. Improvements

For this study, only the Split-Ring resonators have been implemented. As explained, many other structures derived from the SRR exist even if they mainly deal with this basic structure. For example, some types of metamaterials like DSRR are said to reduce the resonant frequency by 30% for the same physical size [16]. All the different metamaterial structures behave differently, and theory is not enough to estimate those differences. That is why implementing additional structures in the antenna could be interesting.

It could also be useful to study the effect of a DNG material on the antenna, by adding thin wires to layers of SRRs in order to reuse the backward waves.

As the 2 layers configuration shows the best improvement of the peak E field, additional cases including more layers with the different distances between them could be investigated.

For this study only the case without substrate has been investigated to be able to understand the behavior of the metamaterial itself. However, adding a substrate would modify the resonant frequency of the antenna depending on the thickness and permittivity of the substrate. This could allow investigating different SRR sizes while matching a more realistic case.

As the simulator used in this study has a uniform mesh, the cell size of the domain has been reduced to 0.2mm in order to design the smallest dimension encountered in the SRR (see 1.3.1). Therefore the simulation time has been dramatically increased. Models including a high number of different tissues with varying permittivity exist. This kind of models could be simulated faster with a simulator with non-uniform mesh. This is why the only remaining option, even though not so realistic, was to include a cube with a permittivity corresponding to human tissue.

Only a few SAR simulations could be launched in this study for the reason explained in the previous paragraph. As SAR calculations are very long, it has been chosen to use the electric and magnetic field investigations, the SAR being proportional to the electric field. Ideally, it would be easier to directly investigate the SAR but calculating the peak of the electric field is a good compromise to estimate the peak of SAR in this case.

List of Figures

CHAPTER I - METAMATERIALS

Figure 2.1 : Basic classification of materials in the ϵ, μ plane [31].....	9
Figure 2.2 : Classification of extreme materials in the ϵ, μ plane [31].....	10
Figure 2.3 : Classification of bi-isotropic materials [30].....	11
Figure 3.1 : Dimensions in millimeter of a SRR pattern in mm [6].....	12
Figure 3.2. Discontinuity of the permittivity [32]	13
Figure 3.3 : $SRR_{parallel}, SRR_{random}, SRR_{perpendicular}$	14
Figure 3.4 : Orientation of B-fields on a SRR structures	14
Figure 3.5 : Excitation of the U-shaped SRR by electric field [9].....	15
Figure 3.6 : Excitation of the U-shaped SRR by magnetic field [9]	15
Figure 3.7 : Design of CLS on the left, and SRR on the right ($1 \text{ mil} = 2.54 \cdot 10^{-2} \text{ mm}$). [10]	15
Figure 3.8 : Planar MM designed with CLS and SRR.....	16
Figure 3.9 : Arrangement of thin-wire structure for metamaterials	17
Figure 3.10 : Two types of isotropic magnetic 3D cubical resonators.....	18
Figure 3.11 : Scheme of 3D DNG metamaterial with dielectric particles and conducting wire frame	18
Figure 3.12 : Metamaterials with both electric and magnetic polarization presented as a set of crystal planes [15].	19
Figure 3.13 : Front view of an I-m-lattice metamaterial [15].....	19
Figure 3.14 : Sum up of the different combinations of structures and their effects.....	20
Figure 3.15 : The lattice geometry of a p-m crystal	21
Figure 3.16. A SRR and its Equivalent Circuit.....	21
Figure 3.17 : Equivalent circuit of thin wire array with inductor array. ([18]).....	22
Figure 4.1 : Dipole antenna surrounded by a DNG shell	23
Figure 4.2 : Configuration for the SAR calculation	24
Figure 4.3 : The different types of filters	24
Figure 4.4. Design of a DSRR	26
Figure 4.5 : Measurement of S parameter for a layer of SRRs	26

CHAPTER II - SIMULATIONS

Figure 1.1 : Detailed dipole model used in the simulations.....	30
Figure 1.2 : Detailed PIFA models used in the simulations.....	30
Figure 1.3 : PIFA used for simulations	31
Figure 1.4 : S11 parameter showing the resonance of the PIFA	31
Figure 1.5 : Shape and dimensions of the square SRR used	32
Figure 1.6 : μ_{eff} plot showing the resonance.....	32
Figure 1.7 : closer look at the resonance in μ_{eff}	33
Figure 2.1 : Detailed dipole with SRR configuration used in simulation.....	34
Figure 2.2 : Different planes where the fields are studied (dipole case) (cell size = 0.2mm).....	34
Figure 2.3 : E field peak plot on different planes.....	34
Figure 2.4 : H field peak plot on different planes	35
Figure 2.5 : Dipole with SRR and cube configuration	36
Figure 2.6 : Investigation of E and H fields in the purple array	36
Figure 2.7 : S11 parameters for dipole and cube configuration at different distances.....	37
Figure 2.8 : S11 parameters for dipole with SRR (at 4mm) and cube configuration at different distances.....	38
Figure 2.9 : Absorption loss depending on the distance (dipole-cube).....	38
Figure 2.10 : Variation of effective bandwidth depending on the distance {dipole-cube}.....	39
Figure 2.11 : Radiation patterns of dipole and cube for three distances (dB).....	40
Figure 2.12 : Radiation patterns for high distance with and without SRR (dB).....	40
Figure 2.13 : E field peak plot on the different planes.....	41
Figure 2.14 : H field peak plot on the different planes.....	41
Figure 2.15 : SAR peak plot for dipole and cube configuration	42
Figure 3.1 : Areas of E and H fields extraction for the PIFA 'bottom'	44

Figure 3.2 : Variation of the position of the SRR into the PIFA.....	44
Figure 3.3 : Resonant frequencies for different PIFA models	45
Figure 3.4 : S11 parameters for the different types of PIFA configurations investigated	46
Figure 3.5 : Initial S11 parameter plots before retuning	46
Figure 3.6 : S11 parameter plot after the retuning.....	47
Figure 3.7 : Smith chart of the PIFA alone and with a SRRs layer at 4mm	47
Figure 3.8 : E field peak plot depending on SRRs layer distance to the ground plane calculated at 5mm.....	48
Figure 3.9 : E field peak plot depending on SRRs layer distance to the ground plane calculated at 10mm.....	49
Figure 3.10 : E field peak plot depending on SRRs layer distance to the ground plane calculated at 15mm.....	49
Figure 3.11 : E field peak plot depending on SRRs layer distance to the ground plane calculated in 3 planes.....	50
Figure 3.12 : H field peak plot depending on SRRs layer distance to the ground plane calculated at 5mm.....	50
Figure 3.13 : H field peak plot depending on SRRs layer distance to the ground plane calculated at 10mm.....	51
Figure 3.14 : H field peak plot depending on SRRs layer distance to the ground plane calculated at 15mm.....	51
Figure 3.15 : E field peak plot depending on SRRs layer distance to the ground plane calculated in 3 planes.....	52
Figure 3.16 : Areas of E and H fields extraction for the PIFA 'top'	52
Figure 3.17 : E field peak plot depending on SRRs layer distance to the ground plane calculated at 5mm.....	53
Figure 3.18 : E field peak plot depending on SRRs layer distance to the ground plane calculated at 10mm.....	53
Figure 3.19 : E field peak plot depending on SRRs layer distance to the ground plane calculated at 15mm.....	54
Figure 3.20 : E field peak plot depending on SRRs layer distance to the ground plane calculated in 3 planes.....	54
Figure 3.21 : H field peak plot depending on SRRs layer distance to the ground plane calculated at 5mm.....	55
Figure 3.22 : H field peak plot depending on SRRs layer distance to the ground plane calculated at 10mm.....	55
Figure 3.23 : H field peak plot depending on SRRs layer distance to the ground plane calculated at 15mm.....	56
Figure 3.24 : H field peak plot depending on SRRs layer distance to the ground plane calculated in 3 planes.....	56
Figure 3.25 : Areas of E and H fields extraction for the PIFA 'crossed'.....	57
Figure 3.26 : E field peak plot depending on SRRs layer distance to the ground plane calculated in 3 planes.....	57
Figure 3.27 : H field peak plot depending on SRRs layer distance to the ground plane calculated in 3 planes.....	58
Figure 3.28 E fields of the 3 configurations and 3 distances.....	59
Figure 3.29 : S11 parameter for 2 and 3 layers of SRRs	60
Figure 3.30 : Peak of electric field for a PIFA with 2 and 3 layers	60
Figure 3.31 : positions of the cube of tissue for 'top' and 'bottom' simulations with SRRs layer.....	62
Figure 3.32 : Peaks E field at different planes into the cube place at 1mm and 5mm for a PIFA 'bottom'.....	62
Figure 3.33 : Peaks E field at different planes into the cube place at 1mm and 5mm for a PIFA 'top'	63
APPENDIX - ANTENNAS	
Figure 1.1 : Radiation pattern of a dipole antenna (YZ plane).....	II
Figure 1.2. Antenna with transmission line.....	III
Figure 1.3 : Return loss (S11) and bandwidth	V
Figure 3.1 : Whip antenna.....	VII
Figure 3.2 : Coil antenna	VIII
Figure 3.3 : PCB antenna.....	VIII
Figure 3.4 : Inverted F antenna	VIII
Figure 3.5 : Dual-band PIFA.....	IX
Figure 3.6 : Quad-band PCB antenna [27].....	IX
APPENDIX - FDTD	
Figure 1.1 : Representation of the Yee algorithm solution.....	XII

List of Tables

CHAPTER I – METAMATERIALS

Table 4.1 : Five configurations of finger rings [23]..... 27

Table 4.2 : Planar and vertical configurations (same sizes than in the previous table) [23]..... 27

CHAPTER II - SIMULATIONS

Table 2.1 : SAR values with and without SRRs layer..... 42

Table 3.1 : Variation of the bandwidth for the different types of PIFA investigated..... 48

APPENDIX - ANTENNAS

Table 1.1 : Frequency bands, nomenclatures and uses.[26] VI

APPENDIX - SAR

Table 1.1 : Classification of the different SAR legislations XV

Bibliography

- [1] CR. Simovski, SA. Tretyakov, *Local constitutive parameters of metamaterials from an effective-medium perspective.*
- [2] Boltasseva, V M. Shalaev, *Fabrication of optical negative-index metamaterials: Recent advances and outlook.*
- [3] X Cai, Rui Zhu, Gengkai Hu, *Experimental study for metamaterials based on dielectric resonators and wire frame.*
- [4] E. Shamonina, L. Solymar, *Metamaterials: How the subject started.*
- [5] CR. Simovski, *Bloch material parameters of magneto-dielectric metamaterials and the concept of Bloch lattices.*
- [6] Vasundara V. Varadan, A. R. (2006). *Effective properties of SRR metamaterials using measured scattering parameters : effect of gap orientation.*
- [7] Zhongyan Sheng, V. V. (2006). *Tuning the effective properties of metamaterials by changing the substrate properties.*
- [8] Hongcang Guo, Na Liu, Liwei Fu, Todd P. Meyrath, Thomas Zentgraf, Heinz Schweizer, and Harald Giessen, *Resonance hybridization in double split-ring resonators metamaterials*
- [9] E. Ekmekci † and G. Turhan-Sayan, *Comparative investigation of resonance characteristics and electrical size of the double-sized SRR, BC-SRR and conventional SRR type metamaterials for varying substrate parameters*
- [10] Ziolkowski, R. W. (2003). *Design, Fabrication and Testing of double negative metamaterials.*
- [11] Ozbay, Aydin, Cubukcu, Bayindir, *Transmission and reflection properties of composite DNG metamaterials in free space*
- [12] Q. Wu, FY. Meng, MF. Wu, J. Wu, LW. Li, *Research on the macro effect of the thin wire array in Metamaterials by equivalent circuit method.*
- [13] C.L. Holloway, E.F. Kuester, J. Baker-Jarvis, P. Kabos, Gengkai Hu, *A double negative (DNG) composite medium composed of magnetodielectric spherical particles embedded in a matrix.*
- [14] Hao, Faulkner, Stevens, Edwards, *Comparison of simulation and measurement for 1-D metamaterial devices*
- [15] Ari Sihvola, *Metamaterials in electromagnetics*
- [16] Bilotti, F., A. Toscano, L. Vegni, K. Aydin, K. B. Alici, and E. Ozbay, *Equivalent-circuit models for the design of metamaterials based on artificial magnetic inclusions*
- [17] Liu, Su, Lin, Wu, Tang, Yeh, *Design of antenna radome composed of metamaterials for high gain*
- [18] Shamonina, Kalinin, Syms, Solymar, *A theory of metamaterials based on periodically loaded transmission lines: Interaction between magnetoinductive and electromagnetic waves*
- [19] Erentok, R. W. (2005). *Dipole antennas enclosed in DNG and SNG nested spheres : efficient electrically small antennas.*
- [20] Chen, J.-N. H.-C. (2006). *Reduction of the peak SAR in the human head with metamaterials.*
- [21] Wikipedia online website: http://en.wikipedia.org/wiki/Specific_absorption_rate
- [22] T. Hao, C. S. (2008). *Reducing electrical size of metamaterial elements : simulations and experiments*
- [23] Boardman, King, Mitchell-Thomas, Malnev, Report: *Gain control and diffraction managed solitons in metamaterials*
- [24] Wikipedia Online Website: http://en.wikipedia.org/wiki/Radiation_pattern
- [25] Balanis, A. Constantine. (1997). *Antenna Theory: Analysis and Design*
- [26] Chen, Z. N. (2007). *Antennas For Portable Devices.*
- [27] Miron Douglas, *Small Antenna Design*
- [28] Hirvonen, M. (2008). *Performance enhancement of small antennas and applications in RFID*
- [29] Online website : http://www.nearfield.com/amta/AMTA06_DG.htm
- [30] Ari Sihvola, *Metamaterials in electromagnetics*
- [31] A. Sihvola, S. Tretyakov, A. De Baas, *Metamaterials with extreme material parameters*
- [32] J.B. Pendry, A.J. Holden, D.J. Robbins, W.J. Stewart, *Magnetism from Conductors, and Enhanced Non-Linear Phenomena*

List of Abbreviations

BC-SRR:	Broadside-Coupled SRR
BW:	Backward Propagation Wave
CLS:	Capacity Loading Strips
DNG:	Double Negative
DPS:	Double Positive
DSRR:	Double-Sided SRR
EBL:	Electron-Beam Lithography
EC-SRR:	Edge-Coupled SRR
EM:	Electromagnetic
ENG:	Epsilon Negative
FDTD:	Finite-Difference Time-Domain
FIB:	Focused-Ion Beam
FW:	Forward Propagation Wave
GSM:	Global System for Mobile Communications
HFSS:	High Frequency Selective Surfaces
IIM:	Infinite Impedance Medium
LHM:	Left-Handed Metamaterials
MMs:	Metamaterials
MNG:	Mu Negative
NIL:	Nano-Imprint Lithography
NRW:	Nicolson-Ross-Weir
PCB:	Printed Circuit Board
PEC:	Perfect Electric Conductor
PEMC:	Perfect Electromagnetic Conductor
PIFA:	Planar Inverted F-Antenna
PMC:	Perfect Magnetic Conductor
SAR:	Specific Absorption Rate
SFR:	Shielded Finger Ring
SRR:	Split-Ring Resonator
VS-SRR:	Vertical Spiral SRR
ZIM:	Zero Impedance Medium

Appendix

Antennas

This chapter deals with antennas for portable devices. In a first part, the fundamental parameters of an antenna are reminded, focusing on the elements that are likely to vary when modifying the simulation environment, and physical propagation properties. The second part introduces small antennas by giving elements on what can be considered as small and explaining the specific issues related to these systems. Finally, some examples of integration in mobile devices are shown.

1. Antenna parameters

This section describes the main parameters that have to be investigated for the present study. The goal of this study is not to reduce the SAR at the expense of other parameters like directivity, bandwidth or efficiency. Improving an antenna is thus a compromise between all parameters that can be investigated and modified. That is why the following properties of the antenna have to be observed when changing the system by adding metamaterial elements.

1.1. Radiation pattern

The radiation pattern refers to the directional dependence of radiation from the antenna [24] (See Figure 1.1).

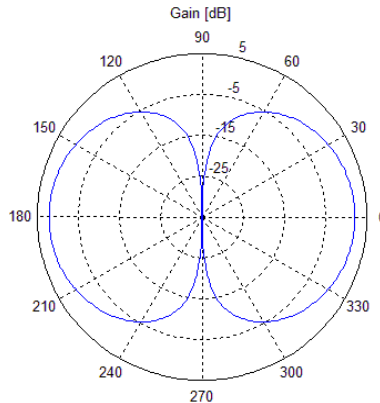


Figure 1.1 : Radiation pattern of a dipole antenna (YZ plane)

It is usually measured during the development of the antenna and is rarely referenced to in mobile communications, because a handset designer has limited ability to influence it and because the user modifies it greatly when using his device. On the other hand, the radiated power in space can be investigated in this study to analyze the impact of modifying the antenna system by adding a metamaterial structure.

The directivity is linked to the radiation pattern and could be expressed by (1.1):

$$D = \max \left(\frac{\text{Radiated_Power_density}(\theta, \phi)}{\frac{\text{Total_Radiated_Power}}{4 \cdot \pi}} \right) \quad (1.1)$$

1.2. Input Impedance

When an antenna terminates a transmission line, its impedance Z_a should be matched to the transmission line impedance Z_o , in order to maximize the power delivered to the antenna. The resonance occurs when Z_a is real.

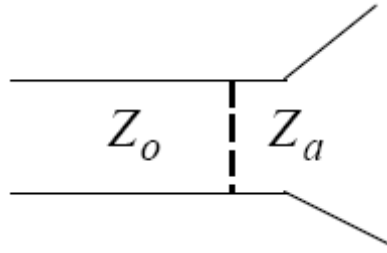


Figure 1.2. Antenna with transmission line

The input impedance is defined as the impedance presented by an antenna at its terminals, the ratio of the voltage to current at a pair of terminals or the ratio of the appropriate components of the electric to magnetic fields at a point [25].

$$Z = R + j.X \quad (1.2)$$

The formula (1.2) can also be understood as:

$$\text{Input impedance} = \text{Self impedance} + \text{Mutual impedance}$$

When the self impedance is calculated in free space, the mutual impedance takes into account anything in the antenna environment that could affect its impedance (also called coupling). When the antenna is isolated enough, then this value is near zero. R is the resistance and the real part of the impedance that is modified when the size of the antenna varies, thus changing the resonant frequency. X is the reactance.

The antenna will typically be coupled to a transmission line that could just be coaxial cables, and so the objective for the impedance is to provide a matching value (50Ω) to ensure that the maximum power is transferred.

1.3. S11

The S11 parameter refers to the signal reflected at Port 1 for the signal incident at Port 1. In fact it is the difference in dB between forward and reflected power measured. Generally this important antenna parameter is referred as the input reflexion coefficient of the network.

1.3.1. VSWR

The voltage standing wave ratio (VSWR) is similar to the return loss but is a scalar linear quantity. It stands for the ratio of the standing wave maximum voltage to the standing wave minimum voltage. It relates to the magnitude of the voltage reflection coefficient and so to the magnitude of S11.[26] So at the input port, the VSWR is given by the equation below.

$$VSWR_{in} = \frac{1 + |s_{11}|}{1 - |s_{11}|} \quad (1.3)$$

When the VSWR value is 1.5:1, it means that the maximum standing wave amplitude is 1.2 times greater than the minimum standing wave value.

1.3.2. Reflexion coefficient

The reflexion coefficient is a measure of the quality of the matching between the input impedance and the characteristic impedance of the transmission line. So the better the match is, the smaller the reflection coefficient will be.

Generally, Γ stands for the reflection coefficient and is defined in (1.4).

$$\Gamma = \frac{VSWR - 1}{VSWR + 1} \quad (1.4)$$

1.3.3. Mismatch Loss

The mismatch loss is referred as the amount of power expressed in dB that will not be available on the output due to impedance mismatches and reflections. In fact it is the amount of power wasted in an imperfect system. The mismatch loss can be defined by the relation below.

$$ML = 10 \cdot \log_{10}(1 - \Gamma^2) \quad (1.5)$$

1.3.4. Return Loss

The Input Return Loss RL_{in} is another way of expressing a mismatch. It is a logarithmic ratio measured in dB that compares the power reflected by the antenna to the power that is fed into the antenna from the transmission line.(1.6)

$$RL_{in} = -20 \cdot \log_{10}(\Gamma)_{dB} \quad (1.6)$$

1.4. Radiation efficiency

The Radiation efficiency is generally more relevant than the Gain to describe a handset antenna. It is the ratio between the radiated power over the input power, which represents how much power is reflected from the antenna.

$$e_r = \frac{P_{rad}}{P_{in}} \quad (1.7)$$

It is basically the input power that will not be available at the output and is also called radiation efficiency. The loss can be created by several reasons [26]:

- Reflection caused by the mismatch between the antenna and its feed line
- Absorption by circuits and other components
- User effects, like presence of hand or head
- Dissipation within the antenna

In the simulation part, two situations happen:

- The case where an antenna has been simulated in free space where the radiation efficiency is thus 1
- The case where an absorbing element is added. The radiation efficiency (or absorption loss) is interesting to study in this case.

1.5. Total Radiated Power (TRP) and Total Isotropic Sensitivity (TIS)

Those two parameters are often used to express the effectiveness of an antenna. The total radiated power which represents the power per unit solid angle is expressed by (1.8):

$$Total_Radiated_Power = \int_{\phi=0}^{\phi=2\cdot\pi} \left(\int_{\theta=0}^{\theta=\pi} Radiated_Power_Density(\theta, \phi) \cdot \sin(\theta) \cdot d\theta \right) \cdot d\phi \quad (1.8)$$

The TIS refers to receiver sensitivity integrated over the sphere and measures ‘the minimum power required achieving a specific bit error rate’ [29].

1.6. Bandwidth

The bandwidth of an antenna is the frequency range over which some specified set of parameters is maintained [21]. This bandwidth has to be large enough to cover the operating frequency. For example, a device operating at 900MHz should cover a frequency range from 890MHz to 960MHz and a device used for GSM 1800 from 1710MHz to 1880MHz.

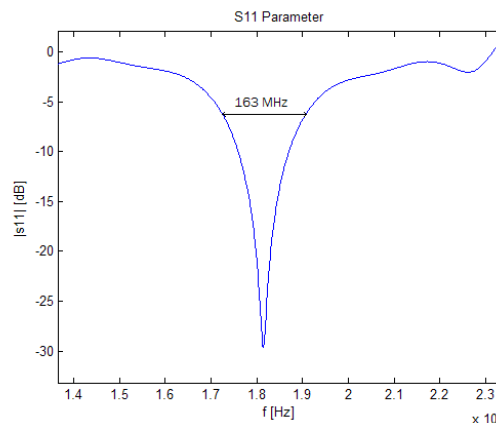


Figure 1.3 : Return loss (S_{11}) and bandwidth

The Figure 1.3 shows the S_{11} parameter for a GSM 1800MHz antenna. The bandwidth observed at -6dB is approximately 163MHz, while the center frequency or resonant frequency is $f_c = 1800MHz$

Nowadays, mobile devices have to resonate at more and more frequencies as the number of services are always increasing. We can consider today that modern handsets have to operate on different bandwidths from 450MHz up to 5GHz. It can be important to investigate the effect of metamaterials on different frequencies to observe if their influence differs according to the bandwidth. It is particularly relevant to analyze this influence on the DVB-H domain, which is the lowest frequency with the highest bandwidth and represents the most difficult scenario.

Here is shown a table containing the main frequencies used in modern communications:

Frequency band	Short reference	Service
550–1600 kHz	MF radio	Radio broadcast
2–30MHz	HF radio	Radio broadcast
88–108MHz	Band II	Radio broadcast
174–240MHz	Band III	T-DMB TV
450–470MHz	450MHz	Phone + data

470–750MHz	Band IV/V	DVB-H TV
824–890MHz	850MHz	Phone + data
870 (880)–960MHz	900MHz	Phone + data
824–960MHz (850 and 900 MHz)	Low bands	Phone + data
1575MHz	GPS	Geolocation
1710–1880MHz	1800MHz	Phone + data
1850–1990MHz	1900MHz	Phone + data
1900–2170MHz	2100MHz	Phone + data
1710–2170MHz (1800, 1900 and 2100 MHz)	High bands	Phone + data
2.4–2.485MHz	2.4 GHz	WLAN
2.5–2.69 GHz	2.5 GHz	WiMAX™
3.4–3.6 GHz	3.6 GHz	WiMAX™
4.9–5.9 GHz	5 GHz	WLAN, WiMAX™

Table 1.1 : Frequency bands, nomenclatures and uses.[26]

2. Small antennas

2.1. Definition of ‘small’

The term ‘small’ is only a comparative term and is usually used for a comparison with an element that has a ‘normal’ size. In the antenna domain this physical definition of small is not so practical as there is no normal size, and is often used compared to Human size. An antenna of 20m will thus be large whereas an antenna in someone’s hand will be small. However, this definition of physically small is only important looking at the mechanical design but not pertinent at all concerning the electrical design process.[26]

The term ‘electrically small’ is therefore introduced, and the scale of interest will be the size of the operating wavelength. Let us consider the fundamental relation:

$$\lambda = \frac{c}{f} \quad (2.1)$$

Where λ is the wavelength, [m]
 c the speed of light [m.s⁻¹]
 f the frequency. [Hz]

An antenna is generally considered small when its size is smaller than $\lambda/10$. Let us consider the GSM system operating at 1800MHz: $\lambda = \frac{300}{1800} = 17cm$
As no mobile device is longer than 15cm, the antenna included can be taken as physically small.

2.2. Problems encountered

Without size constraints, most antennas would be designed to size multiples of $\frac{\lambda}{4}$ because the terminal impedance would be real in this case and easily made compatible with the radio or transmission line it is connected with ([27]) and would thus be called “resonant size”. The problem with electrically small antennas is that their impedance is more and more reactive, making the power transfer more difficult. This implies a reduction in the radiation resistance, due to the lack of coupling between the antenna and the circuit. The overall quality of the system is thus degraded because of the relative loss.

2.3. Q-factor

The quality factor Q is an important measure for small antennas. It relates stored energy and dissipated energy, and is defined by (2.2) [28]:

$$Q = \frac{\omega W}{P} \quad (2.2)$$

Where ω is the angular frequency [rad.s⁻¹]
 W the energy stored in the reactive fields [W]
 P the loss power [W.s-1]

There is a relationship between the bandwidth and the quality factor, and relation (2.3) is commonly admitted:

$$B = \frac{1}{Q} \quad (2.3)$$

Practically, the higher the quality factor is, the more rapidly the antenna impedance varies as a function of frequency. As said before, a small antenna has very reactive impedance with an associated very narrow bandwidth. It is possible to compensate this impedance by adding an opposite reactance, but this would lead Q to increase and B to decrease. The objective is to achieve the highest possible efficiency and still enough bandwidth to cover the mobile bands [26].

3. Antenna design in portable devices

This section shows the different classes of antennas used in mobile handsets. Although this study focuses on PIFA antennas, it is interesting to compare the influence of metamaterials on the different types of antennas. However, the implementation of antennas in the handset will not be discussed, as the simulations focus on the interaction between the antenna and metamaterials, not between the mobile case and the antenna.

3.1. Classes ([26])

3.1.1. Whip antennas

These are the first external antennas that have been implemented, and are still a standard to judge other antennas efficiency. Usually one-quarter wavelength sized, their main inconvenient is that they often have to be pulled in or out when the mobile is in use or not. This implies that the costly mechanical parts become fragile and are often broken.



Figure 3.1 : Whip antenna

3.1.2. Meanders and coils

These are variants of the whip antennas, designed to be more convenient for the user. The antenna that is contained in a short housing is flexible and does not need to be pulled out.



Figure 3.2 : Coil antenna

3.1.3. Dual-band whips and coils

The rapid appearance of the second generation mobiles led to requirement of dual-band handsets, operating at both GSM frequencies (900MHz and 1800MHz). The designed antennas were quite similar to classical coils but with two concentric helix structures. Nowadays, their use is decreasing due to the generalization of internal antennas.

3.1.4. Early internal antennas

One of the first internal antennas designed was a conductor fixed on the main circuit board (Figure 3.3).



Figure 3.3 : PCB antenna

Then the addition of shunt-feeding to the usually used PCB L-inverted antenna created the inverted F antenna, which is now a standard form for internal antennas (Figure 3.4)

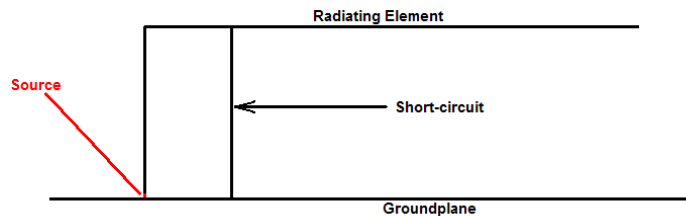


Figure 3.4 : Inverted F antenna

The PIFA (Planar Inverted F Antenna) relies on this model, the upper loading wire becoming a flat plate.

3.1.5. Dual-band internal antennas

PIFA are useful to obtain dual-band antennas, as two radiating elements are used and fed in parallel at the common point. One short element used for high-band provides capacitance in parallel with the lower impedance of the resonant (low-band) element.



Figure 3.5 : Dual-band PIFA

3.1.6. Triple-, quad-, penta-band antennas

The growth of services provided is increasing the frequencies a mobile phone has to support, and early dual-band antennas cannot cover them.



Figure 3.6 : Quad-band PCB antenna [27]

3.1.7. Multiple antennas

The new challenge of mobile designers is to implement several antennas in the handset. For example, the use of Dual-Antenna Interference Cancellation (DAIC) needs the second antenna to be free from user interference. One of the next objectives is although to implement MIMO (Multiple Input Multiple Output) structures and schemes in mobiles using multipath transmission or Space-Time Coding to improve communications.

3.1.8. Additional services

The major difficulty is now to design antennas capable of supporting all mobile services shown in Table 1.1 and even more in the future.

FDTD method

Based upon the mathematical derivation of the wave equation by Maxwell, the FDTD method (Finite-Difference Time-Domain) allows to sample the space considered for the study and extract the expressions of the electromagnetic fields. In three dimensions, the Yee algorithm is used to solve both E and H fields at the same time in space inducing a reinforcement of the Curl's equations.

1. FDTD

1.1. Method choice

In order to be able to demonstrate the effectiveness of metamaterials in specific conditions relative to the human head, the simulations must give some relevant results. Thus, the choice of the method of simulation has to be carefully done and the FDTD seems to fit perfectly with the needs so far. Each method which can be found makes assumptions or approximations that do not fit exactly to the reality. Therefore, the method which will be privileged here is the one that fit the best with the reality.

1.2. Why using FDTD method?

1.2.1. Advantages

1.2.1.1. Spatial modelisation

FDTD is based on the discretization of the physical space, it could be performed on any kind of modelable object around the antenna like the phone itself (Chassis, display, etc...), the human head and hand, and of course metamaterials. As soon as an object is sampled in space, FDTD could be applied on it and then extract the expressions of the E and H fields.

1.2.1.2. Accuracy

The approximations in this method at a mathematical level are not roughly done and provide enough relevance of the results. Moreover, a specific configuration of the simulation according to the CLF number (Courant, Levy, and Friedrich) also known as the Magic Time Step allows to reduce the loss of accuracy of the approximations.

1.2.1.3. Model acceptance

Also, FDTD method allows to make evaluations upon any modeled objects defined with a specific permittivity (ϵ) and permeability (μ). FDTD is an easy way to evaluate electromagnetic waves with all types of materials which could affect them as conductive, capacitive, dissipative, dispersive and non-linear materials.

1.2.1.4. Radiation fields tolerance

No special physics need to be built in the method, as the evolution through the near-field to the far-field is allowed gently. Therefore, the radiation patterns, impedances and fields can be determined by FDTD.

1.2.2. Drawbacks

Despite all the advantages FDTD provides, the major drawbacks are about the computational issues. The simulations done with this method could take a lot of time because of the calculation done for all unit cells defined. Depending on the size of those units and the spatial area of the study, simulations can take a long time to compute. The simulations that are done in this thesis have been performed by a super computer so that the computation time can be increased a lot.

The other main drawback is about the ability to create difficult shaped models as spheres, diagonal planes, etc... As the space is sampled in cells, those particular shapes lead to staircase representations. A trade-off can be found saying that it can be considered as continuous shapes as soon as the unit cells are defined small enough.

1.3. Principles

Maxwell's equations can be expressed in Differential or Integral form and FDTD method is based on the differential one. It induces the assumptions that the medium, in which \mathbf{E} and \mathbf{H} fields have to be calculated, is linear (field independent), isotropic (direction independent) and non-dispersive (frequency independent).

It starts from the Wave equation (1.1) and Maxwell's Curl Equations (1.2) (1.3): (u is E or H field)

Wave equation:

$$\frac{\partial^2 u(x,t)}{\partial t^2} = c^2 \cdot \frac{\partial^2 u(x,t)}{\partial x^2} \quad (1.1)$$

Maxwell's Curl equations:

$$\frac{\partial \vec{D}}{\partial t} = \nabla \times \vec{H} - \vec{J} \quad \nabla \cdot \vec{D} = \rho \quad (1.2)$$

$$\frac{\partial \vec{B}}{\partial t} = -\nabla \times \vec{E} - \vec{M} \quad \nabla \cdot \vec{B} = 0 \quad (1.3)$$

Derivating again the wave equations with Taylor's series and summing them, a second order derivative is obtained (1.4):

$$\left. \frac{\partial^2 u}{\partial x^2} \right|_{x_i, t_n} = \frac{u_{i+1}^n - 2 \cdot u_i^n + u_i^{n+1}}{(\Delta x)^2} + O[(\Delta x)^2] \quad (1.4)$$

Then, the fields that have been already calculated lead to the expression of the same field a time step further (1.5):

$$u_i^{n+1} = \left(\frac{c \cdot \Delta t}{\Delta x} \right)^2 \cdot [u_{i+1}^n - 2 \cdot u_i^n + u_i^{n+1}] + 2 \cdot u_i^n - u_i^{n-1} + O[(\Delta t)^2] + O[(\Delta x)^2] \quad (1.5)$$

This calculus strategy allows defining a specific step to avoid any theoretical losses with the magic time step. This method permits to find out the equations of electric and magnetic waves individually.

1.4. Yee algorithm

The Yee algorithm is designed especially for the 3D case by solving E and H fields at the same time. It solves both E and H fields in time and space relying on the fully explicit time stepping. As this algorithm is not dissipative (2nd order accuracy), it brings enough reliability to the outcome explaining why this algorithm is really useful in this thesis. Moreover, Yee's algorithm reinforces the initial Maxwell's equations due to the coupled resolution of the derivatives between E and H fields (E depending on H and vice-versa).

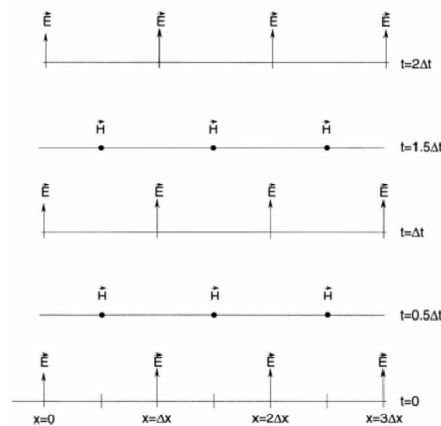


Figure 1.1 : Representation of the Yee algorithm solution

It is also possible to model specific features as keeping the continuity of the tangential E and H fields across the boundaries (§1.5). It allows simulating the infinite space that could not be simulated by a computer as infinite.

1.5. Absorbing Boundaries Conditions

When simulating features on computers, it is often needed to define open regions where the space domain is unbounded in one or more directions. Thus, a trick is needed to be able to simulate this space as an unbounded one. The extension to the infinity could be simulated by a special boundary called 'Absorbing Boundary'.

1.5.1. Definition

As any computer has to deal with its own memory capacity, the simulation space is needed to be clearly defined. This space cannot be infinite even if desired. Therefore, the ABC trick is a solution to do simulations in a space which can be assimilated as unbounded.

The absorbing boundaries allow to all out coming waves, willing to go off the defined space, to be considered as evacuating this space inducing the effect of disappearance. The purpose of those boundaries is to

forbid any waves reflections at best. All unit cells of the simulation space are not affected by the wave reflection that depends only on the limitation of the fixed domain.

In practice, layers of electromagnetic wave absorbers are laid all around the simulation space exactly as the walls of an anechoic chamber but for EM waves.

1.5.2. Solution

The PML (Perfect Matching Layer) is a solution to fit perfectly with the expectations of the ABC. The principle of a PML is that plane incidence, polarization and frequency are matched at the boundary. Choosing a lossless medium in those conditions allows having a perfectly matched layer as the simulation domain end surfaces.

1.6. Models

As the simulations described before this section, some approximations are done on the parameters of the domain considered. The models in which we will be interested in are the models used for approximation of the medium parameters ϵ and μ . Metamaterials are defined with nearly exclusively these two parameters and the approximation with a proper model lead to accurate investigations. Here follow the two models generally used to simulate metamaterials. In the thesis, a specific model for SRR (described in §1.3).

1.6.1. Drude Model

The simple Drude model provides very good explanations for the conductivity in metals and allows approximating the expressions of the two fundamental parameters ϵ and μ . The conductivity of the material is implied into the definition formula of the SAR (Specific Absorption Rate depicted in §1). Permeability (μ) and permittivity (ϵ) take an important place in the simulations which cannot be denied. Therefore, the Drude model allows taking all these parameters and making them evolved as a group during the simulations.

As a computer relies on fixed data that cannot be extent to the infinite, a Lossy Drude Model (LDM) is introduced in order to simplify the simulation computations. Thus, the permittivity and the permeability are modeled as follow:

$$\epsilon_D = \epsilon_0 \cdot \left(1 - \frac{\omega_{PE}^2}{\omega(\omega + i\Gamma_E)} \right) \quad (1.6)$$

$$\mu_D = \mu_0 \cdot \left(1 - \frac{\omega_{PM}^2}{\omega(\omega + i\Gamma_M)} \right) \quad (1.7)$$

Where:	μ_0 is the permeability in free space	[H.m ⁻¹]
	ϵ_0 is the permittivity in free space	[F.m ⁻¹]
	Γ is the damping frequency	[rad.s ⁻¹]
	ω_P is the plasmatic frequency	[rad.s ⁻¹]

(1.6) and (1.7) are approximations, and researches to find even better approximations for the accuracy or the computational time has to be investigated.

1.6.2. Lorentz Model

The Lorentz' model (or Minkowski's model) is based upon geometrical approach where the points are points on one sheet of a hyperboloid of two sheets. Applied to the Drude model previously depicted, slightly different expressions than (1.6) and (1.7) can be described for the two main parameters:

$$\epsilon_L = \epsilon_0 \cdot \left(1 - \frac{\omega_{PE}^2}{\omega^2 + i \cdot \Gamma_E \cdot \omega - \omega_{OE}^2} \right) \quad (1.8)$$

$$\mu_L = \mu_0 \cdot \left(1 - \frac{\omega_{PM}^2}{\omega^2 + i \cdot \Gamma_M \cdot \omega - \omega_{OM}^2} \right) \quad (1.9)$$

Where:	μ_0 is the permeability in free space	[H.m ⁻¹]
	ϵ_0 is the permittivity in free space	[A.m ⁻¹]
	Γ is the damping frequency	[rad.s ⁻¹]
	ω_p is the plasmatic frequency	[rad.s ⁻¹]

By doing this ((1.8) and (1.9)), the metamaterials could be considered as homogeneous materials with frequency dispersive material parameter.

SAR – Specific Absorption Rate

In 2000, the publication of the Stewart Report contained a lot of recommendations about the use of mobile phones and more generally about RF (Radio Frequencies) for adults and children. To be able to put limitations that could be applied everywhere, a specific ratio had been determined to evaluate the effect on the human body (and especially on human heads).

1. Introduction

In the recent years, the use and the impact of RF on the human body has been discussed. In order to prevent some inconvenient diseases from the use of mobile phones, standards had been applied in many countries. The SAR (Specific Absorption Rate) is the standard evaluation of the ability of human tissue to absorb electromagnetic wave per volume of tissue. Each country made its own assumptions about the maximum ratio that could be reached, depending on the use of the phone, the volume of tissue taken for calculations, and of course the frequency range used for handset.

Here is the classification of the different SAR maximum ratios around the world:

	Australia	Europe	USA	Japan	Taiwan	China
Measurement Method	ASA ARPANSA	(ICNIRP) EN50360	ANSI C95.1b:2004	TTC/MPTC ARIB		
Whole body	0.08 W/kg	0.08 W/kg	0.08 W/kg	0.04 W/kg	0.08 W/kg	
Spatial Peak	2 W/kg	2 W/kg	1.6 W/kg	2 W/kg	1.6 W/kg	1 W/kg
Averaged over	10 g cube	10 g cube	1 g cube	10 g cube	1 g cube	10 g
Averaged for	6 min	6 min	30 min	6 min	30 min	

Table 1.1 : Classification of the different SAR legislations

The study of reducing the electromagnetic impact on human body by placing metamaterials is mainly based upon the evolution of the SAR peaks resulting of the mobile phone's radiations.

2. Definition

The SAR is mathematically defined as follow:

$$SAR = \sigma \cdot \frac{|E|^2}{\rho} \quad (2.1)$$

Where: E is the value of electric strength in the tissue [V/m]
 σ is the conductivity of the tissue [S/m]
 ρ is the density of the tissue [kg/m³]

Previous studies have shown that the conductivity takes an important part in the ability to absorb energy from electromagnetic sources. However, the same ratio could be expressed with the difference of temperatures in the medium, as the heating capacity of it. So, SAR could be also expressed as:

$$SAR = C \cdot \left. \frac{\Delta T}{\Delta t} \right|_{t=0} \quad (2.2)$$

Where: C is the specific heat capacity [J/kg.°C]
 ΔT is the change of temperature [°C]
 Δt is the duration of the exposure [s]

3. Simulations

For this thesis, the SAR has been calculated only for the configuration {dipole-cube} because of time issues due to the reduction of the cell size in the domain. In fact, each SAR calculation takes more than one or two days because the supercomputer cannot be used in this case. The result of these measurement are shown in §2.2.7.